Convex Reparameterizations for Efficient Mixed $\mathcal{H}_2/\mathcal{H}_\infty$ Feedback Control

by

Zhong Fang

A thesis
presented to the University of Waterloo
in fulfillment of the
thesis requirement for the degree of
Master of Applied Science
in
Electrical and Computer Engineering

Waterloo, Ontario, Canada, 2025

Author's Declaration

I hereby declare that I am the sole author of this thesis. This is a true copy of the thesis, including any required final revisions, as accepted by my examiners.

I understand that my thesis may be made electronically available to the public.

Abstract

The design of controllers with mixed $\mathcal{H}_2/\mathcal{H}_\infty$ cost functions remains a challenging problem in control theory, with pervasive applications across diverse engineering fields. The main difficulties arise from nonconvexity and infinite dimensionality of the associated optimization problem for the design. Recently, several new approaches were developed to tackle nonconvexity by reparameterizing the variables to transform the optimization into a convex but infinite-dimensional formulation incorporating additional affine constraints in the design problem. For state feedback design, system level synthesis is focused since input output parameterization is primarily intended for output feedback. To make the problem tractable, and to address limitations of historical approximation methods, a new Galerkin-type method for finite-dimensional approximations of transfer functions in Hardy space with a selection of simple poles was recently developed.

However, prior applications of this simple pole approximation resulted in a design problem that required an additional approximation of a finite time horizon to compute $\mathcal{H}_2$ and $\mathcal{H}_\infty$ norms for the closed-loop response. This finite horizon resulted in increased suboptimality, degraded performance, and increased problem size and memory requirements. To address these limitations, this thesis presents a novel control design framework that combines the frequency domain convex reparameterization affine constraints with a state space formulation of the $\mathcal{H}_2$ and $\mathcal{H}_\infty$ norms using linear matrix inequality. This state space formulation eliminates the need for a finite time horizon approximation, and results in a convex and tractable semidefinite program for the control design. Suboptimality bounds are provided for the method which guarantee convergence to the global optimum of the infinite dimensional problem as the number of poles approaches infinity with a convergence rate that depends on the geometry of the pole selection.

The recently developed convex reparameterization methods have been challenging to adapt to continuous time control design in practice, because they typically rely on finite dimensional approximations for tractability that lead to numerical ill-conditioning or even closed-loop instability. In this work, the hybrid state space and frequency domain control design method is adapted to develop the first practical and tractable continuous time control design based on these convex reparameterizations that does not suffer from ill-conditioning and that guarantees closed-loop stability for stabilizable plants. Approximation error bounds are established for the first time for the simple pole approximation in continuous time. These bound the error based on the geometry of the pole selection, and show that this error goes to zero as the number of poles approaches infinity. These bounds are particularly challenging to obtain compared to the discrete time case due to the noncompactness of the domain of integration for computing the $\mathcal{H}_2$ and $\mathcal{H}_\infty$ norms

in continuous time. These approximation error bounds are then used to develop suboptimality guarantees of an analogous nature to those in discrete time. This is the first time that suboptimality bounds with zero asymptotic error have been developed for a control design method using these recent convex reparameterization approaches in continuous time. Again, the noncompactness represents a major challenge that must be overcome to establish these results.

There exist several recently developed convex reparameterizations for output feedback control design in discrete time (including system level synthesis and input output parameterization). However, all of these methods currently lack rigorous suboptimality guarantees that establish convergence to the solution of the infinite dimensional problem as the approximation dimension approaches infinity. This is largely due to the additional complexity introduced by the output feedback case compared to state feedback. This work develops novel output feedback control design methods using four different convex reparameterization approaches, each with different benefits and trade-offs, that result in convex and tractable control design formulations. Moreover, a single unified approximation theory is developed that simultaneously establishes suboptimality bounds for all four methods that recovers analogous results to the state feedback setting. In particular, they show a convergence rate to the global optimum that depends on the geometry of the pole selection in a similar fashion to the state feedback case.

The novel methods are applied to design controllers for power converter interfaced devices to provide frequency and voltage regulation to the power grid. Practical case studies demonstrate the ability of the methods to match desired dynamic behavior for these services. We consider multi-controller scenarios involving distributed energy resources where multiple power converters must coordinate to provide grid services while respecting physical and engineering constraints, including state, input, and output limits for each device, enabling coordinated control of dynamic virtual power plants. Case studies involving power converter voltage and frequency regulation, as well as multi-controller coordination in the IEEE 9-bus system, demonstrate superior performance.

Acknowledgements

I could never have come this far alone.

I would like to express my deepest gratitude to Dr. Michael Walter Fisher, my advisor and dear friend, for his unwavering support and kindness even when I was inexperienced, naive, and vulnerable. Without his trust and guidance, I would not have spent these two incredible years in Waterloo, marveling at the world darkened by solar eclipses and the Northern Lights dancing alongside the setting moon, let alone reached these milestones in my academic journey.

Specifically, I am grateful for two of the most important things I have learned from you. First, you helped me shape my research taste. I appreciate how you consistently respected my ideas and gave me the freedom to explore. Over the past two years, you introduced me to this captivating field and gradually gave me more independence, eventually becoming a collaborator standing shoulder-to-shoulder with me. Research is inherently filled with uncertainty and challenges, but your mentorship has not only made me more resilient but also deepened my passion for discovery. More importantly, you reminded me that being a graduate student is not just about research, but also about growing as a whole person with relationships, values, and a life beyond academia. Your genuine care for your students shines through in your teaching, our weekly meetings, and your support during my talk at CDC. You always provided generous encouragement and affirmation especially when I lacked confidence. Your commitment to family has also left a lasting impression on me. Watching you balance professional excellence with care for your loved ones has reshaped how I understand what it means to live a full and grounded life. On a personal note, please also extend my thanks to Navedeep for welcoming us to your home with such a lovely dinner and memorable conversation. In a nutshell, you've made me believe that I, too, can become someone like you.

I would also like to thank Dr. Stephen L. Smith and Dr. Christopher Nielsen for offering excellent courses in areas I had barely ventured into, and for exemplifying through their teaching what outstanding instruction looks like. Thank you to Dr. Stephen L. Smith and Dr. Jun Liu for being my committee members and for providing many insightful comments and suggestions that greatly improved this thesis. Special shout-out to Dr. Dan Davison, one of the best professors at Waterloo, whom I was truly honored to work with as the MATH 213 teaching assistant. Your dedication to teaching goes far beyond obligation and has inspired me to begin developing my own teaching philosophy.

I would like to deeply thank the DOCS group members, you are the best and kindest people. I am truly privileged to have had the opportunity to work alongside such exceptional future scholars and engineers.

First, I would like to express my gratitude to my two incredible cohorts, Murphy and Penny. Your trusted companionship and steadfast support have been indispensable in helping me navigate this challenging yet rewarding journey. From tackling coursework together to commuting to Toronto as student volunteers during ACC, and from countless research discussions to mutual encouragement during difficult moments, you enriched the path and made it far less lonely. Without you, this achievement would not have been possible.

Elin, I'm grateful for the unique perspective you brought to our discussions which truly reshaped my thinking. Your initiative and infectious energy transformed DOCS's dynamic in the best way. I appreciate you cheering me up and helping me all the time, tough days especially.

Thank you, Peng and Garrett, for making my final semester much more enjoyable.

Last but certainly not least, I would like to thank Jinghan for being a constant friend throughout my journey, whether maple leaves colored crimson or cherry blossoms were blooming. Your warmth and understanding created a space where I felt truly at home, which carried me through the most challenging transitions. As I've often told you, I have no doubt you will become the person you aspire to be.

I would like to thank all the sincere humans at Waterloo who made this journey meaningful. Blake (Biochem), Christel (Civil), Kevin (SYDE), LiHsin (MME), Sherly (MSE), Xi (Stats), and the incredible ECE community: Chengyi Li, Yuxuan Qi, Shechem Sumanthiran, Prajwal Thakur, Bin Yan, and many others. Although I cannot name everyone here, each conversation and moment we shared has stayed with me. You wonderful people have broadened my perspective across so many fields, and I wish you all the very best in your lives ahead.

I would like to thank all my friends from high school and undergraduate studies who supported me at the beginning and throughout this journey. I cannot imagine how lost I would have been without you by my side. I look forward to seeing you again.

My deepest love goes to my family, especially the extraordinary women who have shielded and sustained me. Your love made all of this possible. I owe you a lot and I will never be able to make up for it. By now, my tears would have soaked through the paper, had I been writing by hand. Please forgive me.

No matter where life leads, I will never forget where I am from.

Dedication

To my nanas beyond the stars, my mama, my aunt, all my family.

Table of Contents

List of Figures

List of Tables

List of Abbreviations

f-p	active power frequency
v-q	reactive power voltage
c.s.	Cauchy-Schwarz inequality
DER	distributed energy resource
DVPP	dynamic virtual power plant
ES	energy storage system
FIR	finite impulse response
IOP	input output parameterization
KYP	Kalman-Yakubovich-Popov
LMI	linear matrix inequality
LTI	linear time invariant
MI	mixed I
MII	mixed II
MIMO	multiple input multiple output
PV	photovoltaic

SDP	semidefinite program
SISO	single input single output
SLS	system level synthesis
SPA	simple pole approximation
VPP	virtual power plant
WT	wind turbine

List of Symbols

B_r	closed ball of radius r centered at the origin
$\mathbb{C}^-$	open left half plane of the complex plane
$\mathbb{D}$	open unit disk
$\partial\mathbb{D}$	unit circle
$\overline{\mathbb{D}}$	closed unit disk
$\otimes$	Kronecker product
$\mathcal{RH}_\infty$	set of real, rational, proper, and stable transfer function matrices
$\frac{1}{s}\mathcal{RH}_\infty$	set of real, rational, strictly proper, and stable transfer function matrices in continuous time
$\frac{1}{z}\mathcal{RH}_\infty$	set of real, rational, strictly proper, and stable transfer function matrices in discrete time

Chapter 1

Introduction

Mixed $\mathcal{H}_2/\mathcal{H}_\infty$ control synthesis is valuable for applications and has a long history (see, e.g., [7,8]). $\mathcal{H}_2$ norm minimization reduces the energy of the closed-loop behavior resulting from disturbances, whereas $\mathcal{H}_\infty$ norm minimization reduces the worst-case of this behavior. Therefore, it is valuable to combine both into mixed $\mathcal{H}_2/\mathcal{H}_\infty$ design in order to balance and trade-off between the two extremes. However, it remains challenging to solve efficiently as methods for $\mathcal{H}_2$ and $\mathcal{H}_\infty$ synthesis alone do not readily yield optimal solutions to mixed $\mathcal{H}_2/\mathcal{H}_\infty$ synthesis. The first major difficulty is that the design problem is nonconvex in the controller. Convex reparameterization, which involves a change of variables to render the optimization problem convex, is one approach to address this. A classical example is the Youla parametrization [23], while more recent methods include system level synthesis (SLS) [3], input output parameterization (IOP) [16], mixed I (MI) and mixed II (MII) [24]. Althought these four methods and Youla parameterization were later shown to be equivalent in [25], these four new approaches each parameterize a class of stable closed-loop transfer matrices and enforce a set of equality constraints in terms of these transfer functions. As mentioned in [24], they represent the only known methods that can guarantee internal stability and do not rely on the doubly coprime factorization technique. They show several advantages over Youla parameterization, including directly parameterizing the control design via the closed-loop system responses rather than coprime decomposition, and more naturally accommodating structural, robustness, and performance constraints via convex formulations [24]. For state feedback control design, this thesis primarily focuses on the SLS framework, as the other three reparameterizations (IOP, MI, and MII) are primarily designed for output feedback scenarios. Subsequently, all four convex reparameterization methods are examined in the context of output feedback control design.

Convex reparameterization methods result in convex control design problems, yet re-

main infinite dimensional because their decision variables are transfer functions lying in Hardy space and, hence, intractable in general. Different finite dimensional approximation methods have been proposed with convex reparameterizations to tackle this. In [9, 16, 24], the finite impulse response (FIR) approximation is used for the closed-loop system responses. This requires all closed-loop poles to lie at the origin, causing infeasibility for stabilizable but uncontrollable systems, high computational cost in systems with large separation of time scales, and inability to incorporate prior knowledge about optimal closed-loop poles. Additionally, FIR results in deadbeat control, which often has poor robustness to uncertainty and disturbances due to large control gains. The simple pole approximation (SPA) [13] was developed to circumvent these drawbacks by using poles of multiplicity one (i.e., simple poles) to approximate the closed-loop system responses. SPA gives the designer the freedom to form an approximation using any finite selection of stable poles in the unit disk that are closed under complex conjugation, and can therefore easily include prior knowledge about optimal closed-loop poles. Futhermore. the resulting control design has bounded suboptimality with a convergence rate that depends on the geometry of the pole selection, which converges to the global optimum of the infinite dimensional problem as the number of poles diverges to infinity.

For discrete-time linear time invariant (LTI) systems, the mixed $\mathcal{H}_2/\mathcal{H}_\infty$ state feedback control design problem has been studied by combining SLS with FIR in [3], and with SPA in [14]. However, to compute the $\mathcal{H}_2$ and $\mathcal{H}_\infty$ norms of the closed-loop system responses, these approaches use finite time horizon approximations of the closed-loop impulse response and convolution operators. This additional approximation results in increased suboptimality leading to degraded performance, higher memory and storage requirements, and longer runtimes. The suboptimality bounds for the optimzization problem after SLS and SPA do not apply for their methods, thus the suboptimality may not tend to zero even as the number of poles approaches infinity.

The recently developed convex reparameterization methods have been challenging to adapt to continuous time control design in practice, because they typically rely on finite dimensional approximation FIR for tractability that leads to numerical ill-conditioning or even closed-loop instability [3, 16, 25]. The absence of continuous-time SPA theory requires developing approximation error bounds that parallel the discrete-time results in [13]. One of the biggest theoretical challenges is the noncompactness of the domain over which the $\mathcal{H}_2$ and $\mathcal{H}_\infty$ norms are calculated, which affects the key assumptions and derivation of bounds that enable tractable discrete-time solutions. Consequently, deriving error bounds for SPA requires new theoretical developments in the continuous-time setting. Beyond the limitations of the extra finite time horizon approximation error in the discrete-case control design, truncating the time domain response does not yield an approximation to the $\mathcal{H}_2$ or

$\mathcal{H}_\infty$ norm in continuous time. This is because these norms involve integration or supremum over the entire imaginary axis, and there is no natural finite time horizon surrogate that guarantees convergence to the exact continuous-time norms. As a result, directly evaluating $\mathcal{H}_2$ and $\mathcal{H}_\infty$ norms using finite time horizon approximations in continuous time is inherently intractable and may lead to uncontrolled conservatism or infeasibility in control design, and an alternative approach is needed for control synthesis. Furthermore, suboptimality certificates for control design problems involving SLS and SPA have not been established in continuous time, which this thesis aims to address.

Several recently developed convex reparameterizations (including SLS and IOP) are combined with FIR to solve the $\mathcal{H}_2$ output feedback control design in discrete time in prior work (e.g., [9, 16, 24]). Not only do these approaches suffer from the drawbacks of FIR methods discussed above, but they also lack rigorous theoretical guarantees ensuring convergence to the infinite dimensional optimal solution as the approximation order increases. This is largely due to the additional complexity introduced by the output feedback case compared to state feedback. These gaps highlight the need for unified theoretical frameworks that can address mixed $\mathcal{H}_2/\mathcal{H}_\infty$ synthesis across both state and output feedback scenarios while providing rigorous performance guarantees.

The concept of virtual power plants (VPPs) was introduced as early as 1997 to address the transition to future power converter-based grids [6]. VPPs aggregate multiple distributed generators, each with individual operational constraints, to collectively achieve the controllability, visibility, and market participation of a traditional power plant [21]. Despite significant progress, both commercial implementations and much of the academic research to date have primarily focused on VPPs delivering static ancillary services, such as tracking predefined power and voltage reference signals [10]. This thesis investigates the concept of DVPPs composed of heterogeneous distributed energy resources (DERs), aimed at providing dynamic ancillary services beyond setpoint tracking. In contrast to existing VPPs, DVPPs can deliver fast frequency and voltage regulation through coordinated control of diverse devices. Heterogeneity is essential for reliable dynamic ancillary services, as different devices with varying capacities and response times are necessary to provide these services across multiple power levels and time scales. However, previous efforts combining heterogeneous resources, such as hydropower with batteries or synchronous condensers with converter-based generation [18], have been highly specialized and heuristic, and lack general applicability or optimal dynamic performance. Moreover, they do not provide frameworks for enforcing desired aggregate system behavior under operational constraints.

The main goal of this thesis is to develop optimal mixed $\mathcal{H}_2/\mathcal{H}_\infty$ control design methods and to establish rigorous suboptimality bounds for them. The methods are then applied to design controllers for power converter interfaced devices for frequency and voltage reg-

ulation, and demonstrate superior performance.

This thesis is structured as follows. Preliminaries and notation are stated in Chapter 2. The theoretical foundation spans three chapters covering state feedback design in discrete time (Chapter 3) and continuous time (Chapters 4), and output feedback design in discrete time (Chapter 5). All frameworks are equipped with convergence certificates. The practical application (Chapter 6) demonstrates the effectiveness of control design methods on control of constrained DVPPs in power systems, where superior performance is achieved compared to existing methods. Chapter 7 concludes the thesis and identifies future research opportunities. More details and our contributions will be introduced in Section 1.1.

1.1 Contributions

A hybrid state space and frequency domain formulation of the mixed $\mathcal{H}_2/\mathcal{H}_\infty$ optimal discrete-time state feedback control design is proposed to address the limitations of of the finite time horizon approximation used to evaluate the $\mathcal{H}_2$ and $\mathcal{H}_\infty$ norms in [14]. SLS requires additional constraints, which are affine if expressed in the frequency domain but become nonconvex when represented in state space. Therefore, our method maintains this frequency domain representation of the SLS constraints. However, unlike in prior work of SLS [3, 14], we use the Kalman-Yakubovich-Popov (KYP) lemma to express the $\mathcal{H}_2$ and $\mathcal{H}_\infty$ norms of the closed-loop system responses in state space in the form of linear matrix inequalitys (LMIs). To do so, we use the simple pole approximation to obtain state space realizations of the closed-loop system responses. Our method does not require any finite time horizon approximation, and thus does not suffer from the drawbacks discussed above. A key innovation of our method is to use SPA to simultaneously preserve the affine nature of the SLS constraints in the frequency domain, while also evaluating the $\mathcal{H}_2$ and $\mathcal{H}_\infty$ norms of the closed-loop transfer functions using LMIs in state space. The resulting control design problem is a convex and tractable semidefinite program (SDP) which can be solved accurately and efficiently. Furthermore, the suboptimality bounds developed from [14] apply exactly to our proposed method, and ensure that the suboptimality converges to zero as the number of poles approaches infinity with a convergence rate that depends on the geometry of the pole selection. An example of power converter control design demonstrates superior performance of the method.

This method is introduced in Chapter 3, which is based on

- Zhong Fang and Michael W. Fisher. Hybrid state space and frequency domain system

level synthesis for sparsity-promoting $\mathcal{H}_2/\mathcal{H}_\infty$ control design. In *2024 IEEE 63rd Conference on Decision and Control (CDC)*, pages 8473–8478, 2024.

The framework is then adapted to mixed $\mathcal{H}_2/\mathcal{H}_\infty$ continuous-time state feedback, though this requires overcoming the fundamental differences between discrete and continuous Hardy spaces. In Chapter 4, we develop for the first time approximation error bounds for SPA to approximate arbitrary transfer functions in Hardy space. These bounds are proportional to the geometric distance between the poles of SPA and the poles of the desired transfer function. A key challenge arises from the noncompactness of the imaginary axis when computing the $\mathcal{H}_2$ and $\mathcal{H}_\infty$ norms in continuous time, which are upper bounded by the Cauchy-Schwarz inequality and Cauchy's root bound, respectively. Combining these approximation error bounds with the notion of a space-filling sequence of poles and considering a SPA with poles selected from any arbitrary compact set in the left half plane closed under complex conjugation, it is shown that SPA converges to any transfer function whose poles lie in this compact set at this same uniform convergence rate, which depends purely on the geometry of the pole selection. Therefore, unlike with Lorentz approximations in general, and FIR in particular, the convergence rate of SPA is not reduced for transfer functions with long settling times, such as those resulting from systems with large separation of time scales. Combine SLS with SPA in continuous time and use the continuous time KYP lemma to obtain a hybrid control design method, where SLS constraints remain in the frequency domain and $\mathcal{H}_2$ and $\mathcal{H}_\infty$ norms of the objective are represented in state space, similar to the discrete time case. Also, this method results in a convex and tractable optimization problem for the control design, without any finite time horizon approximation or discrete time approximation to the continuous time systems, which is the first tractable method capable of solving mixed $\mathcal{H}_2/\mathcal{H}_\infty$ control design with SLS in continuous time. Suboptimality certificates are provided for SLS showing the convergence rate of SPA to the ground-truth optimal solution of the infinite dimensional problem as the number of poles diverges based on the geometry of the pole selection. Finally, a particularly interesting space-filling sequence of poles is proposed based on the idea of selecting poles from the intersection of a grid with a trapezoid in the left half plane. This selection leads to a uniform convergence rate of the suboptimality bounds based on the geometry of the pole selection, similar to the discrete time case, showing the explicit convergence to the compact set and the suboptimality bounds for the optimization after SLS and SPA. The hybrid state space and frequency domain continuous-time control design method with convergence certificates has been established to provide the first solution method for mixed $\mathcal{H}_2/\mathcal{H}_\infty$ with SLS in continuous time, and an example of power converter control design for frequency and voltage regulation shows the superior performance of SPA in continuous time.

The continuous-time SPA methods and the results developed in this paper are presented in a general form, without being limited to the setting of SLS with state feedback. As a result, they have the potential to be applied to a range of other control design techniques, including IOP, Youla parameterization, and SLS with output feedback. In addition, the approach used to derive approximation error bounds and suboptimality bounds may serve as a general methodology for deriving similar guarantees in these alternative continuous-time control settings.

In Chapter 5, the control design framework is adapted to output feedback control for all four known convex reparameterization methods that can guarantee internal stability without involving the doubly coprime factorization technique, SLS, IOP, MI, MII, with the SPA. Although output feedback involves different objectives, after choosing different closed-loop realizations, they all result in convex and tractable control design formulations as state feedback case. Suboptimality certificates for output feedback control design under each convex reparameterization method combined with SPA are provided for the first time, which characterize the convergence rate of SPA to the ground-truth optimal solution based on the geometry of the pole selection. These certificates are then specialized to a particular pole selection based on an Archimedes spiral as in [13, Theorem 4]. These are the first rigorous suboptimality bounds for output feedback $\mathcal{H}_2/\mathcal{H}_\infty$ control with these four convex reparameterizations that guarantee convergence to the global optimum as the number of poles diverges.

In Chapter 6, we apply the design framework to a multi-controller case for DVPPs that simultaneously delivers multiple dynamic ancillary services while explicitly addressing device constraints and adapting to resource variations, including state, input, and output limits, which also provides guaranteed suboptimality bounds and results in a convex and tractable SDP for the control design. Our proposed control synthesis framework successfully handles challenging state, input, output, and coupling constraints without introducing conservatism, thereby highlighting the structured and systematic approach enabled by modern convex reparameterization methods and SPA. We demonstrate the effectiveness of our control strategy in a case study based on the IEEE 9-bus system.

Chapter 6 is based on

- Zhong Fang and Michael W. Fisher. Constrained $\mathcal{H}_2/\mathcal{H}_\infty$ control design of dynamic virtual power plants via system level synthesis and simple pole approximation. In *2025 IEEE Electrical Power and Energy Conference (EPEC)*, 2025. to appear.

Chapter 2

Preliminaries and Notation

Prior to presenting the main results of the thesis, we establish the necessary foundation by introducing notation used throughout the thesis in Section 2.1, and reviewing mixed $\mathcal{H}_2/\mathcal{H}_\infty$ state feedback control design in both discrete-time and continuous-time settings in Section 2.2. Although SLS and SPA were combined in [14] to solve the optimization problem in discrete time. Several challenges remain,

- convergence guarantees do not immediately apply to the control design method in [14] due to the error introduced by finite time horizon approximation in discrete time,
- the continuous time control design framework is underexplored, particularly regarding the difficulties in extending SPA theory and SLS suboptimality bounds to continuous time systems,

and preliminaries about SPA are elaborated in Section 2.3.

2.1 Notation

The superscript "$\intercal$" and $\mathrm{Tr}\{\cdot\}$ denote the transpose and trace of a matrix, respectively. For a complex number z (or s), let $\mathrm{Re}(z)$, $\mathrm{Im}(z)$, and $\overline{z}$ represent the real part, imaginary part, and complex conjugate of z. For any matrix A, its spectral norm is written as $\|A\|_2 = \sigma_{\max}(A)$ (the largest singular value of A), and its Frobenius norm is written as $\|A\|_F = \sqrt{A^\intercal A}$. We say a matrix A is Hurwitz (Schur) if all of its eigenvalues lie in $\mathbb{C}^-$ ($\mathbb{D}$). A positive definite (semidefinite) matrix P is denoted by $P \succ 0$ ($P \succeq 0$). The set

of real (symmetric) matrices of dimension $n \times m$ (n) is denoted by $\mathbb{R}^{n\times m}$ ($\mathbb{S}^n$). 0 and I are the zero and identity matrices. We use calligraphic letters such as $\mathcal{S}$ to denote sets, and let $|\mathcal{S}|$ be its cardinality (i.e., the number of elements it contains). Let $\mathcal{M}$ denote a collection of matrices $\{M_i\}_{i=1}^l$, define the block diagonal concatenation operator by $\mathcal{D}(\mathcal{M}) := \begin{bmatrix} M_1 & & \\ & \ddots & \\ & & M_l \end{bmatrix}$ where the off-diagonal entries are all zero, and define the block row concatenation operator by $\mathcal{R}(\mathcal{M}) := \begin{bmatrix} M_1 & \cdots & M_l \end{bmatrix}$. We define the floor function $\lfloor x \rfloor := \max\{n \in \mathbb{Z} \mid n \le x\}$ for any $x \in \mathbb{R}$. Let m and n be nonnegative integers, and let $m!$ denote the standard factorial. Define the rising factorial $m^{(n)} = \prod_{k=0}^{n-1}(m+k)$ and the falling factorial $m_n = \prod_{k=0}^{n-1}(m-k)$. Define the double factorial $m!! = \prod_{k=0}^{\lfloor (m-1)/2 \rfloor}(m-2k)$. We have $m^{(n)} = \frac{(m+n-1)!}{(m-1)!}$ and $m_n = \frac{m!}{(m-n)!}$. The following facts hold:

Fact 1. $0! = 1$, $-1!! = 0!! = 1$

Fact 2. $(-1)^n m^{(n)} = (-m)_n$

Fact 3. $\sum_{j=0}^{n} \binom{n}{j} m_j (m')_{n-j} = (m+m')_n$

Hardy space is the space of real, rational, stable transfer functions. For continuous-time systems with $S(s) \in \mathcal{RH}_\infty$, define the norms

$$\|S\|_{\mathcal{H}_\infty} = \sup_{\omega\in\mathbb{R}} \sigma_{\max}(S(j\omega)) \qquad \|S\|_{\mathcal{H}_2}^2 = \frac{1}{2\pi} \operatorname{trace} \int_{-\infty}^{\infty} S(j\omega)S(j\omega)^* \, \mathrm{d}\omega.$$

For discrete-time systems with $S(z) \in \mathcal{RH}_\infty$, define the norms

$$\|S\|_{\mathcal{H}_\infty} = \sup_{z\in\partial\mathbb{D}} \|S(z)\|_2 \qquad \|S\|_{\mathcal{H}_2}^2 = \frac{1}{2\pi} \int_{z\in\partial\mathbb{D}} \|S(z)\|_F^2 \, \mathrm{d}z.$$

Given a discrete-time linear system $G(z) = C(zI - A)^{-1}B$, we define its left and right strictly proper factors as

$$G_C(z) := C(zI-A)^{-1} = G(z)B^\dagger \qquad G_B(z) := (zI-A)^{-1}B = C^\dagger G(z), \tag{2.1}$$

where $B^\dagger$ and $C^\dagger$ denote the Moore–Penrose pseudoinverses of B and C, respectively. These factor functions satisfy $G(z) = G_C(z)B = CG_B(z)$. For any transfer matrix $S \in \frac{1}{z}\mathcal{RH}_\infty$, let $\mathcal{J}(S)(k)$ denote its impulse response at time k. The convolution operator $\mathcal{C}(S)$ maps an input sequence $u(n)$ to an output sequence $y(n) = \sum_{k=1}^{\infty} \mathcal{J}(S)(k)u(n-k)$. We denote $\mathcal{J}_T(S)$ as a stacked vector of the first T impulse responses, and $\mathcal{C}_T(S)$ as a lower-triangular block Toeplitz matrix formed from $\mathcal{J}(S)(k)$.

2.2 Mixed $\mathcal{H}_2/\mathcal{H}_\infty$ State Feedback Control Design

We consider LTI systems in discrete time and continuous time described by the following state space representation respectively:

$$\begin{aligned} x(k+1) &= Ax(k) + Bu(k) + \hat{B}w(k) \\ y(k) &= Cx(k) \end{aligned} \qquad \begin{aligned} \dot{x}(t) &= Ax(t) + Bu(t) + \hat{B}w(t) \\ y(t) &= Cx(t) \end{aligned} \tag{2.2}$$

where $x \in \mathbb{R}^n$, $u \in \mathbb{R}^p$, $w \in \mathbb{R}^q$, $y \in \mathbb{R}^m$ are the state, controller signal, disturbance input, and performance output vectors, respectively. For the sake of simplicity, the results in this chapter applied to both discrete-time and continuous-time systems are denoted as $\circ$ to represent either the s-domain or z-domain accordingly. It will be useful to define the signal $v(\circ) = \hat{B}w(\circ)$.

The closed-loop transfer function mapping disturbance w to output y is $T_{w\to y}(\circ)$, and $T_{w\to u}(\circ)$, $T_{v\to x}(\circ)$, and $T_{v\to u}(\circ)$ are defined analogously. Let $T_{\text{des}}(\circ)$ be some desired closed-loop transfer function for model matching control design, which can also be set to zero if preferred.

Consider a linear state feedback control law of the form $u(\circ) = K(\circ)x(\circ)$ where $K(\circ)$ is a dynamic controller. The goal of Chapter 3 and 4 is to design a controller $K(\circ)$ that is a solution to the mixed $\mathcal{H}_2/\mathcal{H}_\infty$ control design problem given by

$$\underset{K(\circ)}{\text{minimize}} \quad \left\| \begin{bmatrix} Q & 0 \\ 0 & R \end{bmatrix} \begin{bmatrix} T_{w\to y}(\circ) - T_{\text{des}}(\circ) \\ T_{w\to u}(\circ) \end{bmatrix} \right\|_{\mathcal{H}_2/\mathcal{H}_\infty} \tag{2.3a}$$

$$\text{subject to} \quad T_{v\to x}, T_{v\to u} \in \frac{1}{z}\mathcal{RH}_\infty \Big/ \frac{1}{s}\mathcal{RH}_\infty \tag{2.3b}$$

where the mixed $\mathcal{H}_2/\mathcal{H}_\infty$ norm is given by $\|T\|_{\mathcal{H}_2/\mathcal{H}_\infty} = \|T\|_{\mathcal{H}_2} + \lambda\|T\|_{\mathcal{H}_\infty}$ for some constant $\lambda \in [0, \infty]$. The constant matrices Q and R represent the weights on output and input, respectively. We make the following feasibility assumption:

(A1) A solution to (2.3) exists, i.e., (A,B) is stabilizable, and the optimal closed-loop transfer functions are rational (hence they have finitely many poles).

Note that (2.3) is nonconvex in $K(\circ)$ since $T_{w\to y}(\circ)$ and $T_{w\to u}(\circ)$ are, so this problem is challenging to solve in this form.

As discussed in Chapter 1, SLS focuses on state feedback control (we refer the reader to [3] for further details about SLS). Using SLS, (2.3) can be equivalently reformulated as

follows

$$\underset{\Phi_x(\circ),\Phi_u(\circ)}{\text{minimize}} \quad \left\| \begin{bmatrix} Q & 0 \\ 0 & R \end{bmatrix} \begin{bmatrix} \tilde{\Phi}_x(\circ) - T_{\text{des}}(\circ) \\ \tilde{\Phi}_u(\circ) \end{bmatrix} \right\|_{\mathcal{H}_2/\mathcal{H}_\infty} \tag{2.4a}$$

$$\text{subject to} \quad (zI - A)\Phi_x(\circ) - B\Phi_u(\circ) = I \tag{2.4b}$$

$$\Phi_x(\circ), \Phi_u(\circ) \in \frac{1}{z}\mathcal{RH}_\infty \Big/ \frac{1}{s}\mathcal{RH}_\infty \tag{2.4c}$$

where $\Phi_x(\circ)$ and $\Phi_u(\circ)$ are the design variables and represent the closed-loop transfer functions $T_{v\to x}(\circ)$ and $T_{v\to u}(\circ)$, respectively, and where $\tilde{\Phi}_x(\circ) = T_{w\to y}(\circ) = C\Phi_x(\circ)\hat{B}$ and $\tilde{\Phi}_u(\circ) = T_{w\to u}(\circ) = \Phi_u(\circ)\hat{B}$. Note that (2.4c) ensures stability and well-posedness of the closed-loop system. SLS requires the additional affine constraint (2.4b). Note that (2.4) is now convex, although still infinite dimensional as $\Phi_x(\circ)$ and $\Phi_u(\circ)$ lie in the infinite dimensional function space $\frac{1}{z}\mathcal{RH}_\infty$ or $\frac{1}{s}\mathcal{RH}_\infty$.

2.3 Simple Pole Approximation

SPA is adopted to circumvent this issue, that is, transfer functions with only simple poles (i.e., poles with multiplicity no greater than one) can be used to approximate any transfer function in Hardy Space, including those with repeated poles, to arbitrary accuracy. [14] approximates the closed-loop transfer functions using a finite selection of simple stable poles $\mathcal{P}$, closed under complex conjugation, as

$$\Phi_x(z) = \sum_{p\in\mathcal{P}} G_p \frac{1}{z-p} \qquad \Phi_u(z) = \sum_{p\in\mathcal{P}} H_p \frac{1}{z-p}, \tag{2.5}$$

where G_p and H_p are (complex) coefficient matrices for each $p \in \mathcal{P}$. This SPA renders (2.4) finite dimensional. In [14] it is proposed to select the closed-loop poles $\mathcal{P}$ along an Archimedes spiral in the unit disk. It was then shown in [13, Corollary 1] that for this pole selection, the solution to (2.4) with the SPA (2.5) satisfies the following suboptimality bound

$$\frac{J(\mathcal{P}_n) - J^*}{J^*} \leq \frac{\hat{K}}{\sqrt{n}}, \tag{2.6}$$

where $\hat{K}$ is a constant that depends on the ground-truth optimal solution, J^* is the ground-truth optimal cost of problem (2.4), and $J(\mathcal{P}_n)$ is the optimal cost of (2.4) with the SPA (2.5) for the selection $\mathcal{P}_n$ of n poles from the Archimedes spiral. By (2.6), the suboptimality of the solution of SLS with SPA will tend to zero as the number of poles approaches infinity.

However, (2.6) was derived under the assumption that (2.4) with (2.5) could be solved exactly, but this was not the case in [13] due to a finite time horizon approximation used to calculate the $\mathcal{H}_2$ and $\mathcal{H}_\infty$ norms, so the suboptimality may not tend to zero as the number of poles diverges for the method in [13]. In contrast, this suboptimality bound will be shown to apply to the novel control design method we develop in Chapter 3.

For SPA, since $\Phi_x(z)$ and $\Phi_u(z)$ are real, it is straightforward to show that for any real pole p, G_p and H_p are real, and for any complex pole p, $G_{\overline{p}} = \overline{G_p}$ and $H_{\overline{p}} = \overline{H_p}$. Let $\mathcal{P}_r$ denote the real poles in $\mathcal{P}$, and let $\mathcal{P}_c$ denote its complex poles. Then $\mathcal{P} = \mathcal{P}_r \cup \mathcal{P}_c$.

Chapter 3

Mixed $\mathcal{H}_2/\mathcal{H}_\infty$ State Feedback Control in Discrete Time

In this chapter, we develop a novel control design framework that eliminates the finite time horizon approximation error in [14], avoiding the degraded performance, higher memory and storage requirements, and longer runtimes that it causes. Furthermore, this also ensures that the suboptimality bounds developed in [14], which did not include the suboptimality resulting from the finite time horizon approximation, accurately apply to our method. In addition, although this control design framework is presented in the context of discrete-time state feedback control, it extends seamlessly to continuous-time (Chapter 4), output feedback (Chapter 5), and aggregative control (Chapter 6) settings.

Section 3.1 develops a novel state space realization for the closed-loop transfer functions that is specially designed to preserve convexity of the novel control design method, and which provides the structurethat will enable adaptation to the settings of Chapters 4, 5, and 6. The novel hybrid state space and frequency domain control design method is presented in Section 3.2. Section 3.3 details the derivation of the control design, providing a unified approach for extending the framework throughout the remainder of this thesis. The effectiveness of the proposed method is demonstrated through a numerical example in Section 3.4. Section 3.5 concludes this chapter.

3.1 Closed-Loop Realization

To derive the proposed hybrid state space and frequency domain control design method, we will require state space realizations of the closed-loop transfer functions. In this section,

we propose novel state space realizations of the closed-loop dynamics based on the simple pole approximation.

For any $p \in \mathcal{P}_c$, its conjugate $\overline{p}$ is also in $\mathcal{P}_c$, their corresponding coefficient matrices are:

$$\begin{aligned} G_p &= \mathrm{Re}(G_p) + \mathrm{Im}(G_p)j \quad G_{\overline{p}} = \mathrm{Re}(G_p) - \mathrm{Im}(G_p)j, \\ H_p &= \mathrm{Re}(H_p) + \mathrm{Im}(H_p)j \quad H_{\overline{p}} = \mathrm{Re}(H_p) - \mathrm{Im}(H_p)j. \end{aligned} \tag{3.1}$$

We first find real state space realizations for $\tilde{\Phi}_x(z)$ and $\tilde{\Phi}_u(z)$. To do so, for each complex conjugate pair $p, \overline{p} \in \mathcal{P}_c$, define the matrix

$$M(p) = \begin{bmatrix} \mathrm{Re}(p) & \mathrm{Im}(p) \\ -\mathrm{Im}(p) & \mathrm{Re}(p) \end{bmatrix},$$

and let $\mathcal{M}_c$ be the collection of $M(p)$ for all such complex conjugate pairs. Let $\mathcal{M}_r$ be the collection of each scalar matrix p for all $p \in \mathcal{P}_r$. Then we can define

$$\begin{aligned} \overline{A} &= \begin{bmatrix} \mathcal{D}(\mathcal{M}_r) & \\ & \mathcal{D}(\mathcal{M}_c) \end{bmatrix} \otimes I, \\ \overline{B} &= \big[\underbrace{I \quad \cdots \quad I}_{|\mathcal{P}_r|} \quad \underbrace{2I \quad 0 \quad \cdots \quad 2I \quad 0}_{|\mathcal{P}_c|} \big]^{\intercal} \hat{B}. \end{aligned}$$

Next, for each complex conjugate pair $p, \overline{p} \in \mathcal{P}_c$, define the matrices

$$G(p) = \begin{bmatrix} \mathrm{Re}(G_p) & \mathrm{Im}(G_p) \end{bmatrix}, H(p) = \begin{bmatrix} \mathrm{Re}(H_p) & \mathrm{Im}(H_p) \end{bmatrix},$$

and let $\mathcal{G}_c$ and $\mathcal{H}_c$ be the collection of $G(p)$ and $H(p)$, respectively, for all such complex conjugate pairs. Let $\mathcal{G}_r$ and $\mathcal{H}_r$ be the collection of G_p and H_p, respectively, for each $p \in \mathcal{P}_r$. Then we define

$$\begin{aligned} \overline{C}_x &= C \begin{bmatrix} \mathcal{R}(\mathcal{G}_r) & \mathcal{R}(\mathcal{G}_c) \end{bmatrix}, \\ \overline{C}_u &= \begin{bmatrix} \mathcal{R}(\mathcal{H}_r) & \mathcal{R}(\mathcal{H}_c) \end{bmatrix}. \end{aligned}$$

It is straightforward to verify that $(\overline{A}, \overline{B}, \overline{C}_x, 0)$ is a real state space realization of $\tilde{\Phi}_x(z)$, and that $(\overline{A}, \overline{B}, \overline{C}_u, 0)$ is a real state space realization of $\tilde{\Phi}_u(z)$. To see this, first note that $\tilde{\Phi}_x(z)$ and $\tilde{\Phi}_u(z)$ can be decomposed into the contributions from individual real poles and from complex conjugate pairs of poles since $\overline{A}$ is block diagonal. For any real pole p, it follows

$$CG_p \left[zI - pI \right]^{-1} \hat{B} = CG_p \frac{1}{z-p} \hat{B}.$$

For any complex conjugate pair of poles p and $\overline{p}$,

$$\begin{aligned}
&\begin{bmatrix}\mathrm{Re}(G_p) & \mathrm{Im}(G_p)\end{bmatrix}\begin{bmatrix} zI-\mathrm{Re}(p)I & -\mathrm{Im}(p)I \\ \mathrm{Im}(p)I & zI-\mathrm{Re}(p)I\end{bmatrix}^{-1}\begin{bmatrix}2I\\0\end{bmatrix}\\
&=\begin{bmatrix}\mathrm{Re}(G_p) & \mathrm{Im}(G_p)\end{bmatrix}\frac{1}{(z-p)(z-\overline{p})}\begin{bmatrix}2zI-2\mathrm{Re}(p)I\\-2\mathrm{Im}(p)I\end{bmatrix}\\
&=\frac{2z\mathrm{Re}(G_p)-2\mathrm{Re}(G_p)\mathrm{Re}(p)-2\mathrm{Im}(G_p)\mathrm{Im}(p)}{(z-p)(z-\overline{p})}\\
&\overset{(3.1)}{=} G_p\frac{1}{z-p}+G_{\overline{p}}\frac{1}{z-\overline{p}}
\end{aligned}\tag{3.2}$$

and $C(G_p\frac{1}{z-p}+G_{\overline{p}}\frac{1}{z-\overline{p}})\hat{B}$ can be obtained by left multiplying (3.2) by C and right multiplying (3.2) by $\hat{B}$. Therefore $(\overline{A},\overline{B},\overline{C}_x,0)$ is a real state space realization of $\tilde{\Phi}_x(z)$, and $(\overline{A},\overline{B},\overline{C}_u,0)$ can be shown to be a real state space realization of $\tilde{\Phi}_u(z)$ analogously.

Let $(A_{\mathrm{des}},B_{\mathrm{des}},C_{\mathrm{des}},0)$ be any real state space realization of T_{des}. Now we can represent the transfer function in the objective (2.4a) using the following real state space realization

$$\tilde{A}=\begin{bmatrix}\overline{A}&0\\0&A_{\mathrm{des}}\end{bmatrix}\qquad \tilde{B}=\begin{bmatrix}\overline{B}\\B_{\mathrm{des}}\end{bmatrix}\qquad \tilde{C}=\begin{bmatrix}Q\overline{C}_x & -QC_{\mathrm{des}}\\ R\overline{C}_u & 0\end{bmatrix},\tag{3.3}$$

which satisfies

$$\tilde{C}(zI-\tilde{A})^{-1}\tilde{B}=\begin{bmatrix}Q&0\\0&R\end{bmatrix}\begin{bmatrix}\tilde{\Phi}_x(z)-T_{\mathrm{des}}(z)\\ \tilde{\Phi}_u(z)\end{bmatrix}=:\Phi(z).\tag{3.4}$$

Thus, we have obtained an equivalent state space representation of the closed-loop transfer function $\Phi(z)$, which will be used to develop our novel control design method. Note that for a fixed collection of simple poles $\mathcal{P}$, as used for SPA, $\tilde{A}$ and $\tilde{B}$ are constant matrices, and $\tilde{C}$ is an affine function of all of the variable coefficients G_p and H_p.

3.2 Hybrid State Space and Frequency Domain Design

In this section we present our hybrid state space and frequency domain control design method which does not require any finite time horizon approximations for computing the $\mathcal{H}_2$ and $\mathcal{H}_\infty$ norms of the closed-loop transfer functions. As a result, it has reduced suboptimality, better performance, and lower computational cost compared to prior work

[14]. The full derivation of the method is presented in Section 3.3, but the key idea is to use the state space realizations provided in Section 3.1 together with the KYP lemma to derive an equivalent state space representation of the $\mathcal{H}_2$ and $\mathcal{H}_\infty$ norms of the closed-loop transfer functions as LMIs. However, the additional SLS constraints required for the SLS formulation no longer remain affine if we represent them in state space, so we choose to retain their frequency domain representation. Combining these two representations, we obtain the following control design formulation for the solution to (2.4) with the SPA (2.5)

$$\underset{K_1,K_2,Z,G_p,H_p,\gamma_1,\gamma_2}{\text{minimize}} \quad \gamma_1 + \lambda\gamma_2 \tag{3.5a}$$

$$\text{subject to} \quad \begin{bmatrix} K_1 & K_1\tilde{A} & K_1\tilde{B} \\ \tilde{A}^\intercal K_1 & K_1 & 0 \\ \tilde{B}^\intercal K_1 & 0 & \gamma_1 I \end{bmatrix} \succ 0 \tag{3.5b}$$

$$\begin{bmatrix} K_1 & 0 & \tilde{C}(G_p,H_p)^\intercal \\ 0 & I & 0 \\ \tilde{C}(G_p,H_p) & 0 & Z \end{bmatrix} \succ 0 \tag{3.5c}$$

$$\mathrm{Tr}(Z) < \gamma_1 \tag{3.5d}$$

$$\begin{bmatrix} K_2 & 0 & \tilde{A}^\intercal K_2 & \tilde{C}(G_p,H_p)^\intercal \\ 0 & \gamma_2 I & \tilde{B}^\intercal K_2 & 0 \\ K_2\tilde{A} & K_2\tilde{B} & K_2 & 0 \\ \tilde{C}(G_p,H_p) & 0 & 0 & \gamma_2 I \end{bmatrix} \succ 0 \tag{3.5e}$$

$$\sum_{p\in\mathcal{P}_r} G_p + 2\sum_{p\in\mathcal{P}_c} \mathrm{Re}(G_p) = I \tag{3.5f}$$

$$(pI - A)G_p - BH_p = 0, \quad p \in \mathcal{P}_r \tag{3.5g}$$

$$(\mathrm{Re}(p)I - A)\mathrm{Re}(G_p) - \mathrm{Im}(p)\mathrm{Im}(G_p) - B\mathrm{Re}(H_p) = 0, \quad p \in \mathcal{P}_c \tag{3.5h}$$

$$(\mathrm{Re}(p)I - A)\mathrm{Im}(G_p) + \mathrm{Im}(p)\mathrm{Re}(G_p) - B\mathrm{Im}(H_p) = 0, \quad p \in \mathcal{P}_c \tag{3.5i}$$

where $K_1, K_2 \in \mathbb{S}^{n\times|\mathcal{P}|}$, $Z \in \mathbb{S}^m$, and γ_1, γ_2 are scalar variables that represent the $\mathcal{H}_2$ and $\mathcal{H}_\infty$ norms of the closed-loop transfer functions, respectively. Recall that $\tilde{A}$, $\tilde{B}$, and $\tilde{C}$ were defined in (3.3), but we write $\tilde{C} = \tilde{C}(G_p, H_p)$ to emphasize that $\tilde{C}$ is an affine function of the coefficients G_p and H_p for all $p \in \mathcal{P}$. Since, using SPA, we have already selected the closed-loop poles $\mathcal{P}$, $\tilde{A}$ and $\tilde{B}$ are constant matrices, along with A, B, and C. Thus, the objective (3.5a) is linear, the constraints (3.5g)-(3.5i) are linear, the constraint (3.5f) is affine, and the constraints (3.5b)-(3.5e) are LMIs in the decision variables. Therefore, overall (3.5) is a convex SDP that can be solved efficiently. Note that the state space realizations of the closed-loop transfer functions from Section 3.1 were deliberately constructed to ensure

that the constraints (3.5b)-(3.5e) become LMIs rather than nonconvex bilinear matrix inequalities by including all the decision variables G_p, H_p in $\tilde{C}$ and leaving $\tilde{A}, \tilde{B}$ as constant matrices.

As we will see in Section 3.3, the objective (3.5a) and constraints (3.5b)-(3.5e) are derived from a state space representation, whereas the constraints (3.5f)-(3.5i) represent the SLS constraints in the frequency domain, which together yield a truly hybrid control design. Notably, the design method (3.5) exactly determines the $\mathcal{H}_2$ and $\mathcal{H}_\infty$ norms of the closed-loop transfer function, whereas [14] using Frobenius and spectral norms, respectively, to approximate them over a finite time horizon. The error of this finite time horizon approximation is thus entirely eliminated by the proposed design approach. As a result, for the Archimedes spiral pole selection proposed in [13], the suboptimality bound (2.6) from [14] applies exactly to (3.5), and ensures that the suboptimality converges to zero as the number of poles approaches infinity. As we will see in the numerical example in Section 3.4, even a small number of poles can often result in low suboptimality, and thus good performance, in practice.

3.3 Control Design Derivation

This section presents the derivation of our control design optimization problem (3.5). We begin with the problem formulation of SLS (2.4) together with SPA (2.5). First we will derive the representation of the SLS constraints (2.4b) for SPA, and then we will derive the state space representation of the objective function (2.4a).

For the SLS constraint (2.4b), substituting in the SPA (2.5) and matching coefficients of $\frac{1}{z-p}$ for each pole $p \in \mathcal{P}$ since these functions are linearly independent, we obtain

$$I = \sum_{p \in \mathcal{P}_r} G_p + 2 \sum_{p \in \mathcal{P}_c} \mathrm{Re}(G_p) \tag{3.6}$$

for the constant term,

$$0 = (pI - A)\, G_p - B H_p \tag{3.7}$$

for each $p \in \mathcal{P}_r$, and

$$\begin{aligned} 0 &= (\mathrm{Re}(p)I - A)\mathrm{Re}(G_p) - \mathrm{Im}(p)\mathrm{Im}(G_p) - B\mathrm{Re}(H_p) \\ 0 &= (\mathrm{Re}(p)I - A)\mathrm{Im}(G_p) + \mathrm{Im}(p)\mathrm{Re}(G_p) - B\mathrm{Im}(H_p) \end{aligned} \tag{3.8}$$

for each complex conjugate pair $p, \overline{p} \in \mathcal{P}_c$. Thus, the SLS constraint (2.4b) with the SPA (2.5) can be equivalently represented using (3.6)-(3.8).

Next, we will express the $\mathcal{H}_2$ and $\mathcal{H}_\infty$ norms of the closed-loop transfer functions from the objective function (2.4a) using a state space representation. To do so, we begin with the real state space realization $(\tilde{A}, \tilde{B}, \tilde{C}, 0)$ from (3.3), which is a realization of the closed-loop transfer function $\Phi(z)$ by (3.4). In order to calculate the objective (2.4a), we need to express $\|\Phi(z)\|_{\mathcal{H}_2}$ and $\|\Phi(z)\|_{\mathcal{H}_\infty}$ in terms of LMIs using a state space representation. To accomplish this, we apply the KYP lemma to obtain bounds on the $\mathcal{H}_2$ and $\mathcal{H}_\infty$ norms of our state space representation $(\tilde{A}, \tilde{B}, \tilde{C}, 0)$. This yields the following result from [22, Section 4.6]

Theorem 1 (KYP lemma in discrete time) *For the transfer function $\Phi(z) = \tilde{C}(zI - \tilde{A})^{-1}\tilde{B}$, if $\tilde{A}$ is Schur then the following statements hold.*

(1) $\|\Phi(z)\|_{\mathcal{H}_2} < \gamma_1$ if and only if there exist $K_1 \in \mathbb{S}^{n\times|\mathcal{P}|}$, $Z \in \mathbb{S}^m$, such that

$$\begin{bmatrix} K_1 & K_1\tilde{A} & K_1\tilde{B} \\ \tilde{A}^\intercal K_1 & K_1 & 0 \\ \tilde{B}^\intercal K_1 & 0 & \gamma_1 I \end{bmatrix} \succ 0, \qquad \begin{bmatrix} K_1 & 0 & \tilde{C}^\intercal \\ 0 & I & 0 \\ \tilde{C} & 0 & Z \end{bmatrix} \succ 0, \qquad \operatorname{Tr}(Z) < \gamma_1. \tag{3.9}$$

(2) $\|\Phi(z)\|_{\mathcal{H}_\infty} < \gamma_2$ if and only if there exists $K_2 \in \mathbb{S}^{n\times|\mathcal{P}|}$,

$$\begin{bmatrix} K_2 & 0 & \tilde{A}^\intercal K_2 & \tilde{C}^\intercal \\ 0 & \gamma_2 I & \tilde{B}^\intercal K_2 & 0 \\ K_2\tilde{A} & K_2\tilde{B} & K_2 & 0 \\ \tilde{C} & 0 & 0 & \gamma_2 I \end{bmatrix} \succ 0. \tag{3.10}$$

Note that $\tilde{A}$ is Schur by construction because its eigenvalues consist of the poles $\mathcal{P}$ from SPA, which all lie inside the unit disk, so the assumptions of Theorem 1 are automatically satisfied. To use Theorem 1 to reexpress the objective function (2.4a), we note that

$$\min_{\Phi(z)\in\frac{1}{z}\mathcal{RH}_\infty} \|\Phi(z)\|_{\mathcal{H}_2} + \lambda\|\Phi(z)\|_{\mathcal{H}_\infty}$$

is equivalent to

$$\min_{\gamma_1,\gamma_2,\Phi(z)\in\frac{1}{z}\mathcal{RH}_\infty} \gamma_1 + \lambda\gamma_2 \tag{3.11a}$$

$$\text{s.t.} \quad \|\Phi(z)\|_{\mathcal{H}_2} < \gamma_1 \tag{3.11b}$$

$$\|\Phi(z)\|_{\mathcal{H}_\infty} < \gamma_2 \tag{3.11c}$$

since the two inequalities $\|\Phi(z)\|_{\mathcal{H}_2} < \gamma_1$ and $\|\Phi(z)\|_{\mathcal{H}_\infty} < \gamma_2$ will become tight at optimality. Now we can apply Theorem 1 to (3.11) to express the objective function (2.4a) equivalently in terms of LMIs. Thus, combining (3.9), (3.10), (3.11a), and (3.6)-(3.8), we arrive at the final control design optimization problem (3.5), which is equivalent to (2.4) with the SPA (2.5).

3.4 Numerical Example

In this section, we demonstrate the proposed control synthesis method on the control of a wind turbine interfaced to the power grid via a power converter. We model the turbine and converter system using the model proposed in [17]. Let w represent the frequency and voltage magnitude at the connection point, and let y represent the power output of the converter. Then this can be formulated in the form of (2.2) with matrices given by

$$A = \begin{bmatrix} 0.8046 & 0 & 0 & 0 & 0 \\ 0 & 0 & 0.1177 & -0.0112 & -0.1332 \\ 1 & 0 & 0 & 0 & 0 \\ 0 & 0 & 0 & 0.9889 & 0 \\ 0 & 0 & 0 & 0 & 0 \end{bmatrix}, \quad B = \begin{bmatrix} 0 & 0 \\ 0 & 0 \\ 0 & 0 \\ 0.0111 & 0 \\ 0 & 1 \end{bmatrix}, \quad \hat{B} = \begin{bmatrix} -0.4885 & 0 \\ 0 & 1.0069 \\ 2.5 & 0 \\ 0 & 0 \\ 0 & 0 \end{bmatrix},$$

$$C = \begin{bmatrix} 0 & 0.9066 & -0.0364 & 1.0218 & 0 \\ 0 & 0.364 & 0.9066 & -0.2406 & -1.0201 \end{bmatrix}, \quad A_{\text{des}} = \begin{bmatrix} 0.944 & \\ & 0.944 \end{bmatrix}, \quad B_{\text{des}} = \begin{bmatrix} -1.1052 & \\ & -1.1389 \end{bmatrix}, \quad C_{\text{des}} = I_2.$$

For the control design, we choose $Q = I_2$, $R = 0.01I_2$, and $\lambda = 0.5$. For the SPA pole selection $\mathcal{P}$, we set the maximum number of closed-loop poles at $l = 10$. To form $\mathcal{P}$ we first incorporate the plant poles and the poles of the desired transfer function. The remaining poles are chosen based on the spiral method, involving selecting the remaining poles along an Archimedes spiral as in [13]. We also compare the proposed hybrid state space and frequency domain control design method, which we call the hybrid domain method, to the finite time horizon approximation method from [14] with 30 time steps. We solve the SDP for the control design using MOSEK [2] in conjunction with YALMIP [19] in MATLAB.

The step responses for the desired transfer function and the solutions of the finite time horizon approximation method with spiral pole selection [14], and the hybrid domain method with spiral pole selection are shown in Fig. 3.1. The proposed hybrid domain method shows much closer matching to the desired step response than the finite time horizon approximation method, even though both methods use the same spiral pole selection, indicating that the absence of truncation error leads to improved performance for our proposed approach. In particular, the finite time horizon approximation method has a much larger deviation and longer transient during the step response, while the hybrid domain method yields almost perfect matching with the desired response.

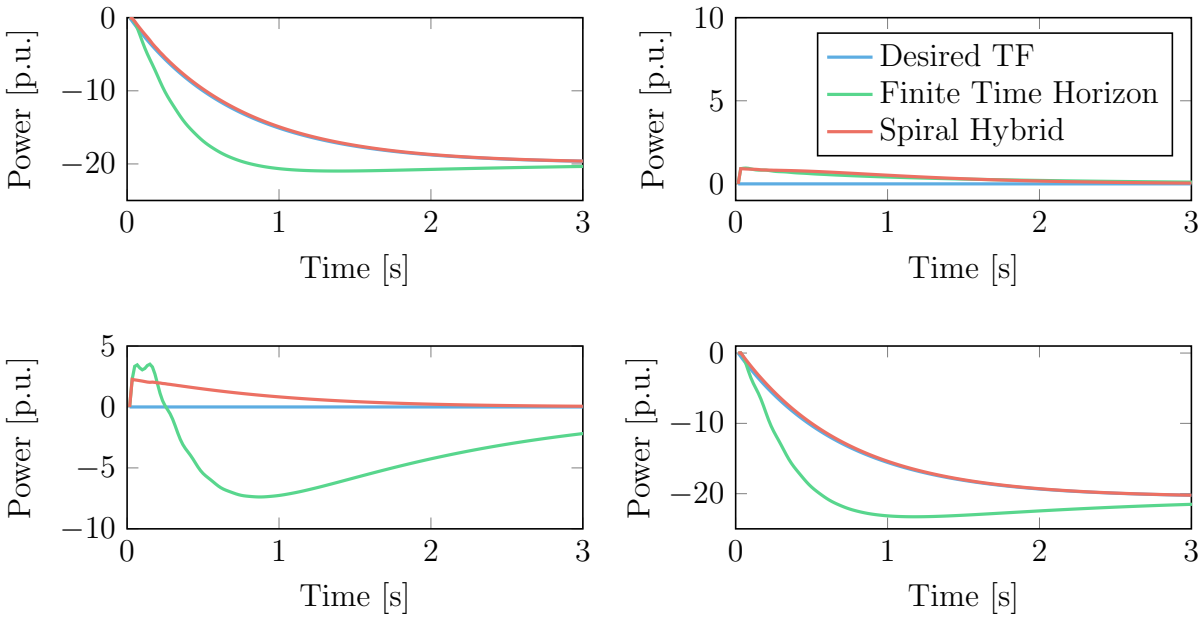

Figure 3.1: Step responses of the desired transfer function (Desired TF) and of the solutions of the finite time horizon approximation method with spiral pole selection (Finite Time Horizon), and the hybrid domain method with spiral pole selection (Spiral Hybrid).

3.5 Conclusion

In this chapter, a novel hybrid state space and frequency domain method for mixed $\mathcal{H}_2/\mathcal{H}_\infty$ control design was developed. The method uses SLS with SPA, but unlike prior work it does not require any finite time horizon approximations to evaluate the $\mathcal{H}_2$ and $\mathcal{H}_\infty$ norms of the closed-loop transfer functions. Therefore, it has reduced suboptimality, improved performance, and less computational cost than prior methods. The state space representations were derived using the KYP lemma applied to a deliberately constructed state space realization in order to obtain a convex and tractable SDP for the control design consisting of LMIs and affine constraints, which can be solved efficiently. The hybrid domain control design method was demonstrated on the test case of control design for a wind turbine with power converter interface, and showed superior performance compared to the prior methods.

Chapter 4

Mixed $\mathcal{H}_2/\mathcal{H}_\infty$ State Feedback Control in Continuous Time

In this chapter, we develop the first method for solving mixed $\mathcal{H}_2/\mathcal{H}_\infty$ control design in continuous time using SLS. This method inherits all of the same advantages of SLS over historical methods, such as Youla parameterization, and also results in a tractable convex optimization problem for the control design, but now in the continuous time setting. Furthermore, we derive the first approximation error bounds for SPA in continuous time, overcoming the difficulty of noncompact domain of integration for evaluating the $\mathcal{H}_2$ and $\mathcal{H}_\infty$ norms, and are able to recover analogous results to the simpler discrete time case. Then, these error bounds are applied to derive suboptimality bounds for our proposed method, again recovering similar results, including a geometric convergence rate and convergence to the ground truth global optimum of the infinite dimensional problem, as in the discrete time setting. Section 4.1 develops continuous-time SPA and derives approximation error bounds, establishes convergence of SPA to the subspace of transfer functions whose poles lie in any given compact set in the left half plane, and derives a uniform convergence rate based on the geometry of the pole selection. Next, Section 4.2 develops the novel hybrid state space and frequency domain method for mixed $\mathcal{H}_2/\mathcal{H}_\infty$ control using SLS with SPA. It also introduces a novel pole selection strategy for SPA, and establishes suboptimality bounds for the control design method both in general and specialized to this particular selection strategy. Section 4.3 presents a numerical example demonstrating the effectiveness of the proposed method. Section 4.4 provides proofs of the theoretical results. Finally, Section 4.5 concludes the chapter.

4.1 Simple Pole Approximation in Continuous Time

Extension of SPA to continuous-time systems introduces substantial challenges. Unlike in discrete time, where stable transfer functions have their poles in the (bounded) unit disk, in continuous time stable transfer functions have poles in the (unbounded) left half plane. This leads to two major difficulties. First, the frequency variable in the definitions of $\mathcal{H}_2$ and $\mathcal{H}_\infty$ norms spans the entire (noncompact) imaginary axis, rather than being confined to the (compact) unit circle, making norm estimation significantly harder. Second, a crucial inequality in discrete time, $\mathcal{H}_2$ norm being upper bounded by a constant multiple of the $\mathcal{H}_\infty$ norm, does not hold in continuous time. The approximation error bounds derived for SPA, and the suboptimality bounds derived for SLS with SPA, in discrete time both relied heavily on these two properties [13]. Consequently, deriving error and suboptimality bounds for SPA and SLS in continuous-time settings requires the development of novel techniques that are particularly well suited for the continuous time setting. Towards that end, we begin with the necessary theoretical foundations.

For any $S \in \frac{1}{s}\mathcal{RH}_\infty$, let $\mathcal{Q}$ be the poles of S. For each pole $q \in \mathcal{Q}$, let m_q be its multiplicity in S and let $m_{\max}$ be the maximum multiplicity, i.e., $m_{\max} = \max_{q\in\mathcal{Q}} m_q$. Then the partial fraction decomposition of S can be written

$$S(s) = \sum_{q\in\mathcal{Q}} \sum_{j=1}^{m_q} G_{(q,j)} \frac{1}{(s-q)^j}$$

for some constant coefficient matrices $G_{(q,j)}$. Let $\mathcal{P}$ be a set of simple and distinct poles, hereafter referred to as approximating poles, which will be used to construct a transfer function for approximating S (i.e., $S \approx \sum_{p\in P} G_p \frac{1}{s-p}$). The key idea is that for each pole $q \in \mathcal{Q}$, an approximating transfer function is constructed to approximate q's contribution to the partial fraction decomposition of S. The poles of this approximation are selected to be the m_q closest poles in $\mathcal{P}$ to q, which we denote by $\mathcal{P}(q)$. Then, the overall approximating transfer function for S is obtained by summing over the individual approximating transfer functions for each $q \in \mathcal{Q}$.

We make the following assumptions regarding the set of approximating poles $\mathcal{P}$ and the control design problem.

(A2) *There exists a compact set $\mathcal{K} \subset \mathbb{C}^-$ that is symmetric with respect to the real axis, such that $\mathcal{P}, \mathcal{Q} \subset \mathcal{K}$.*

(A3) $|\mathcal{P}| \geq m_{\max}$.

(A4) $\mathcal{P}$ *is closed under complex conjugation (i.e.,* $p \in \mathcal{P}$ *implies that* $\overline{p} \in \mathcal{P}$*).*

(A5) Let $\sigma \subset \mathcal{K}$ *be finite. Then for every* $q \in \mathcal{Q}$ *and every* $\lambda \in \sigma$ *with* $\lambda \neq q, \lambda \notin \mathcal{P}(q)$*.*

Assumption A2 ensures that $\mathcal{P}$ and $\mathcal{Q}$ consist of stable poles lying in a compact set of the open left half plane, which is crucial for upper bounding the worst-case approximation error. The symmetry of $\mathcal{K}$ helps ensure that the SPA will result in a real transfer function (whose poles therefore come in complex conjugate pairs) and will converge to any real transfer function whose poles lie in $\mathcal{K}$. Assumption A3 requires that the size of $\mathcal{P}$ is at least as large as $m_{\max}$. Assumption A4 guarantees that $\mathcal{P}$ can be used to construct a transfer function with real coefficients (as will be seen in the proof of Theorem 2), and Assumption A5 is used for Theorem 6 to maintain a positive $\delta = \min_{q\in\mathcal{Q},\lambda\in\sigma,\lambda\neq q} d(\lambda, \mathcal{P}(q))$ where σ will represent the poles of the plant, and can be easily satisfied in practice.

To evaluate the accuracy of the approximation, for each $q \in \mathcal{Q}$ let $\hat{d}(q)$ be the distance from q to the furthest of the m_q simple poles being used to approximate it, i.e., $\hat{d}(q) = \max_{p\in\mathcal{P}(q)} |p-q|$. Let $D(\mathcal{P})$ be the maximum of these distances over all the poles in $\mathcal{Q}$, i.e., $D(\mathcal{P}) = \max_{q\in\mathcal{Q}} \hat{d}(q)$. Then $D(\mathcal{P})$ represents the largest distance between approximating poles in $\mathcal{P}$ and the poles in $\mathcal{Q}$ they are being used to approximate, so it measures the worst-case geometric error in this pole approximation. Intuitively one might therefore expect that as $D(\mathcal{P}) \to 0$, the approximating transfer function would approach S. This intuition is formalized in Theorem 2, which provides an approximation error bound in terms of standard Hardy space norms of the simple pole approximation, which is linear in $D(\mathcal{P})$. Thus, Theorem 2 shows that the simple pole approximating transfer function converges to S at least linearly with $D(\mathcal{P})$ and, therefore, that this convergence rate depends purely on the geometry of the pole selection.

Toward that end, a few important concepts introduced in [13] will be useful to build the uniform convergence rate in Theorem 3 and then specialized to a particular grid pole selection in Theorem 4 and Corollary 1. We define a sequence of poles, denoted $\{\mathcal{P}_n\}_{n=1}^{\infty}$, to be a sequence where for each n, $\mathcal{P}_n$ is a finite collection of poles contained in $\mathcal{K}$ and closed under complex conjugation. We say that a sequence of poles $\{\mathcal{P}_n\}_{n=1}^{\infty}$ exhibits geometric convergence if, for any $S \in \frac{1}{s}\mathcal{RH}_\infty$, its worst-case geometric approximation error converges to zero, i.e., $\lim_{n\to\infty} D(\mathcal{P}_n) = 0$. This definition relates naturally to the approximation error bound provided in Theorem 2. For any $k > 0$, we say that a sequence of poles $\{\mathcal{P}_n\}_{n=1}^{\infty}$ has a geometric convergence rate $\frac{1}{n^k}$ if for each $S \in \frac{1}{s}\mathcal{RH}_\infty$ there exists a constant $c_S > 0$ such that $D(\mathcal{P}_n) \leq \frac{c_S}{n^k}$ for all positive integers n. Note that this is in fact a uniform convergence rate since the rate k is independent of the choice of $S \in \frac{1}{s}\mathcal{RH}_\infty$. However, it is valuable to introduce the related notion of a space-filling sequence of poles. In particular, we say that a sequence of poles $\{\mathcal{P}_n\}_{n=1}^{\infty}$ is space-filling if it is a sequence of pole selections

such that $\mathcal{P}_n \to \mathcal{K}$ with respect to the Hausdorff distance, i.e., the pole sequence converges to the entire compact set.

Theorem 2 (Simple pole approximation) *Let $S \in \frac{1}{s}\mathcal{RH}_\infty$ and let $\mathcal{P}$ be a set of poles satisfying Assumptions A2-A4. Then there exist constants $c_S = c_S(\mathcal{Q}, G^*_{(q,j)}, \mathcal{K}) > 0$ and $c'_S = c'_S(\mathcal{Q}, G^*_{(q,j)}, \mathcal{K}) > 0$, and constant matrices $\{G_p\}_{p\in\mathcal{P}}$ such that $\sum_{p\in\mathcal{P}} G_p \frac{1}{s-p} \in \frac{1}{s}\mathcal{RH}_\infty$ and*

$$\left\| \sum_{p\in\mathcal{P}} G_p \frac{1}{s-p} - S \right\|_{\mathcal{H}_2} \leq c_S D(\mathcal{P}) \qquad \left\| \sum_{p\in\mathcal{P}} G_p \frac{1}{s-p} - S \right\|_{\mathcal{H}_\infty} \leq c'_S D(\mathcal{P}). \tag{4.1}$$

Theorem 2 shows that a transfer function with only simple poles, namely, $\sum_{p\in\mathcal{P}} G_p$, can approximate any transfer function S in the Hardy space $\frac{1}{s}\mathcal{RH}_\infty$ whose poles lie in the compact set $\mathcal{K}$ to arbitrary accuracy in the $\mathcal{H}_2$ and $\mathcal{H}_\infty$ norms as long as each pole q in S has m_q poles in $\mathcal{P}$ that are sufficiently close to it. Recall also that the choice of the compact set $\mathcal{K}$ is arbitrary, so it could be chosen to contain the poles of any transfer function in $\frac{1}{s}\mathcal{RH}_\infty$. Note that the constants c_S and c'_S appearing in Theorem 2 depend on $S \in \frac{1}{s}\mathcal{RH}_\infty$ and on the diameter $\ell(\mathcal{K})$ of the compact set $\mathcal{K}$ in which $\mathcal{P}$ is contained, and do not otherwise depend on the specific pole selection $\mathcal{P}$. This feature will play a crucial role in the proofs of the following uniform convergence results.

The goal of the Theorem 3 is to show that simple pole approximations using suitable pole selections are dense in a compact set containing the poles of transfer functions symmetric with respect to the real axis, and that a uniform convergence rate of the simple pole approximation to any transfer function in the set can be provided, which depends only on the geometry of the pole selection. The equivalence of space-filling and geometric convergence that was shown in discrete time [13, Lemma 1] can be obtained immediately in continuous time by replacing the unit disk in discrete time with the compact set $\mathcal{K}$ in the proof of [13, Lemma 1]. The proof that the space of simple pole approximations converges to the full Hardy space in discrete time [13, Theorem 2] is even more straightforward to complete in continuous time since K is a compact set in the left half plane, so there is no need (as in discrete time) to construct a closed ball inside the open unit disk. As a result, the uniform convergence rate can be given by Theorem 3 in continuous time analogously to the discrete time result.

Theorem 3 shows that if a sequence of poles has geometric convergence rate $\frac{1}{n^k}$, then for any $S \in \frac{1}{s}\mathcal{RH}_\infty$ the simple pole approximation converges to S in the $\mathcal{H}_2$ and $\mathcal{H}_\infty$ norms at the rate $\frac{1}{n^k}$.

Theorem 3 (Uniform convergence rate) *For some $k > 0$, let $\{\mathcal{P}_n\}_{n=1}^{\infty}$ be a sequence of poles with geometric convergence rate $\frac{1}{n^k}$. Then for any $S \in \frac{1}{s}\mathcal{RH}_\infty$, there exist constants $c_S = c_S(\mathcal{Q}, G^*_{(q,j)}, \mathcal{K}) > 0$, $c'_S = c'_S(\mathcal{Q}, G^*_{(q,j)}, \mathcal{K}) > 0$, and $N > 0$ such that for any $n \geq N$ there exist $\{G^n_p\}_{p\in\mathcal{P}_n}$ such that $\sum_{p\in\mathcal{P}_n} G^n_p \frac{1}{s-p} \in \frac{1}{s}\mathcal{RH}_\infty$ and*

$$\left\| \sum_{p\in\mathcal{P}_n} G^n_p \frac{1}{s-p} - S \right\|_{\mathcal{H}_2} \leq \frac{c_S}{n^k} \qquad \left\| \sum_{p\in\mathcal{P}_n} G^n_p \frac{1}{s-p} - S \right\|_{\mathcal{H}_\infty} \leq \frac{c'_S}{n^k}. \tag{4.2}$$

As discussed in [13] for discrete time, in continuous time we also incorporate both the plant poles and any prior information about the optimal poles (if known a priori) into the pole selection for SPA. Since we do not know the locations of the other optimal poles, a natural choice for the remaining poles in the selection for SPA would be to choose them uniformly (i.e., evenly spaced) over $\mathcal{K}$ in order to maximize the probability that every optimal pole has a nearby approximating pole in the SPA selection. However, finding exactly uniformly spaced pole selections over $\mathcal{K}$ is a challenging problem in general - typically nonconvex - so instead we resort to finding approximately uniform pole selections instead. These approximations also have the advantage that, unlike for the exact solution methods, they can be used to derive analytic approximation error bounds with a geometric convergence rate based on Theorem 3. As a special case of practical interest, the compact set $\mathcal{K} \subset \mathbb{C}^-$ in Assumption A2 is selected to be a trapezoidal region symmetric with respect to the real axis, shown in Fig. 4.1a, where k_a, k_b, and k_c denote half the height, half the length of the shorter base, and half the longer base, respectively. This trapezoidal geometry is a practical approximation of the stable region in the continuous-time complex plane, commonly used in model reduction and control design to restrict pole locations to a bounded subset of the open left half plane (see e.g., [5, 11]).

A commonly used heuristic for generating approximately evenly spaced points over arbitrary shapes is to select the centers of uniformly spaced grid cells, a method that has proven effective in various applications including numerical analysis and control design (e.g., [15]). We adopt this approach by overlaying a uniform grid onto the trapezoidal region $\mathcal{K}$ and aligning its center with that of the trapezoid (see the green circle in Fig. 4.1a). Once the cell size l is specified, the grid dimensions are fixed, and pole candidates are selected from the centers of grid cells that lie within $\mathcal{K}$, yielding an approximately even distribution. This method provides a practical heuristic for minimizing $D(\mathcal{P}_n)$ and will make it possible to establish convergence of the approximation error bounds with a geometric convergence rate of $\frac{1}{n^{1/2}}$ based on the grid geometry (see Corollary 1).

The trapezoidal region $\mathcal{K}$ is divided by the lines $y = \pm k_c$ into three parts: a central rectangle and two symmetric upper and lower triangles with angle θ. Since both the

grid and $\mathcal{K}$ are symmetric with respect to the imaginary axis and already center-aligned, the resulting pole set $\mathcal{P}_n$ is closed under complex conjugation, satisfying Assumption A4. Therefore, it suffices to consider pole selection only in the upper half of $\mathcal{K}$ (i.e., $\mathrm{Im}(s) > 0$), since the remaining poles in the selection are automatically determined by the poles with positive imaginary parts by complex conjugation. The upper half of $\mathcal{K}$ consists of one triangle and half of the rectangle. covering one triangle and half of the rectangle. For the rectangular region, pole selection is straightforward to take the centers of all grid cells that lie within this area (see Fig. 4.1c). In contrast, the triangular region presents a challenge due to the presence of the slanted boundary (the hypotenuse). Rather than attempting ideal pole placement along the hypotenuse (as illustrated in Fig. 4.1a), we adopt a more practical approach based on grid cell coverage.

Specifically, we identify all grid cells intersecting the hypotenuse, these are marked by red staircase frames in Figs. 4.1b and 4.1d. Cells within and above this red staircase region are excluded from pole selection. The remaining cells, located beneath the lower boundary of the red staircase, contribute their center points to $\mathcal{P}_n$. This construction ensures that the entire triangular region, including the hypotenuse zone, is effectively covered. It also allows us to provide an upper bound on the distance from any point in $\mathcal{K}$ to its nearest pole in $\mathcal{P}_n$, as shown in Theorem 4.

Theorem 4 (Grid geometric convergence rate) *Let $\mathcal{K} \subset \mathbb{C}^-$ be the trapezoidal region defined in Fig. 4.1a, and let the grid cell size satisfy $l \le \bar{l} := \min\{k_a, k_c\}$. Construct a uniform $n_b l \times n_a l$ grid aligned with the center of $\mathcal{K}$ (as described previously), where $n_\bullet = \lfloor 2k_\bullet/l \rfloor + 1$, for $\bullet \in \{a, b, c\}$. Select poles according to the procedure described above: center points in the rectangular subgrid of size $n_c l \times n_a l$, and valid points in the triangular region below the staircase cells, with symmetry imposed about the real axis.*

Let $n(l)$ denote the number of selected poles under grid size l, and let $\mathcal{P}_{n(l)}$ be the resulting set of poles. Note that $n(l)$ depends on l in a non-monotonic but asymptotically increasing fashion: while a smaller l does not always produce more poles due to grid alignment and staircase effects, the overall trend is that $n(l) \to \infty$ as $l \to 0$. Define the set of achievable pole counts as $\mathcal{N} := \{n \in \mathbb{Z}^+ \mid \exists\, 0 < l \le \bar{l},\ \mathcal{P}_n = \mathcal{P}_{n(l)}\}$. Then, for each $n \in \mathcal{N}$,

$$D(\mathcal{P}_n) \le \frac{c_S}{\sqrt{n}}, \tag{4.3}$$

$$c_S = (m_{\max} - 1)\, l + d_{\min}, \tag{4.4}$$

$$d_{\min} = l\sqrt{\frac{5}{2} + \lceil \tan\theta \rceil^2 + 3\lceil \tan\theta \rceil}. \tag{4.5}$$

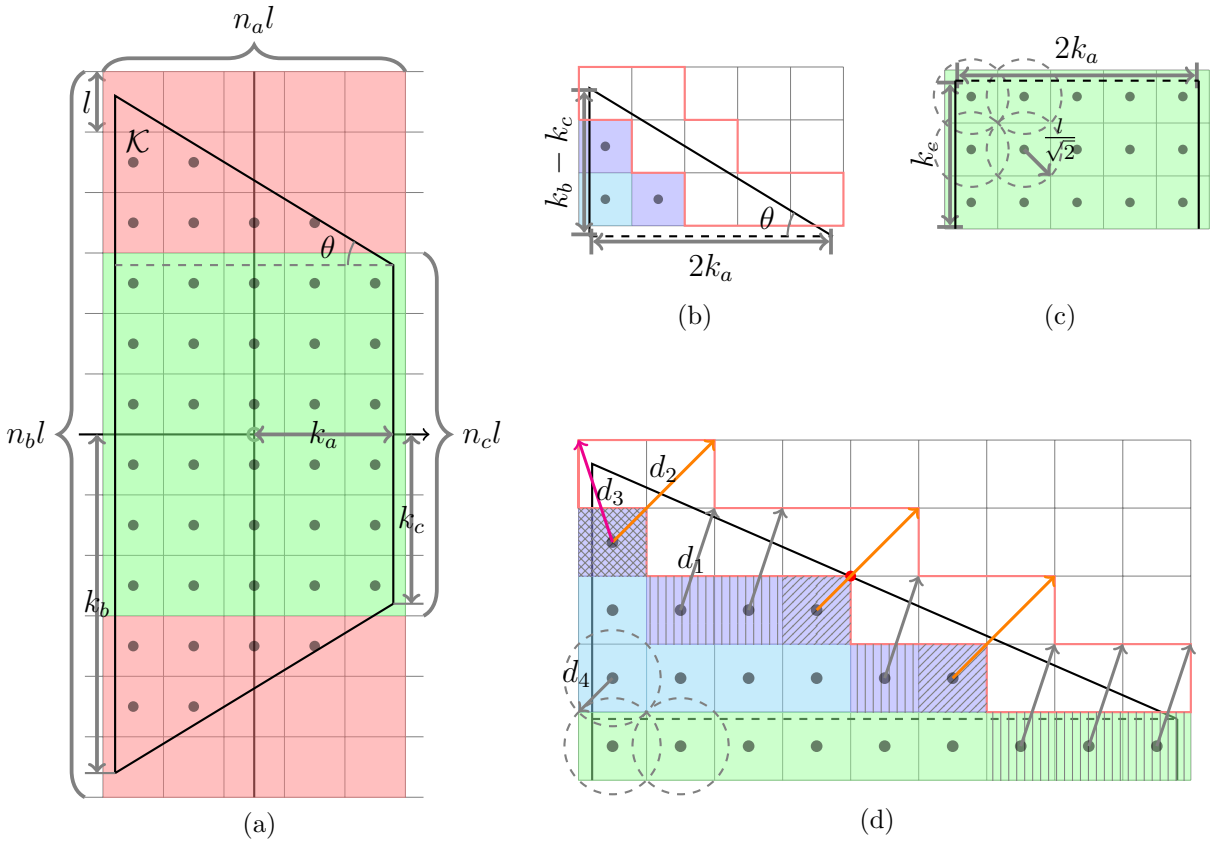

Figure 4.1: (a) is the trapezoidal region $\mathcal{K}$ in the open left half plane overlaid with a uniform grid and the ideal pole selection from the center points of grid cells. The green and red shaded regions are preassigned cells corresponding to the rectangular and triangular subregions, respectively. The corresponding actually chosen poles from them for analyzing convergence rate are illustrated in (b) and (c). (d) shows the stair-step effect on covering the triangle and cell task allocation with different distances; see more details in the proof of Theorem 4.

The coefficient c_S provides a conservative upper bound on the approximation error, which tends to be loose in practice due to the inclusion of all grid center points within $\mathcal{K}$ in the pole set.

Corollary 1 shows that for this choice of pole selection, the SPA converges to the full Hardy space at a rate of $\sqrt{n}$ in the $\mathcal{H}_2$ and $\mathcal{H}_\infty$ norms.

Corollary 1 (Grid approximation convergence rate) *Consider the pole selection of Theorem 4. Then for any $S \in \frac{1}{s}\mathcal{RH}_\infty$ there exist constants $c_S = c_S(\mathcal{Q}, G^*_{(q,j)}, \mathcal{K}) > 0$, $c'_S = c'_S(\mathcal{Q}, G^*_{(q,j)}, \mathcal{K}) > 0$, and $N > 0$ such that for each integer $n \geq N$ there exist $\{G^n_p\}_{p\in\mathcal{P}_n}$ such that*

$$\left\| \sum_{p\in\mathcal{P}_n} G^n_p \frac{1}{s-p} - S \right\|_{\mathcal{H}_2} \leq \frac{c_S}{n^{1/2}} \qquad \left\| \sum_{p\in\mathcal{P}_n} G^n_p \frac{1}{s-p} - S \right\|_{\mathcal{H}_\infty} \leq \frac{c'_S}{n^{1/2}}. \tag{4.6}$$

4.2 Hybrid State Space and Frequency Domain Design

The goal of this section is to design a state feedback controller $K(s)$ that is a solution to the mixed $\mathcal{H}_2/\mathcal{H}_\infty$ control design problem given by

$$\begin{aligned} \underset{K(s)}{\text{minimize}} \quad & \left\| \begin{bmatrix} Q & 0 \\ 0 & R \end{bmatrix} \begin{bmatrix} T_{w\to y}(s) - T_{\text{des}}(s) \\ T_{w\to u}(s) \end{bmatrix} \right\|_{\mathcal{H}_2/\mathcal{H}_\infty} \\ \text{subject to} \quad & T_{v\to x}(s), T_{v\to u}(s) \in \frac{1}{s}\mathcal{RH}_\infty \end{aligned} \tag{4.7}$$

where the mixed $\mathcal{H}_2/\mathcal{H}_\infty$ norm is given by $\|T\|_{\mathcal{H}_2/\mathcal{H}_\infty} = \|T\|_{\mathcal{H}_2} + \lambda\|T\|_{\mathcal{H}_\infty}$ for some constant $\lambda \in [0, \infty]$. The constant matrices Q and R represent the weights on output and input, respectively. Note that (4.7) is nonconvex in $K(s)$ since $T_{w\to y}(s)$ and $T_{w\to u}(s)$ are, so this problem is challenging to solve in this form.

Using SLS, (4.7) can be equivalently reformulated as follows

$$\underset{\Phi_x(s),\Phi_u(s)}{\text{minimize}} \quad \left\| \begin{bmatrix} Q & 0 \\ 0 & R \end{bmatrix} \begin{bmatrix} \tilde{\Phi}_x(s) - T_{\text{des}}(s) \\ \tilde{\Phi}_u(s) \end{bmatrix} \right\|_{\mathcal{H}_2/\mathcal{H}_\infty} \tag{4.8a}$$

$$\text{subject to} \quad (sI - A)\Phi_x(s) - B\Phi_u(s) = I \tag{4.8b}$$

$$\Phi_x(s), \Phi_u(s) \in \frac{1}{s}\mathcal{RH}_\infty \tag{4.8c}$$

where $\Phi_x(s)$ and $\Phi_u(s)$ are the design variables and represent the closed-loop transfer functions $T_{v\to x}(s)$ and $T_{v\to u}(s)$, respectively, and where $\tilde{\Phi}_x(s) = T_{w\to y}(s) = C\Phi_x(s)\hat{B}$ and $\tilde{\Phi}_u(s) = T_{w\to u}(s) = \Phi_u(s)\hat{B}$. Note that (4.8c) ensures stability and well-posedness of the closed-loop system. SLS requires the additional affine constraint (4.8b). Note that (4.8) is now convex, although still infinite dimensional as $\Phi_x(s)$ and $\Phi_u(s)$ lie in the infinite dimensional function space $\frac{1}{s}\mathcal{RH}_\infty$.

To circumvent the issue, we consider the SPA in continuous time in Section 4.1. Using SPA for the closed-loop transfer functions after SLS in (4.8c) can result in

$$\Phi_x(s) = \sum_{p\in\mathcal{P}} G_p \frac{1}{s-p} \qquad\qquad \Phi_u(s) = \sum_{p\in\mathcal{P}} H_p \frac{1}{s-p}, \tag{4.9}$$

where G_p and H_p are (complex) coefficient matrices for each $p \in \mathcal{P}$, which renders (4.8) finite dimensional.

Mixed $\mathcal{H}_2/\mathcal{H}_\infty$ control design requires efficiently evaluating the $\mathcal{H}_2$ and $\mathcal{H}_\infty$ norms of the closed-loop transfer functions using a tractable finite dimensional formulation. Motivated by the method in [14], one way to achieve this finite dimensional formulation in continuous time would be to combine a discrete time approximation with a finite time horizon approximation of the continuous time closed-loop impulse response and convolution operators. Such approximations would introduce additional error, potentially leading to uncontrolled conservatism or infeasibility in control design, higher dimensionality, and computational cost. Consequently, there is a need for an alternative design methodology. To address this, the previously developed novel control design framework in discrete time [12] that avoids finite time horizon approximation errors and possesses suboptimality bounds that ensure convergence to the infinite dimensional global optimum as the number of poles diverges is adapted to develop the first tractable and convex method for $\mathcal{H}_2/\mathcal{H}_\infty$ control design with SLS in in continuous time in this section.

The key idea is to combine the carefully designed state space realizations (continuous-time and discrete-time share analogous realizations, and $(\tilde{A}, \tilde{B}, \tilde{C}, 0)$ from (3.3) is a realization for the closed-loop system in continuous time as well) together with the KYP lemma to derive an equivalent state space representation of the $\mathcal{H}_2$ and $\mathcal{H}_\infty$ norms of the closed-loop transfer functions in the objective as LMIs, and leave SLS constraints in the frequency domain to maintain their linearity. The continuous-time framework employs an analogous derivation to the discrete-time case in Section 3.3, with the KYP lemma being the only distinguishing element, as shown below

Theorem 5 (KYP lemma in continuous time [22, Section 3.3]) *For the transfer function $\tilde{\Phi}(s) = \tilde{C}(sI - \tilde{A})^{-1}\tilde{B}$, if A is Hurwitz then the following statements hold.*

1) $\|\tilde{\Phi}(s)\|_{\mathcal{H}_2} < \gamma_1$ *if and only if there exist* $K_1 \in \mathbb{S}^{n\times|\mathcal{P}|}$, $Z \in \mathbb{S}^m$, *such that*

$$\begin{bmatrix} \tilde{A}^\intercal K_1 + K_1 \tilde{A} & K_1 \tilde{B} \\ \tilde{B}^\intercal K_1 & -\gamma_1 I \end{bmatrix} \prec 0, \qquad \begin{bmatrix} K_1 & \tilde{C}^\intercal \\ \tilde{C} & Z \end{bmatrix} \succ 0, \qquad \mathrm{Tr}(Z) < \gamma_1.$$

2) $\|\tilde{\Phi}(s)\|_{\mathcal{H}_\infty} < \gamma_2$ *if and only if there exists* $K_2 \in \mathbb{S}^{n\times|\mathcal{P}|}$,

$$\begin{bmatrix} \tilde{A}^\intercal K_2 + K_2 \tilde{A} & K_2 \tilde{B} & \tilde{C}^\intercal \\ \tilde{B}^\intercal K_2 & -\gamma_2 I & 0 \\ \tilde{C} & 0 & -\gamma_2 I \end{bmatrix} \prec 0.$$

We can follow the flow to apply it in continuous time analogously: SLS constraint in (4.8b) follows completely the same derivation, and the $\mathcal{H}_2/\mathcal{H}_\infty$ norms of the closed-loop transfer function in (4.8a) are transformed to LMIs via KYP lemma in continuous time in Theorem 5 with respect to the same state space realization (3.3) of the closed-loop transfer function. Combining these two representations, we obtain the following control design formulation for the solution to (4.8) with the SPA (4.9).

$$\underset{K_1,K_2,Z,G_p,H_p,\gamma_1,\gamma_2}{\text{minimize}} \quad \gamma_1 + \lambda\gamma_2 \tag{4.10a}$$

$$\text{subject to} \quad \begin{bmatrix} -\tilde{A}^\intercal K_1 - K_1 \tilde{A}^\intercal & -K_1 \tilde{B} \\ -\tilde{B}^\intercal K_1 & \gamma_1 I \end{bmatrix} \succ 0 \tag{4.10b}$$

$$\begin{bmatrix} K_1 & \tilde{C}(G_p, H_p)^\intercal \\ \tilde{C}(G_p, H_p) & Z \end{bmatrix} \succ 0 \tag{4.10c}$$

$$\mathrm{Tr}(Z) < \gamma_1 \tag{4.10d}$$

$$\begin{bmatrix} -\tilde{A}^\intercal K_2 - K_2 \tilde{A} & -K_2 \tilde{B} & -\tilde{C}(G_p, H_p)^\intercal \\ -\tilde{B}^\intercal K_2 & \gamma_2 I & 0 \\ -\tilde{C}(G_p, H_p) & 0 & \gamma_2 I \end{bmatrix} \succ 0 \tag{4.10e}$$

$$\sum_{p\in\mathcal{P}} G_p = I \tag{4.10f}$$

$$(pI - A)\, G_p - B H_p = 0 \tag{4.10g}$$

where $K_1, K_2 \in \mathbb{S}^{n\times|\mathcal{P}|}$, $Z \in \mathbb{S}^m$, and γ_1, γ_2 are scalar variables that represent the $\mathcal{H}_2$ and $\mathcal{H}_\infty$ norms of the closed-loop transfer functions, respectively. Recall that $(\tilde{A}, \tilde{B}, \tilde{C}, 0)$ defined in (3.3) is a real realization of the closed-loop system (4.8a). Note that for a fixed collection of simple poles $\mathcal{P}$, as used for SPA, $\tilde{A}$ and $\tilde{B}$ are constant matrices, and $\tilde{C}$ is an affine function of all of the variable coefficients G_p and H_p for all $p \in \mathcal{P}$, where we write

$\tilde{C} = \tilde{C}(G_p, H_p)$ to emphasize. This state space realization was deliberately constructed in this fashion to ensure that the constraints (4.10b)-(4.10e) become LMIs rather than nonconvex bilinear matrix inequalities.

Thus, the objective (4.10a) is linear, the constraints (4.10b)-(4.10e) are LMIs in the decision variables, and both of them are derived from a state space representation. The SLS constraints (4.10g) and (4.10f) are linear and affine respectively in the frequency domain. Therefore, overall the hybrid domain control design (4.10) is a convex SDP that can be solved efficiently.

Our main theoretical result shows that the relative error of this SPA method decays at least linearly with $D(\mathcal{P})$.

Theorem 6 (General suboptimality bound) *Let J^* denote the optimal cost of the infinite dimensional SLS problem (4.8), and let $J(\mathcal{P})$ denote the optimal cost applying SPA for any choice of $\mathcal{P}$ (4.10). Suppose Assumption A1 is met, and $\mathcal{P}$ satisfies Assumptions A2-A5. Then there exists a constant $\hat{K} = \hat{K}(\mathcal{Q}, G^*_{(q,j)}, H^*_{(q,j)}, \mathcal{K}, \delta) > 0$ such that*

$$\frac{J(\mathcal{P}) - J^*}{J^*} \leq \hat{K} D(\mathcal{P}). \tag{4.11}$$

Corollary 2 shows that, for the grid pole selection in Theorem 4, the relative error of SPA converges to zero at a rate of $\sqrt{n}$.

Corollary 2 (Grid suboptimality bound) *Consider the setup of Theorem 6 with pole selection $\mathcal{P}_n$ given as in Theorem 4 for each integer $n > 0$. Then there exists a constant $\hat{K} = \hat{K}(\mathcal{Q}, G^*(q,j), H^*(q,j), \mathcal{K}) > 0$ and $N > 0$ such that $n \geq N$ implies*

$$\frac{J(\mathcal{P}) - J^*}{J^*} \leq \frac{\hat{K}}{\sqrt{n}}. \tag{4.12}$$

Notably, the design method (4.10) exactly determines the $\mathcal{H}_2$ and $\mathcal{H}_\infty$ norms of the closed-loop transfer function, and so does not require the discrete time or finite time horizon approximations to compute these norms, so it does not suffer from additional suboptimality resulting from these approximations. As a result, for the grid pole selection proposed in Section 4.1, the suboptimality bound (4.12) applies exactly to (4.10), and ensures that the suboptimality converges to zero as the number of poles approaches infinity. This is the first tractable convex method for $\mathcal{H}_2/\mathcal{H}_\infty$ control with SLS in continuous time. As we will see in the numerical example in Section 4.3, even a small number of poles can often result in low suboptimality, and thus good performance, in practice.

4.3 Numerical Example

In this section, we demonstrate the proposed control synthesis method on the control of a wind turbine interfaced to the power grid via a power converter. We model the turbine and converter system using the model proposed in [17]. Let w be a vector whose components represent the frequency and voltage magnitude at the connection point, respectively, and let y represent the active and reactive power output of the converter. To improve grid performance, our goal is to design fast frequency and voltage control and to enforce decoupling between their respective control loops. To do so, we choose a desired closed-loop transfer function that we attempt to match in design, which is diagonal and whose diagonal elements are low pass filters with equal time constants. Then this can be formulated in the form of (2.2) with matrices given by

$$A = \begin{bmatrix} -11.725 & 0 & 0 & 0 & 0 \\ 0 & -60 & 7.0606 & -0.6729 & -7.9931 \\ 60 & 0 & -60 & 0 & 0 \\ 0 & 0 & 0 & -0.6667 & 0 \\ 0 & 0 & 0 & 0 & -60 \end{bmatrix}, \quad B = \begin{bmatrix} 0 & 0 \\ 0 & 0 \\ 0 & 0 \\ 0.6667 & 0 \\ 0 & 60 \end{bmatrix}, \quad \hat{B} = \begin{bmatrix} -29.3125 & 0 \\ 0 & 60.414 \\ 150 & 0 \\ 0 & 0 \\ 0 & 0 \end{bmatrix}$$

$$C = \begin{bmatrix} 0 & 0.9066 & -0.0364 & 1.0218 & 0 \\ 0 & 0.0364 & 0.9066 & -0.2406 & -1.0201 \end{bmatrix}, \; A_{\text{des}} = \begin{bmatrix} -1.4286 & \\ & -1.4286 \end{bmatrix}, \; B_{\text{des}} = \begin{bmatrix} -28.4275 & \\ & -29.2857 \end{bmatrix}, \; C_{\text{des}} = I_2.$$

For the control design, we choose $Q = I_2$, $R = 0.01 I_2$, and $\lambda = 0.5$. For the SPA pole selection $\mathcal{P}$, we set the maximum number of closed-loop poles at $l = 10$. To form $\mathcal{P}$ we first incorporate the plant poles and the poles of the desired transfer function, and the remaining poles are chosen from the grid as we discussed in Theorem 4. We solve the SDP (4.10) for the control design with the proposed hybrid state space and frequency domain method using MOSEK [2] in conjunction with YALMIP [19] in MATLAB.

The multiple input multiple output (MIMO) step responses for the desired transfer function and the solutions of the hybrid state space and frequency method are shown in Fig. 4.2, which yields almost perfect matching with the desired response. Thus, SLS with SPA in continuous time was successfully used to control a power converter for providing desired frequency and voltage regulation in the power grid.

4.4 Proofs

4.4.1 Proof of Theorem 2

The continuous-time SPA shares several features with its discrete-time counterpart. To avoid repetition, the following lemmas present useful identities for developing approxi-

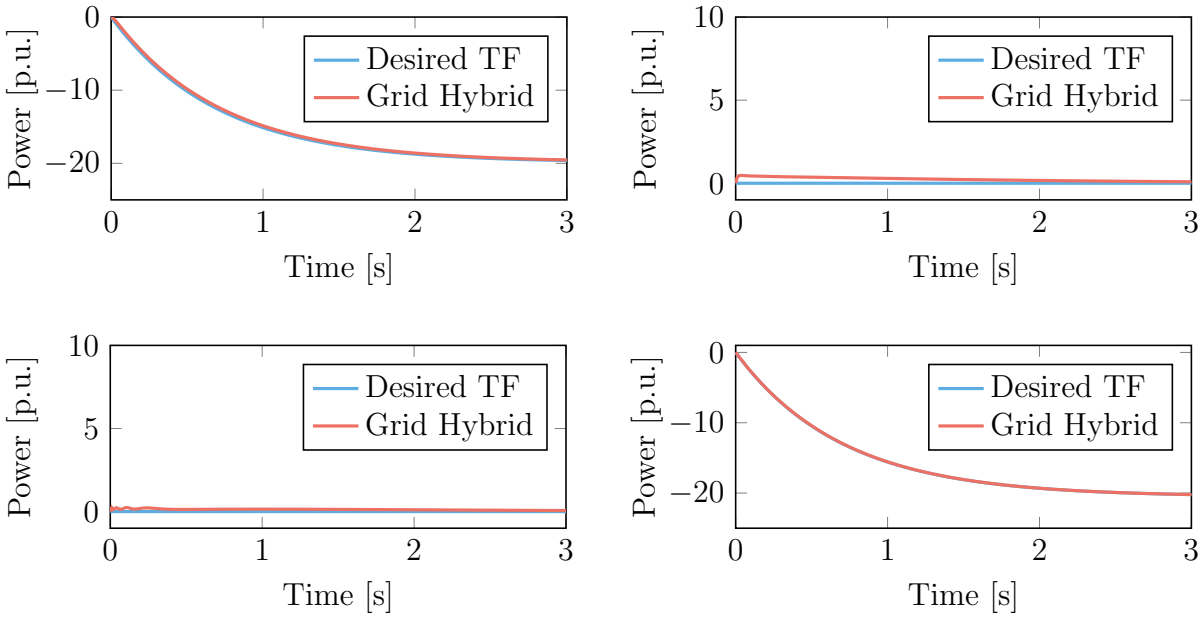

Figure 4.2: Step responses of the desired transfer function (Desired TF) and of the solutions of the hybrid domain method with grid pole selection (Grid Hybrid).

mation error bounds for a single repeated pole in the single input single output (SISO) case.

Lemma 1 *For any positive integer m, let $p_1, \ldots, p_m, q \in \mathcal{K}$, $I_m = \{1, 2, \ldots, m\}$, and $\mathcal{P} = \cup_{i=1}^m p_i$. Define the diameter of $\mathcal{K}$ is $\ell(\mathcal{K})$. Let $\hat{d}(q) = \max_i |p_i - q|$. Let s be in the imaginary axis and $s = j\omega$, $\forall \omega \in \mathbb{R}$. Then there exist constants $c_1, \ldots, c_m$ such that*

$$\begin{aligned} \left| \sum_{i=1}^{m} c_i \frac{1}{s - p_i} - \frac{1}{(s-q)^m} \right|_{s=j\omega} &\leq \frac{((|q|+2)^m - (|q|+1)^m)\ell(\mathcal{K})^{m-1}\hat{d}(q) \sum_{k=0}^{m-1} |\omega|^k}{|j\omega - q|^m \prod_{i=1}^m |j\omega - p_i|} \\ &= d \underbrace{\frac{1}{\prod_{i=1}^m |j\omega - p_i|}}_{\Delta_a} \underbrace{\frac{\sum_{k=0}^{m-1} |\omega|^k}{|j\omega - q|^m}}_{\Delta_b} \end{aligned} \tag{4.13}$$

where $d = ((|q|+2)^m - (|q|+1)^m)\ell(\mathcal{K})^{m-1}\hat{d}(q)$.

Proof of Lemma 1: Since the number of approximating poles is finite and all poles lie within a compact set $\mathcal{K}$, the approximating distance $\hat{d}(q)$ is also finite and can be bounded by the diameter of $\mathcal{K}$. We have

$$\hat{d}(q)^k = \hat{d}(q)^{k-1}\hat{d}(q) \leq \ell(\mathcal{K})^{m-1}\hat{d}(q) \tag{4.14}$$

for $k \in I_m$. It can be shown analogously that the following partial fraction decomposition holds in the s-domain with a similar derivation from [13, Proof of Lemma 3]

$$\sum_{i=1}^{m} c_i \frac{1}{s - p_i} = \frac{1}{\prod_{i=1}^m (s - p_i)} \tag{4.15}$$

where

$$c_i = \frac{1}{\prod_{\substack{j=1 \\ j \neq i}}^m (p_i - p_j)} \tag{4.16}$$

for all $i \in I_m$, which satisfies (4.15). After choosing constants $\{c_i\}_{i=1}^m$ by (4.16), to prove the claim, it suffices to show that $\left| \frac{1}{\prod_{i=1}^m (s-p_i)} - \frac{1}{(s-q)^m} \right|$ satisfies the inequality of Lemma 1. We compute

$$\frac{1}{\prod_{i=1}^m (s - p_i)} - \frac{1}{(s-q)^m} = \frac{(s-q)^m - \prod_{i=1}^m (s - p_i)}{(s-q)^m \prod_{i=1}^m (s - p_i)}. \tag{4.17}$$

Then, recalling [13, Lemma 2],

$$\left| q^m - \prod_{i=1}^{m} p_i \right| \leq \sum_{k=1}^{m} \sum_{\substack{S \subset I_m \\ |S|=k}} |q|^{m-k} \prod_{i \in S} |p_i - q| \,, \tag{4.18}$$

for all $q, \{p_i\}_{i=1}^m$ in the unit disk for the discrete case, but there is no specific reason in that proof and it can be trivially extended to the open left half plane in the continuous case. Follow the similar derivation and applying (4.18) to poles $-q$ and $\{-p_i\}_{i=1}^k$ for each set S in the sum yields

$$\begin{aligned}
\left| (s-q)^m - \prod_{i=1}^{m} (s-p_i) \right| &\overset{\text{triangle inequality}}{\leq} \sum_{k=1}^{m} |s|^{m-k} \sum_{\substack{S \subset I_m \\ |S|=k}} \left| (-q)^k - \prod_{j \in S} (-p_j) \right| \\
&\overset{\substack{s=j\omega \\ (4.18)}}{\leq} \sum_{k=1}^{m} |\omega|^{m-k} \sum_{\substack{S \subset I_m \\ |S|=k}} \sum_{i=1}^{k} \sum_{\substack{T \subset S \\ |T|=i}} |q|^{k-i} \prod_{j \in T} |p_j - q| \qquad (4.19) \\
&\overset{\substack{\text{[13, Proof of} \\ \text{Corollary 2]}}}{\leq} \sum_{k=1}^{m} |\omega|^{m-k} \binom{m}{k} \left((|q| + \hat{d}(q))^k - |q|^k \right) \\
&\overset{\substack{\text{adding} \\ \text{more terms}}}{\leq} \sum_{k=0}^{m-1} |\omega|^k \sum_{k'=1}^{m} \binom{m}{k'} \left((|q| + \hat{d}(q))^{k'} - |q|^{k'} \right) \\
&\overset{\substack{\text{[13, Proof of} \\ \text{Corollary 2]}}}{\leq} \sum_{k=0}^{m-1} |\omega|^k \sum_{k'=1}^{m} \binom{m}{k'} (|q|+1)^{m-k'} \hat{d}(q)^{k'} \\
&\overset{(4.14)}{\leq} ((|q|+2)^m - (|q|+1)^m) \ell(\mathcal{K})^{m-1} \hat{d}(q) \sum_{k=0}^{m-1} |\omega|^k. \qquad (4.20)
\end{aligned}$$

Furthermore, substituting $s = j\omega$ into the denominator of (4.17) implies $|j\omega - q|^m \prod_{i=1}^m |j\omega - p_i|$.

Note that a key distinction from the discrete-time SISO case considered in [13] lies in the fact that $s = j\omega$ is moving in the imaginary axis, which is unbounded. Consequently, the magnitude of ω in (4.19) can no longer be bounded by radius 1 of the unit circle, as was the case in the discrete-time setting.

We obtain

$$\left| \frac{1}{\prod_{i=1}^m (s-p_i)} - \frac{1}{(s-q)^m} \right| \overset{(4.20)}{\leq} \frac{((|q|+2)^m - (|q|+1)^m) \ell(\mathcal{K})^{m-1} \hat{d}(q) \sum_{k=0}^{m-1} |\omega|^k}{|j\omega - q|^m \prod_{i=1}^m |j\omega - p_i|}. \tag{4.21}$$

By regrouping (4.21), Lemma 1 can be proved. □

To derive the error bounds in Lemma 1 under the $\mathcal{H}_2/\mathcal{H}_\infty$ metrics, the next four lemmas are deployed. Lemma 2 provides even function bounds for the denominators of Δ_a and Δ_b in (4.13), facilitating the simplification of integral computations involved in the $\mathcal{H}_2$ norm. Lemma 3 presents closed-form integral expressions useful for evaluating the $\mathcal{H}_2$ norm. Lemmas 4 and 5 further decompose Δ_a and Δ_b in (4.13) respectively, using the Cauchy–Schwarz inequality to enable norm estimates.

Lemma 2 (Lowerbounds for denominators) *For any positive integer m, let $p_1, \ldots, p_m, q \in \mathbb{C}^-$ and $\omega \in \mathbb{R}$, there exist constants $0 < a, a' \leq 1$, $0 < b, b' \leq q_x^2$ such that*

$$\prod_{i=1}^{m} |j\omega - p_i| \geq (a'\omega^2 + b')^{m/2}. \tag{4.22}$$

In a special case, that is, when $p_i = q$ for all $i \in I_m$,

$$|j\omega - q|^m \geq (a\omega^2 + b)^{m/2}. \tag{4.23}$$

Proof of Lemma 2: We first prove (4.23) and (4.22) follows immediately.

By the definition of the module of complex numbers, $|j\omega - q|^m = ((\omega - q_y)^2 + q_x^2)^{m/2}$. Suppose $q_y \neq 0$, (or it is trivial by choosing $a = 1$, $b = q_x^2$.) It suffices to show that there exists an axisymmetric quadratic function as a lowerbound of $(\omega - q_y)^2 + q_x^2$, $\forall \omega \in \mathbb{R}$.

Define $f(\omega) = (\omega - q_y)^2 + q_x^2$ and $g(\omega) = a\omega^2 + b$, where a $(0 < a < 1)$, b $(0 < b < q_x^2)$ are coefficients related to q_x, q_y, to do so, one intuitive idea is to enforce $g(\omega)$ and $f(\omega)$ intersecting only in one single point (to get a better bound) and having same tangents at the point (to be a lowerbound). Assume ω^* is the intersection point of $f(\omega), g(\omega)$, it satisfies

$$q_x^2 + (\omega^* - q_y)^2 = a\omega^{*2} + b \text{ (intersection point)} \qquad \omega^* - q_y = a\omega^* \text{ (tangent equation)}$$

cancel terms and the relation between a and b can be obtained by

$$a = \frac{q_x^2 - b}{q_x^2 + q_y^2 - b}. \tag{4.24}$$

Let $b = \frac{q_x^2}{4}$, then we have $a = \frac{3q_x^2}{3q_x^2+4q_y^2}$, $\omega^* = \frac{3q_x^2+4q_y^2}{4q_y}$, which is an arbitrary choice.

Note that $f(\omega) \geq g(\omega)$ for all $\omega \in \mathbb{R}$ can be verified by

$$f(\omega) - g(\omega) = (1-a)\omega^2 - 2q_y\omega + q_y^2 + q_x^2 - b \overset{(4.24)}{=} \frac{q_y^2}{q_x^2+q_y^2-b}\left(\omega - \frac{q_x^2+q_y^2-b}{q_y}\right)^2 \geq 0$$

and (4.23) is shown.

By (4.23), there exists an lowerbound sequence $\{a_i, b_i\}_{i=1}^m$ which satisfies $|j\omega - p_i| = \sqrt{(\omega - p_i^y)^2 + (p_i^x)^2} \geq \sqrt{a_i\omega^2 + b_i}$, $\forall i \in I_m$. Therefore $\prod_{i=1}^m |j\omega - p_i| \geq (a'\omega^2 + b')^{m/2}$ where $a' = \min\{a_i\}_{i=1}^m$ and $b' = \min\{b_i\}_{i=1}^m$. □

Lemma 2 provides even functional lowerbounds for denominators of Δ_a, Δ_b, which will be meaningful for their integrals with respect to ω.

Lemma 3 (Integral formulas) *Let a, b be any positive real numbers, m be any positive integer, $n \in \{0, \ldots, 2m-1\}$. Then $I_{(m,n)}^{(a,b)} = \int_0^\infty \frac{\omega^n}{(a\omega^2+b)^m} \mathrm{d}\omega$ can be computed via the following formulas:*

1) n is even

$$I_{(m,n)}^{(a,b)} = \frac{\pi}{2} \frac{(n-1)!!(2m-n-3)!!}{(2m-2)!! b^{\frac{2m-n-1}{2}} a^{\frac{n+1}{2}}} \tag{4.25}$$

2) n is odd

$$I_{(m,n)}^{(a,b)} = \frac{\frac{n-1}{2}!}{2\prod_{i=1}^{\frac{n+1}{2}}(m-i) b^{\frac{2m-n-1}{2}} a^{\frac{n+1}{2}}} \tag{4.26}$$

In fact, no matter what parity of n, we have

$$I_{(m,n)}^{(a,b)} = \left(\frac{\pi}{2}\right)^{\mathcal{I}(n)} \frac{(n-1)!!(2m-n-3)!!}{(2m-2)!! b^{\frac{2m-n-1}{2}} a^{\frac{n+1}{2}}} \qquad \mathcal{I}(n) = \begin{cases} 1 & n \text{ is even} \\ 0 & n \text{ is odd} \end{cases} \tag{4.27}$$

Proof of Lemma 3: The main idea is to use (weak) induction on two variables m, n and calculus techniques. Ignoring the superscript (a, b) is admissible if there is no ambiguity.

1) First we prove (4.25).

1.1) When $n = 0$, we first prove

$$I_{(m,0)} = \int_0^\infty \frac{1}{(a\omega^2+b)^m} \mathrm{d}\omega = \frac{\pi}{2} \frac{(2m-3)!!}{(2m-2)!! b^{\frac{2m-1}{2}} a^{\frac{1}{2}}}$$

for all $m \geq 1$. We compute it from $m = 1$, we have

$$I_{(1,0)} = \int_0^\infty \frac{1}{a\omega^2 + b} \mathrm{d}\omega \overset{u=\frac{\sqrt{a}\omega}{\sqrt{b}}}{=} \int_0^\infty \frac{1}{\sqrt{ba}(u^2+1)} \, \mathrm{d}u = \frac{1}{\sqrt{ba}} \arctan \frac{\sqrt{a}\omega}{\sqrt{b}} \Big|_0^\infty = \frac{\pi}{2\sqrt{ba}}$$

Recall the power reduction formula,

$$\int_0^\infty \frac{1}{(ax^2+b)^m} \mathrm{d}x = \underbrace{\frac{x}{2b(m-1)\left(ax^2+b\right)^{m-1}}}_{F(x)} \Big|_0^\infty + \frac{2m-3}{2b(m-1)} \int_0^\infty \frac{1}{(ax^2+b)^{m-1}} \mathrm{d}x.$$

Since $F(\infty) - F(0) = 0$, we have

$$I_{(m,0)} = \frac{\pi}{2} \frac{(2m-3)!!}{(2m-2)!! b^{\frac{2m-1}{2}} a^{\frac{1}{2}}}.$$

1.2) Suppose $n = k$, k is an even number,

$$I_{(m,k)} = \frac{\pi}{2} \frac{(k-1)!!(2m-k-3)!!}{(2m-2)!! b^{\frac{2m-k-1}{2}} a^{\frac{k+1}{2}}} \qquad I_{(m-1,k)} = \frac{\pi}{2} \frac{(k-1)!!(2m-k-5)!!}{(2m-4)!! b^{\frac{2m-k-3}{2}} a^{\frac{k+1}{2}}}$$

hold, then to prove

$$I_{(m,k+2)} = \frac{\pi}{2} \frac{(k+1)!!(2m-k-5)!!}{(2m-2)!! b^{\frac{2m-k-3}{2}} a^{\frac{k+3}{2}}}. \tag{4.28}$$

We consider the integration by parts, i.e., $\int u\mathrm{d}v = uv - \int v\mathrm{d}u$. Let $u = \omega^{k+1}$, $v = -\frac{1}{2a(m-1)(a\omega^2+b)^{m-1}}$, $\mathrm{d}v = \frac{\omega \mathrm{d}\omega}{(a\omega^2+b)^m}$,

$$\begin{aligned}\int_0^\infty \frac{\omega^{k+2}}{(a\omega^2+b)^m} \mathrm{d}\omega &= -\frac{\omega^{k+1}}{2a(m-1)(a\omega^2+b)^{m-1}} \Big|_0^\infty + \frac{k+1}{2a(m-1)} I_{(m-1,k)} \\ &= \frac{\pi}{2} \frac{(k+1)!!(2m-k-5)!!}{(2m-2)!! b^{\frac{2m-k-3}{2}} a^{\frac{k+3}{2}}}\end{aligned}$$

and (4.28) is obtained.

2) Now we prove (4.26).

2.1) When $n = 1$,

$$I_{(m,1)} = \int_0^\infty \frac{1}{2a(a\omega^2+b)^m} \mathrm{d}(a\omega^2+b) = -\frac{1}{2a(m-1)(a\omega^2+b)^{m-1}} \Big|_0^\infty = \frac{1}{2(m-1)b^{m-1}a}.$$

2.2) Suppose $n = k$, k is an odd number,

$$I_{(m,k)} = \frac{\frac{k-1}{2}!}{2\prod_{i=1}^{\frac{k+1}{2}}(m-i)b^{\frac{2m-k-1}{2}}a^{\frac{k+1}{2}}} \qquad I_{(m-1,k)} = \frac{\frac{k-1}{2}!}{2\prod_{i=1}^{\frac{k+1}{2}}(m-1-i)b^{\frac{2m-k-3}{2}}a^{\frac{k+1}{2}}}$$

hold, then use a similar derivation of integration by parts, we have

$$I_{(m,k+2)} = \int_0^\infty \frac{\omega^{k+2}}{(a\omega^2+b)^m}\mathrm{d}\omega = \frac{k+1}{2a(m-1)}I_{(m-1,k)} = \frac{\frac{k+1}{2}!}{2\prod_{i=1}^{\frac{k+3}{2}}(m-i)b^{\frac{2m-k-3}{2}}a^{\frac{k+3}{2}}}.$$

3) Now we prove (4.27), it's straightforward to verify the equivalence when n is even, the odd case can be shown as follows,

$$\begin{aligned} I_{(m,n)} &= \frac{\frac{n-1}{2}!}{2\prod_{i=1}^{\frac{n+1}{2}}(m-i)b^{\frac{2m-n-1}{2}}a^{\frac{n+1}{2}}} = \frac{(n-1)!!}{\prod_{i=1}^{\frac{n+1}{2}}(2m-2i)b^{\frac{2m-n-1}{2}}a^{\frac{n+1}{2}}} \\ &= \frac{(n-1)!!(2m-n-3)!!}{\prod_{i=1}^{\frac{n+1}{2}}(2m-2i)(2m-n-3)!!b^{\frac{2m-n-1}{2}}a^{\frac{n+1}{2}}} = \frac{(n-1)!!(2m-n-3)!!}{(2m-2)!!b^{\frac{2m-n-1}{2}}a^{\frac{n+1}{2}}}. \end{aligned}$$

□

Lemma 3 expresses explicit integral formulas for upcoming $\mathcal{H}_2$ error bounds.

Lemma 4 *For Δ_a defined in (4.13), then there exists $c_i^* = \frac{1}{\prod_{\substack{j=1\\ j\neq i}}^{2m}(p_i^*-p_j^*)}$ follows the same definition in (4.16), where $p_i^* = p_i^y + p_i^x j$, $p_{i+m}^* = \bar{p}_i^* = p_i^y - p_i^x j$ for all $i \in I_m$, and the integral of Δ_a^4 can be computed by*

$$\int_{-\infty}^{\infty}\Delta_a^4\mathrm{d}\omega = \int_{-\infty}^{\infty}\frac{1}{\prod_{i=1}^m|j\omega-p_i|^4}\mathrm{d}\omega = \underbrace{2\pi\sum_{i=1}^m\left(\frac{|c_i^*|^2}{-p_i^x}+\sum_{k=i+1}^m 4\mathrm{Im}\left(\frac{c_i^*\bar{c}_k^*}{p_i^*-\bar{p}_k^*}\right)\right)}_{=:\alpha_{(p,q)}^m} \tag{4.29}$$

Proof of Lemma 4: We first decompose denominators of Δ_a^2 in the complex domain, and then leverage proved partial fraction decomposition to redefined poles.

$$\Delta_a^2 = \frac{1}{\prod_{i=1}^m((\omega-p_i^y)^2+(p_i^x)^2)} = \frac{1}{\prod_{i=1}^m(\omega-(p_i^y+p_i^x j))(\omega-(p_i^y-p_i^x j))}$$
$$\overset{p_i^*=p_i^y+p_i^x j}{=} \frac{1}{\prod_{i=1}^m(\omega-p_i^*)(\omega-\bar{p}_i^*)} \overset{\substack{\text{rewrite } \bar{p}_i^*\\ \text{subscript}}}{=} \frac{1}{\prod_{i=1}^{2m}(\omega-p_i^*)} \overset{(4.15)}{=} \sum_{i=1}^{2m}c_i^*\frac{1}{\omega-p_i^*} \tag{4.30}$$

where $c_i^* = \frac{1}{\prod_{\substack{j=1 \\ j\neq i}}^{2m}(p_i^* - p_j^*)}$ follows (4.16) for all $i \in I_{2m}$. Note that c_i^* and c_{i+m}^* are complex conjugate by (4.16) for all $i \in I_m$. So we can rewrite $\bar{c}_i^*$ to represent c_{i+m}^*. We also rewrite the subscript of $\bar{p}_i^*$ as p_{i+m}^* and redefine

$$\begin{aligned} p_i^* &= p_i^y + p_i^x j \quad \bar{p}_i^* = p_{i+m}^* = p_i^y - p_i^x j \\ r_i^* &= \bar{r}_i^* = \sqrt{(\omega - p_i^y)^2 + (p_i^x)^2} = \sqrt{(\omega - p_i^*)(\omega - \bar{p}_i^*)}. \end{aligned} \tag{4.31}$$

Representing complex numbers in the polar form can simplify future calculation

$$\omega - p_i^* = (\omega - p_i^y) - p_i^x j \overset{\text{Euler's identity}}{=} r_i^* e^{j\theta_i} \qquad \frac{\omega - p_i^*}{\omega - \bar{p}_i^*} = \frac{r_i^* e^{j\theta_i}}{\bar{r}_i^* e^{j(-\theta_i)}} = e^{2j\theta_i} \tag{4.32}$$

for all $i \in I_m$. Since $p_i^x < 0$ (all poles lie in the open left half plane), the imaginary part of $\omega - p_i^*$ will always be positive, the phase θ_i can be discussed by definition: 1) when $\omega > p_i^y$, it lies in the first quadrant, i.e., $\theta_i = \arctan \frac{-p_i^x}{\omega - p_i^y}$; 2) when $\omega = p_i^y$, it's in the upper imaginary axis, i.e., $\theta_i = \frac{\pi}{2}$; 3) when $\omega = p_i^y$, it's in the second quadrant, so $\theta_i = \arctan \frac{-p_i^x}{\omega - p_i^y} + \pi$. Use complementary angles property and these three occasions can be concluded as

$$\theta_i = \frac{\pi}{2} - \arctan \frac{\omega - p_i^y}{-p_i^x} \tag{4.33}$$

for all $i \in I_m$. The following property will be used in the later derivation.

Property: Suppose x, y are two complex numbers, and $\bar{x}, \bar{y}$ are their corresponding complex conjugates, then $\frac{x}{y}$ and $\frac{\bar{x}}{\bar{y}}$ are also the complex conjugate pairs.

Proof: Let $x = a + bj$, $y = c + dj$, thus $\bar{x} = a - bj$, $\bar{y} = c - dj$

$$\begin{aligned} \frac{x}{y} &= \frac{a + bj}{c + dj} = \frac{(a + bj)(c - dj)}{c^2 + d^2} = \frac{ac + bd + (bc - ad)j}{c^2 + d^2} \\ \frac{\bar{x}}{\bar{y}} &= \frac{a - bj}{c - dj} = \frac{(a - bj)(c + dj)}{c^2 + d^2} = \frac{ac + bd - (bc - ad)j}{c^2 + d^2} \end{aligned}$$

which finishes the proof of the property.

$$\Delta_a^4 = \frac{1}{\prod_{i=1}^m |j\omega - p_i|^4} \overset{(4.30)}{=} \left(\sum_{i=1}^{2m} c_i^* \frac{1}{\omega - p_i^*} \right)^2 = \sum_{i=1}^{2m} \left(\frac{(c_i^*)^2}{(\omega - p_i^*)^2} + 2 \sum_{k=i+1}^{2m} \frac{c_i^* c_k^*}{(\omega - p_i^*)(\omega - p_k^*)} \right)$$

$$= \sum_{i=1}^{2m} \left(\frac{(c_i^*)^2}{(\omega - p_i^*)^2} + 2 \sum_{k=i+1}^{2m} \frac{c_i^* c_k^*}{p_i^* - p_k^*} \left(\frac{1}{\omega - p_i^*} - \frac{1}{\omega - p_k^*} \right) \right)$$

$$= \sum_{i=1}^{2m} \frac{(c_i^*)^2}{(\omega - p_i^*)^2} + 2 \sum_{i=1}^{2m} \sum_{k=i+1}^{2m} \frac{c_i^* c_k^*}{p_i^* - p_k^*} \left(\frac{1}{\omega - p_i^*} - \frac{1}{\omega - p_k^*} \right)$$

Now we simplify the integral of square terms and product terms separately by the additivity of integrals. It's straightforward to show $(c_i^*)^2$ and $(\bar{c}_i^*)^2$ are complex conjugates since c_i^* and $\bar{c}_i^*$ are complex conjugates for all $i \in I_m$. Suppose $(c_i^*)^2 = a_i + b_i j$, and $(\bar{c}_i^*)^2 = a_i - b_i j$, where $a_i = \mathrm{Re}\left((c_i^*)^2\right), b_i = \mathrm{Im}\left((c_i^*)^2\right)$.

Since the calculus method still applies to complex numbers. The integral of the first term will be

$$\begin{aligned}
\int \sum_{i=1}^{2m} \frac{(c_i^*)^2}{(\omega - p_i^*)^2} \mathrm{d}\omega &= \sum_{i=1}^{m} \int \left(\frac{(c_i^*)^2}{(\omega - p_i^*)^2} + \frac{\overline{(c_i^*)^2}}{(\omega - \bar{p}_i^*)^2} \right) \mathrm{d}\omega = \sum_{i=1}^{m} - \left(\frac{(c_i^*)^2}{\omega - p_i^*} + \frac{\overline{(c_i^*)^2}}{\omega - \bar{p}_i^*} \right) \\
&= - \sum_{i=1}^{m} \frac{(a_i + b_i j)(\omega - \bar{p}_i^*) + (a_i - b_i j)(\omega - p_i^*)}{(\omega - p_i^*)(\omega - \bar{p}_i^*)} \\
&= - \sum_{i=1}^{m} \frac{a_i (2\omega - 2p_i^y) - 2 b_i p_i^x}{(\omega - p_i^y)^2 + (p_i^x)^2}
\end{aligned} \tag{4.34}$$

The integral of the second term will be

$$\begin{aligned}
&\int 2 \sum_{i=1}^{2m} \sum_{k=i+1}^{2m} \frac{c_i^* c_k^*}{p_i^* - p_k^*} \left(\frac{1}{\omega - p_i^*} - \frac{1}{\omega - p_k^*} \right) \mathrm{d}\omega \\
=& 2 \sum_{i=1}^{2m} \sum_{k=i+1}^{2m} \frac{c_i^* c_k^*}{p_i^* - p_k^*} (\ln(\omega - p_i^*) - \ln(\omega - p_k^*)) \\
=& 2 \left(\sum_{i=1}^{m} \sum_{k=i+1}^{m} \bullet + \sum_{i=m+1}^{2m} \sum_{k=i+1}^{2m} \bullet + \sum_{i=1}^{m} \sum_{k=m+1}^{2m} \bullet \right) \equiv 2\Sigma
\end{aligned} \tag{4.35}$$

We address Σ with two steps: 1) combine the first two terms with corresponding complex conjugate pairs and 2) take the special case out from the last term and follow the similar derivation in 1). For all $i, k \in I_m$, it's straightforward to see the coefficients $\frac{c_i^* c_k^*}{p_i^* - p_k^*}$ and $\frac{\bar{c}_i^* \bar{c}_k^*}{\bar{p}_i^* - \bar{p}_k^*}$ are complex conjugate by the property since c_i^*, $p_i^* - p_k^*$ and $\bar{c}_i^*$, $\bar{p}_i^* - \bar{p}_k^*$ are complex conjugate, respectively. Suppose $\frac{c_i^* c_k^*}{p_i^* - p_k^*} = a_{i,k} + b_{i,k} j$, and $\frac{\bar{c}_i^* \bar{c}_k^*}{\bar{p}_i^* - \bar{p}_k^*} = a_{i,k} - b_{i,k} j$, where $a_{i,k} = \mathrm{Re}\left(\frac{c_i^* c_k^*}{p_i^* - p_k^*} \right), b_{i,k} = \mathrm{Im}\left(\frac{c_i^* c_k^*}{p_i^* - p_k^*} \right)$. The first two terms $\sum_{i=1}^{m} \sum_{k=i+1}^{m} \bullet + \sum_{i=m+1}^{2m} \sum_{k=i+1}^{2m} \bullet$ can

be combined as

$$\begin{aligned}
&\sum_{i=1}^{m}\sum_{k=i+1}^{m}\frac{c_i^*c_k^*}{p_i^*-p_k^*}\ln\frac{\omega-p_i^*}{\omega-p_k^*}+\overline{\frac{c_i^*c_k^*}{p_i^*-p_k^*}}\ln\frac{\omega-\bar{p}_i^*}{\omega-\bar{p}_k^*}\\
\overset{(4.31)}{=}&\sum_{i=1}^{m}\sum_{k=i+1}^{m}a_{i,k}\ln\frac{r_i^{*2}}{r_k^{*2}}+b_{i,k}j\left(\ln\frac{\omega-p_i^*}{\omega-\bar{p}_i^*}-\ln\frac{\omega-p_k^*}{\omega-\bar{p}_k^*}\right)\\
\overset{(4.32)}{=}&\sum_{i=1}^{m}\sum_{k=i+1}^{m}a_{i,k}\ln\frac{r_i^{*2}}{r_k^{*2}}+b_{i,k}j(2j\theta_i-2j\theta_k)\\
=&\sum_{i=1}^{m}\sum_{k=i+1}^{m}a_{i,k}\ln\frac{r_i^{*2}}{r_k^{*2}}+2b_{i,k}(\theta_k-\theta_i)
\end{aligned}\tag{4.36}$$

The last term $\sum_{i=1}^{m}\sum_{k=m+1}^{2m}\bullet$ can be split into two parts classifying by $k=i+m$

$$\sum_{\substack{i=1\\k=i+m}}^{m}\frac{c_i^*c_{i+m}^*}{2p_i^xj}2j\theta_i+\sum_{i=1}^{m}\sum_{\substack{k=m+1\\k\neq i+m}}^{2m}\bullet\tag{4.37}$$

and the latter term is

$$\sum_{i=1}^{m}\sum_{\substack{k=m+1\\k\neq i+m}}^{2m}\frac{c_i^*c_k^*}{p_i^*-p_k^*}\ln\frac{\omega-p_i^*}{\omega-p_k^*}=\sum_{i=1}^{m}\sum_{k=i+1}^{m}\left(\frac{c_i^*c_{k+m}^*}{p_i^*-p_{k+m}^*}\ln\frac{\omega-p_i^*}{\omega-p_{k+m}^*}+\frac{c_k^*c_{i+m}^*}{p_k^*-p_{i+m}^*}\ln\frac{\omega-p_k^*}{\omega-p_{i+m}^*}\right)$$

We know that c_i^* and $\bar{c}_i^*$, $\bar{c}_k^*$ and c_k^* are complex conjugate. It's easy to see that $c_i^*\bar{c}_k^*$ and $c_k^*\bar{c}_i^*$ are complex conjugate. $p_i^*-\bar{p}_k^*=p_i^y-p_k^y+(p_i^x+p_k^x)j$, $p_k^*-\bar{p}_i^*=p_k^y-p_i^y+(p_k^x+p_i^x)j$, which have the same imaginary parts and opposite real parts. It can also be seen as $p_k^*-\bar{p}_i^*=-\overline{p_i^*-\bar{p}_k^*}$. By the property we know these two coefficients $\frac{c_i^*\bar{c}_k^*}{p_i^*-\bar{p}_k^*}$ and $\frac{c_k^*\bar{c}_i^*}{p_k^*-\bar{p}_i^*}$ will have the same imaginary parts, and the opposite real parts. We denote them as $\frac{c_i^*\bar{c}_k^*}{p_i^*-\bar{p}_k^*}=\alpha_{i,k}+\beta_{i,k}j$, $\frac{c_k^*\bar{c}_i^*}{p_k^*-\bar{p}_i^*}=-\alpha_{i,k}+\beta_{i,k}j$, where $\alpha_{i,k}=\mathrm{Re}\left(\frac{c_i^*\bar{c}_k^*}{p_i^*-\bar{p}_k^*}\right),\beta_{i,k}=\mathrm{Im}\left(\frac{c_i^*\bar{c}_k^*}{p_i^*-\bar{p}_k^*}\right)$.

$$\begin{aligned}
&\sum_{i=1}^{m}\sum_{k=i+1}^{m}\left(\frac{c_i^*\bar{c}_k^*}{p_i^*-\bar{p}_k^*}\ln\frac{\omega-p_i^*}{\omega-\bar{p}_k^*}+\frac{c_k^*\bar{c}_i^*}{p_k^*-\bar{p}_i^*}\ln\frac{\omega-p_k^*}{\omega-\bar{p}_i^*}\right)\\
\overset{(4.31)}{=}&\sum_{i=1}^{m}\sum_{k=i+1}^{m}\left(\alpha_{i,k}\ln\frac{r_i^{*2}}{r_k^{*2}}+\beta_{i,k}j\left(\ln\frac{\omega-p_i^*}{\omega-\bar{p}_i^*}+\ln\frac{\omega-p_k^*}{\omega-\bar{p}_k^*}\right)\right)\\
\overset{(4.32)}{=}&\sum_{i=1}^{m}\sum_{k=i+1}^{m}\alpha_{i,k}\ln\frac{r_i^{*2}}{r_k^{*2}}+\beta_{i,k}j(2j\theta_i+2j\theta_k)
\end{aligned}$$

$$= \sum_{i=1}^{m} \sum_{k=i+1}^{m} \alpha_{i,k} \ln \frac{r_i^{*2}}{r_k^{*2}} - 2\beta_{i,k}(\theta_i + \theta_k) \tag{4.38}$$

Combine (4.36)-(4.38), Σ is given by

$$\sum_{i=1}^{m} \left(\frac{c_i^* c_{i+m}^*}{p_i^x} \theta_i + \sum_{k=i+1}^{m} \left((a_{i,k} + \alpha_{i,k}) \ln \frac{r_i^{*2}}{r_k^{*2}} + 2b_{i,k}(\theta_k - \theta_i) - 2\beta_{i,k}(\theta_i + \theta_k) \right) \right) \tag{4.39}$$

So

$$\begin{aligned} \int_{-\infty}^{\infty} \Delta_a^4 \mathrm{d}\omega &= \int_{-\infty}^{\infty} \sum_{i=1}^{2m} \frac{(c_i^*)^2}{(\omega - p_i^*)^2} \mathrm{d}\omega + 2\Sigma\Big|_{-\infty}^{\infty} \\ &\overset{(4.34)}{=} -\sum_{i=1}^{m} \frac{a_i(2\omega - 2p_i^y) - 2b_i p_i^x}{(\omega - p_i^y)^2 + (p_i^x)^2}\Big|_{-\infty}^{\infty} + 2\Sigma\Big|_{-\infty}^{\infty} = 2\Sigma\Big|_{-\infty}^{\infty} \end{aligned}$$

Recall

$$\begin{aligned} \ln \frac{r_i^{*2}}{r_k^{*2}}\Big|_{-\infty}^{\infty} &\overset{(4.31)}{=} \ln \frac{(\omega - p_i^y)^2 + (p_i^x)^2}{(\omega - p_k^y)^2 + (p_k^x)^2}\Big|_{-\infty}^{\infty} = 0 \\ \theta_i\Big|_{-\infty}^{\infty} &\overset{(4.33)}{=} \frac{\pi}{2} - \arctan \frac{\omega - p_i^y}{-p_i^x}\Big|_{-\infty}^{\infty} = -\pi = \theta_k\Big|_{-\infty}^{\infty} \end{aligned}$$

for all $i, k \in I_m$. Thus

$$2\Sigma\Big|_{-\infty}^{\infty} \overset{(4.39)}{=} 2\pi \sum_{i=1}^{m} \left(\frac{|c_i^*|^2}{-p_i^x} + \sum_{k=i+1}^{m} 4\beta_{i,k} \right)$$

Taking the definition of $\beta_{i,k}$ back will finish the final result. □

Lemma 5 *Consider the expansion of* $(\sum_{k=0}^{m-1} \omega^k)^4$. *After combining like terms and reordering by increasing powers of* ω, *the coefficients of* ω^k *exhibit a symmetric, pyramid-like structure, peaking at* ω^{2m-2}. *Therefore, it suffices to consider the coefficients for* $k \in \{0, \ldots, 2m-3\}$. *The coefficients follow the formulas below:*

1) If k *is even:*

$$\left(\frac{k}{2} + 1\right)^2 + 2 \sum_{j=0}^{\frac{k}{2}} j(m - |m - 2 + j - k|). \tag{4.40}$$

2) If k is odd:

$$2\sum_{j=1}^{\frac{k+1}{2}} j(m-|m-2+j-k|).$$

Moreover, the full expansion of $(\sum_{k=0}^{m-1}\omega^k)^4$ is given by:

$$\begin{aligned}\left(\sum_{k=0}^{m-1}\omega^k\right)^4 &= \sum_{i=1}^{m-1}\Bigg\{\left[\sum_{k=2i-2}^{2m-4}\left(\left(\frac{k}{2}+1\right)^2+2\sum_{j=0}^{\frac{k}{2}} j(m-|m-2+j-k|)\right)\right]\\ &(\underbrace{\omega^k+\omega^{4m-4-k}}_{even})+2\sum_{k=2i-1}^{2m-3}\sum_{j=1}^{\frac{k+1}{2}} j(m-|m-2+j-k|)(\underbrace{\omega^k+\omega^{4m-4-k}}_{odd})\Bigg\}\\ &+\left(m^2+2\sum_{j=1}^{m-1} j^2\right)\omega^{2m-2}.\end{aligned} \tag{4.41}$$

Note that the largest coefficient corresponds to ω^{2m-2}. Regardless of the parity of m, the power $2m-2$ is always even, consistent with the even-index formula (4.40). Since ω^{2m-2} has no symmetric counterpart under the transformation $k \mapsto 4m-4-k$, it remains as an isolated term.

For both even and odd k, the coefficients can be unified using the indicator function $\mathcal{I}(k)$, defined to be 1 when k is even and 0 otherwise. Let $\Gamma_m^k = \left(\frac{k}{2}+1\right)^2\mathcal{I}(k)+2\sum_{j=1}^{\lfloor (k+1)/2\rfloor} j(m-|m-2+j-k|)$. Then the expansion in (4.41) can be compactly expressed as

$$\Gamma_m^{2m-2}\omega^{2m-2}+\sum_{k=0}^{2m-3}\Gamma_m^k(\omega^k+\omega^{4m-4-k}). \tag{4.42}$$

Proof of Lemma 5: First, we show that the coefficients of ω^k and ω^{4m-4-k} are equal for all $k \in \{0,\dots,2m-3\}$. This symmetry allows us to focus only on ω^k for k in that range.

We begin by considering the square of the sum

$$\left(\sum_{k=0}^{m-1}\omega^k\right)^2 = \sum_{i=0}^{m-1}(i+1)\omega^i+\sum_{j=m}^{2m-2}(2m-1-j)\omega^j \tag{4.43}$$

$$=\sum_{i=0}^{m-2}(i+1)(\omega^i+\omega^{2m-2-i})+m\omega^{m-1}\equiv p(\omega). \tag{4.44}$$

It is straightforward to see from (4.44) that the coefficients are symmetric about ω^{m-1}, and thus $(\sum_{k=0}^{m-1}\omega^k)^4 = (p(\omega))^2$. To facilitate further analysis, we write $p(\omega)$ explicitly:

$$a_0\omega^0 + a_1\omega^1 + \ldots + a_{m-2}\omega^{m-2} + \boxed{a_{m-1}\omega^{m-1}} + a_m\omega^m + \ldots + a_{2m-3}\omega^{2m-3} + a_{2m-2}\omega^{2m-2}$$

where $a_0 = a_{2m-2}, a_1 = a_{2m-3}, \ldots, a_{m-2} = a_m$. Recall the identity $\left(\sum_{i=1}^n x_i\right)^2 = \sum_{i=1}^n x_i^2 + \sum_{j\neq i} x_i x_j$, which tells us the odd powers of ω result only from cross-product terms $a_i a_j \omega^{i+j}$ with $i \neq j$, whereas even powers come from both cross-product and square terms.

Now, fix an odd $k \in \{0, \ldots, 2m-3\}$. Any term contributing to ω^k in $p(\omega)^2$ must be of the form $a_i a_j \omega^{i+j}$ with $i + j = k$, while the corresponding term for ω^{4m-4-k} is

$$a_{2m-2-i}a_{2m-2-j}\omega^{4m-4-k} = a_i a_j \omega^{4m-4-k}$$

using the symmetry of the a coefficients.

Now consider even $k \in \{0, \ldots, 2m-3\}$. Cross-product terms follow the same argument, and additionally we include square terms of the form $a_{k/2}^2\omega^k$. It's straightforward to see that $a_{k/2}^2$ is equal to $a_{(4m-4-k)/2}^2$. Therefore, in all cases, the coefficients of ω^k and ω^{4m-4-k} are equal for every $k \in \{0, \ldots, 2m-3\}$.

Then consider the coefficient of ω^k in the expansion of $(\sum_{k=0}^{m-1}\omega^k)^4$, where $k \in \{0, \ldots, 2m-3\}$.

When k is even, the square term in (4.40) clearly originates from squaring ω^i in (4.43) when $i = k/2$, yielding the contribution $(k/2+1)^2$. To account for the product terms, we consider the condition $m-2+j-k \geq 0$, i.e., $j \geq k-m+2$, and define $k_1 = \max\{0, k-m+2\}$. Then, the product term contributes

$$2\sum_{j=0}^{k/2} j(m - |m-2+j-k|) = 2\left(\sum_{j=0}^{k_1} j(2m-2+j-k) + \sum_{j=k_1+1}^{k/2} j\,(2-j+k)\right)$$

if $k \leq m-2$, then $k_1 = 0$. Note (4.43) can also be written as $(\sum_{k=0}^{m-1}\omega^k)^2 = \sum_{i=0}^{m-2}(i+1)\omega^i + \sum_{j=m-1}^{2m-2}(2m-1-j)\omega^j$. The product terms will only come from multiplying two (different) ω^i from $\sum_{i=0}^{m-2}(i+1)\omega^i$. The coefficient of the product term of ω^k is

$$2\sum_{i=0}^{k/2-1}(i+1)(1-i+k)\omega^{i+k-i} = 2\sum_{j=1}^{k/2} j\,(2-j+k)\,\omega^k.$$

When $k > m-2$, then $k_1 \geq 1$, and the product terms include some ω^j terms beyond those in the previous case. However, it is impossible to obtain a square term since the maximum

even k is $2m-4$. The product terms involving ω^i and ω^j fall into two categories. For $i \in \{0,\dots,k_1-1\}$, we have $k-i \geq m-1$, so the contribution is $2\sum_{i=0}^{k_1-1}(i+1)(2m-1-(k-i))$. For $i \in \{k_1,\dots,k/2-1\}$, both ω^i and ω^{k-i} lie in the lower part of the expansion, yielding $2\sum_{i=k_1}^{k/2-1}(i+1)(1-i+k)$.

Thus, the total coefficient of the product term is

$$2\sum_{i=0}^{k_1-1}(i+1)(2m-1-(k-i)) + 2\sum_{i=k_1}^{k/2-1}(i+1)(1-i+k)$$
$$= 2\left(\sum_{j=0}^{k_1} j(2m-2+j-k) + \sum_{j=k_1+1}^{k/2} j\,(2-j+k)\right).$$

By adding the square term, the full coefficient of ω^k when k is even is proved.

For odd k, the analysis simplifies: there is no square term, and the product contribution follows the same recipe as above, making it a degenerate case of the even case. □

Now we can derive an upper bound for $\int_{-\infty}^{\infty}\Delta_b^4 \mathrm{d}\omega$

$$\begin{aligned}\int_{-\infty}^{\infty}\Delta_b^4\mathrm{d}\omega &\overset{(4.23)}{\leq} \int_{-\infty}^{\infty}\frac{(\sum_{k=0}^{m-1}|\omega|^k)^4}{(a\omega^2+b)^{2m}}\mathrm{d}\omega = 2\int_0^{\infty}\frac{(\sum_{k=0}^{m-1}\omega^k)^4}{(a\omega^2+b)^{2m}}\mathrm{d}\omega \\ &\overset{(4.42)}{\underset{(4.27)}{=}} 2\left(\Gamma_m^{2m-2}I_{(2m,2m-2)}^{(a,b)} + \sum_{k=0}^{2m-3}\Gamma_m^k\left(I_{(2m,k)}^{(a,b)} + I_{(2m,4m-4-k)}^{(a,b)}\right)\right) \equiv \beta_{p,q}^m.\end{aligned} \tag{4.45}$$

Corollary 3 provides an approximation error bound for a single repeated pole in the SISO case.

Corollary 3 *Let $p_1,\dots,p_m,q \in \mathcal{K}$, and $\mathcal{P} = \cup_{i=1}^m p_i$, let $\hat{d}(q) = \max_i|p_i-q|$. Let s be in the imaginary axis and $s = j\omega$, $\omega \in \mathbb{R}$. Let $\bullet \in \{2,\infty\}$. Then there exist constants $c_1,\dots,c_m$ such that*

$$\left\|\sum_{i=1}^m c_i\frac{1}{s-p_i} - \frac{1}{(s-q)^m}\right\|_{\mathcal{H}_\bullet} \leq k_\bullet^{(p,q,m)}\hat{d}(q). \tag{4.46}$$

Proof of Corollary 3: We first consider the $\mathcal{H}_2$ case

$$\left\|\sum_{i=1}^m c_i\frac{1}{s-p_i} - \frac{1}{(s-q)^m}\right\|_{\mathcal{H}_2} \overset{(4.13)}{\underset{\text{c.s.}}{\leq}} d\sqrt{\frac{1}{2\pi}\int_{-\infty}^{\infty}\Delta_a^2\Delta_b^2\mathrm{d}\omega} \overset{\text{c.s.}}{\leq} d\frac{1}{\sqrt{2\pi}}\left(\int_{-\infty}^{\infty}\Delta_a^4\mathrm{d}\omega\int_{-\infty}^{\infty}\Delta_b^4\mathrm{d}\omega\right)^{\frac{1}{4}}$$

$$\overset{(4.29)}{(4.45)}{\leq} \frac{(\alpha_{(p,q)}^m \beta_{(p,q)}^m)^{\frac{1}{4}}((|q|+2)^m - (|q|+1)^m)\ell(\mathcal{K})^{m-1}}{\sqrt{2\pi}} \hat{d}(q) \equiv k_2^{(p,q,m)} \hat{d}(q).$$

To analyze the $\mathcal{H}_\infty$ norm, we first observe that the supremum of Δ_b is invariant under sign reversal of q_y. Let $\Delta_b(q_y^+, \omega)$ and $\Delta_b(q_y^-, \omega)$ denote the values of Δ_b for $q_y > 0$ and $q_y < 0$, respectively. Then

$$\begin{aligned}\Delta_b(q_y^-, \omega) &= \frac{\sum_{k=0}^{m-1} |\omega|^k}{((\omega - q_y^-)^2 + q_x^2)^{m/2}} = \frac{\sum_{k=0}^{m-1} |\omega|^k}{((\omega + q_y^+)^2 + q_x^2)^{m/2}} \\ &= \frac{\sum_{k=0}^{m-1} |-\omega|^k}{((-\omega - q_y^+)^2 + q_x^2)^{m/2}} = \Delta_b(q_y^+, -\omega).\end{aligned}$$

For any $\tilde{q}_y^- < 0$, we have $\Delta_b(\tilde{q}_y^-, \omega) = \Delta_b(\tilde{q}_y^+, -\omega)$ where $\tilde{q}_y^+ = -\tilde{q}_y^-$. Thus $\sup_{\omega\in\mathbb{R}} \Delta_b(\tilde{q}_y^-, \omega) = \sup_{\omega\in\mathbb{R}} \Delta_b(\tilde{q}_y^+, \omega)$.

Without loss of generality, we assume $q_y > 0$, then

$$\|\cdot\|_{\mathcal{H}_\infty} \overset{(4.13)}{\leq} d \sup_{\omega\in\mathbb{R}} \Delta_a \Delta_b \overset{\text{c.s.}}{\leq} d \frac{1}{\prod_{i=1}^m (-p_i^x)} \sup_{\omega\in\mathbb{R}} \Delta_b. \tag{4.47}$$

To show that the maximum of Δ_b occurs for $\omega > 0$, we rely on two observations. First, for any $\tilde{\omega} > 0$, we have $\Delta_b(q_y, \tilde{\omega}) > \Delta_b(q_y, -\tilde{\omega})$, since the numerator $\sum_{k=0}^{m-1} |\tilde{\omega}|^k$ remains unchanged under sign reversal, while the denominator increases due to the inequality $(-\tilde{\omega} - q_y)^2 + q_x^2 > (\tilde{\omega} - q_y)^2 + q_x^2$. Second, there exists at least one positive value $\tilde{\omega}^* = \frac{q_y}{2}$ such that $\Delta_b(q_y, \tilde{\omega}^*) > \Delta_b(q_y, 0)$, because

$$\frac{1}{(q_x^2 + q_y^2)^{m/2}} < \frac{\sum_{k=0}^{m-1} \left(\frac{q_y}{2}\right)^k}{\left(\left(\frac{q_y}{2}\right)^2 + q_x^2\right)^{m/2}}.$$

Combine with the fact that $\lim_{\omega\to\infty} \Delta_b = 0$ and the continuity of Δ_b, it follows that the supremum is attained over positive domain

$$\sup_{\omega\in\mathbb{R}} \Delta_b = \sup_{\omega\in\mathbb{R}_+} \Delta_b = \max_{\omega\in\mathbb{R}_+} \Delta_b. \tag{4.48}$$

We now focus on analyzing the maximum of the function

$$h(\omega) = \frac{\sum_{k=0}^{m-1} \omega^k}{((\omega - q_y)^2 + q_x^2)^{m/2}} = \frac{1 - \omega^m}{(1-\omega)((\omega - q_y)^2 + q_x^2)^{m/2}}$$

for $\omega > 0$ and $m \geq 1$. Our goal is to estimate the maximum of this function by analyzing the roots of its derivative $h'(\omega)$. Differentiating, we obtain

$$h'(\omega) = \frac{((m-1)\omega^m - m\omega^{m-1} + 1)((\omega - q_y)^2 + q_x^2)}{((\omega - q_y)^2 + q_x^2)^{m/2+1}} - \frac{(1-\omega^m)(1-\omega)m(\omega - q_y)}{((\omega - q_y)^2 + q_x^2)^{m/2+1}}.$$

To identify the critical points, we set $h'(\omega) = 0$, leading to the equation

$$\begin{aligned} &\omega^{m+2} + (m-2)q_y\omega^{m+1} - ((m-1)r + mq_y)\omega^m - mq_y \\ &+mr\omega^{m-1} - (m+1)\omega^2 + (mq_y + m + 2q_y)\omega - r = 0 \end{aligned}$$

where $r = q_x^2 + q_y^2$. Denote the coefficient of ω^i in this polynomial by a_i. Instead of finding the precise solutions for $m > 2$, we use Cauchy's root bound, which is sharper than Lagrange's bound in this situation and gives an upper bound for the magnitude of any root as $\hat{\omega} = 1 + \max_{i<m+2} |a_i| =$

$$\begin{cases} 1 + \max\{(m-1)r + mq_y, mr, \\ \qquad m+1, mq_y + m + 2q_y\}, & m \geq 2 \\ 1 + \max\{2, 3q_y + 1, r + q_y\}, & m = 1 \end{cases} \tag{4.49}$$

Using this bound $\hat{\omega}$, the $\mathcal{H}_\infty$ norm error can be shown as

$$\left\| \sum_{i=1}^{m} c_i \frac{1}{s - p_i} - \frac{1}{(s-q)^m} \right\|_{\mathcal{H}_\infty} \leq d \frac{\max_{\omega \in (0,\hat{\omega}]} h(\omega)}{\prod_{i=1}^{m}(-p_i^x)} \leq \frac{d \sum_{k=0}^{m-1} \hat{\omega}^k}{\prod_{i=1}^{m}(-p_i^x)(-q_x)^m} \equiv k_\infty^{(p,q,m)} \hat{d}(q).$$

Note that $\sup_{\omega \in \mathbb{R}} \Delta_b(\tilde{q}_y^-, \omega) = \sup_{\omega \in \mathbb{R}} \Delta_b(\tilde{q}_y^+, \omega)$ showed first. Therefore, when $q_y < 0$, we can simply apply the bound by replacing q_y with $-q_y$ in the expression for $\hat{\omega}$. The case $q_y = 0$ is naturally included as a degeneration of this bound. □

Theorem 2 extends the approximation error bound to an arbitrary number of (possibly repeated) poles and to the MIMO case.

Proof of Theorem 2: Both the $\mathcal{H}_2$ and $\mathcal{H}_\infty$ error bounds in the MIMO case follow a similar procedure to the $\mathcal{H}_\infty$ norm derivation in [13, Proof of Theorem 1], by appropriately substituting the error bounds from the SISO case as given in Corollary 3. It is important to note that, in order to ensure the approximating transfer function has real coefficients, Assumption A4 requiring symmetry of the approximating complex conjugate poles must be satisfied. □

4.4.2 Proof of Theorem 4

The following corollary determines the minimum distance from any $q \in \mathcal{K}$ to the closest $p \in \mathcal{P}_n$.

Corollary 4 *Suppose the pole selection from the grid is constructed by Theorem 4. Then, for any $z \in \mathcal{K}$, $d(z, \mathcal{P}_n)$ will be bounded by*

$$d_{\min} = l\sqrt{\frac{5}{2} + \lceil \tan\theta \rceil^2 + 3\lceil \tan\theta \rceil} \tag{4.50}$$

Proof of Corollary 4: If z lies in the rectangular region, then all grid points are centers of the corresponding cells, and the minimum distance is given by $d_4 = \frac{\sqrt{2}}{2}l$ (see Fig. 4.1c).

If z lies within the triangular regions, we adopt a cell-based partitioning strategy. Specifically, cells intersecting the hypotenuse define a new bounding region, while the remaining poles located beneath this region are used to ensure the entire triangular region is covered. To better illustrate this classification and the associated distances, Fig. 4.1d provides an overview of the stair-step structure caused by row discontinuities. We divide the cells into three distinct classes, each serving a unique role in bounding the minimum geometric distance:

i) Unsafe cells (red-framed region): These intersect the hypotenuse and are excluded from pole placement to simplify the analysis. Even if a grid node lies exactly on the hypotenuse, the cell to its upper right is still considered unsafe (see the red intersection point in Fig. 4.1d). When θ is small or l is large (e.g., Fig. 4.3a), the triangle may only intersect one row or at most one additional cell. In such cases, we borrow top-row poles from the rectangle to cover this region with a bound $d_5 = \frac{\sqrt{26}}{2}l$.

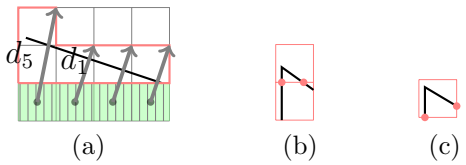

Figure 4.3: Some special cases.

ii) Border cells in purple are the cells below unsafe cells that contact the sides of unsafe cells. They can be classified as two different groups by the number of bordering sides.

a) corner cells (northeast-hatch): These border two sides of unsafe cells and cover the stair-step discontinuities, with distance bound $d_2 = \frac{3\sqrt{2}}{2}l$. A special corner cell (crosshatched)

closest to the acute vertex of the triangle, indicated by a magenta arrow in Fig. 4.1d, yields a key distance d_3 to cover the topleft unsafe cells.

When $\theta \leq \frac{\pi}{4}$, there can be at most two unsafe cells directly above this special corner cell, depending on whether the same side hypotenuse and the vertical leg intersect (see Fig. 4.3b) or not (see Fig. 4.3c). In both cases, we conservatively apply $d_5 = \frac{\sqrt{26}}{2}l$ as an upper bound.

When $\theta > \frac{\pi}{4}$, the maximum number of unsafe cells above the special corner cell increases to $\lceil \tan\theta \rceil + 1$. The distance d_3 from this corner cell to the farthest such unsafe cell (i.e., near the acute vertex) can be calculated geometrically as $\sqrt{(\frac{l}{2} + (\lceil \tan\theta \rceil + 1)l)^2 + (\frac{l}{2})^2}$, and we have

$$d_3 = \begin{cases} d_5 = \dfrac{\sqrt{26}}{2}l, & 0 < \theta \leq \dfrac{\pi}{4} \\ l\sqrt{\dfrac{5}{2} + \lceil \tan\theta \rceil^2 + 3\lceil \tan\theta \rceil}, & \dfrac{\pi}{4} < \theta < \dfrac{\pi}{2} \end{cases}$$

Note that the latter expression also holds for the first case and $d_3 \geq d_5$.

b) pavement cells (vertical lines): These are adjacent to only one side of unsafe cells and serve to cover the row immediately above, with a bound $d_1 = \frac{\sqrt{10}}{2}l$. The top-right cells in the rectangular region also act as pavement cells, covering the lower-right unsafe zone with the same radius.

iii) Safe cells (blue): These cells lie below all border cells and function like standard rectangular cells, with a minimum distance bound of $d_4 = \frac{\sqrt{2}}{2}l$.

This geometric decomposition ensures that every point in the trapezoidal region lies within a distance $d_{\min}$ under this grid pole selection $\mathcal{P}_n$. □

Proof of Theorem 4: Let $S \in \frac{1}{s}\mathcal{RH}_\infty$ and let $\mathcal{Q}$ be the poles of S. The proof considers the grid pole selection $\mathcal{P}$ in Theorem 4. For any pole $q \in \mathcal{Q}$, the analysis above shows that the distance from q to its closest pole in the grid pole selection $\mathcal{P}$ is at most $d_{\min}$. By traversing along a path of neighboring poles in the grid, the cumulative increase in distance from q to each successive pole is bounded by increments of at most l, due to the grid regularity and the triangle inequality. That is, the m_q closest grid points to q are all within a distance of $(m_q - 1)l + d_{\min}$ from q.

Moreover, the fact that the number of selected poles from grid $n(l)$ is upperbounded by the number of all cells in the entire $n_b l \times n_a l$ grid yields

$$n(l) \leq n_b \times n_a = (\lfloor 2k_a/l \rfloor + 1)(\lfloor 2k_b/l \rfloor + 1) \leq (2k_a/l + 1)(2k_b/l + 1)$$

$$0 \geq (n(l)-1)l^2 - 2(k_a+k_b)l + 4k_ak_b,$$

which leads to an upperbound on l

$$0 < l \leq \frac{k_a + k_b + \sqrt{(k_a-k_b)^2 + 4k_ak_bn(l)}}{n(l)-1}. \tag{4.51}$$

At the end of the proof, we characterize the worst case approximating distance for grid pole selection. For any q lying in the compact set $\mathcal{K}$, suppose $p_{\hat{k}}$ and $p_{\hat{i}}$ are the closest and furthest poles in the collection of approximating poles $\mathcal{P}_{n(l)}(q)$ respectively, then the distance from $p_{\hat{k}}$ to $p_{\hat{i}}$ will be less than or equal to $(m_q-1)l$ since each selected pole will have at least one neighboring pole in terms of l distance. Thus

$$\begin{aligned}\hat{d}(q) = \max_{p\in\mathcal{P}_{n(l)}(q)} |p-q| = d\left(q, p_{\hat{i}}\right) &\leq d(q, p_{\hat{k}}) + d(p_{\hat{k}}, p_{\hat{i}}) \\ &\overset{\text{Corollary 4}}{\leq} d_{\min} + (m_q-1)l.\end{aligned}$$

Hence, the worst case approximation error over $\mathcal{Q}$ satisfies $D(\mathcal{P}_m) = \max_{q\in\mathcal{Q}} \hat{d}(q) \leq d_{\min} + (m_{\max}-1)l$. As $(m_q-1)l + d_{\min}$ is bounded by a constant times $\frac{1}{\sqrt{n(l)}}$ by (4.51), this provides a bound on $D(\mathcal{P})$. □

Proof of Corollary 1: By Theorem 4, $\{p_n\}_{n=1}^{\infty}$ is a sequence of poles with geometric convergence rate $\frac{1}{n^{1/2}}$. Thus, the result follows from Theorem 3. □

4.4.3 Proof of Theorem 6

The key technical result required to prove Theorem 6 is Lemma 6, which extends the approximation error bounds of Theorem 2 to bound the error between a feasible solution (Φ_u, Φ_x) of (2.4) and the optimal solution (Φ_u^*, Φ_x^*) of (2.3).

Lemma 6 *let (Φ_x^*, Φ_u^*) denote the optimal solution to (2.3). Then there exist $\Phi_x, \Phi_u \in \frac{1}{s}\mathcal{RH}_\infty$ which are a feasible solution to (2.4), and constants $K_\infty^u, K_2^u, K_\infty^x, K_2^x > 0$, such that*

$$\begin{aligned}\|\Phi_u - \Phi_u^*\|_{\mathcal{H}_\infty} &\leq K_\infty^u D(\mathcal{P}), & \|\Phi_u - \Phi_u^*\|_{\mathcal{H}_2} &\leq K_2^u D(\mathcal{P}) \\ \|\Phi_x - \Phi_x^*\|_{\mathcal{H}_\infty} &\leq K_\infty^x D(\mathcal{P}), & \|\Phi_x - \Phi_x^*\|_{\mathcal{H}_2} &\leq K_2^x D(\mathcal{P}).\end{aligned}$$

Before presenting the proof of Lemma 6, we first establish several supporting lemmas.

Lemma 7 *Let k be any integer, m a nonnegative integer, and s any complex number. Let $p_1, \ldots, p_m, q \in \mathcal{K}$. Denote the diameter of $\mathcal{K}$ as $\ell(\mathcal{K})$. Let $\hat{d}(q) = \max_i |p_i - q|$, then there exists a function $f(s)$ such that*

$$\left| \frac{(s-q)^k}{\prod_{i=1}^m (s-p_i)} - (s-q)^{k-m} \right| \leq f(s)\hat{d}(q). \tag{4.52}$$

If m is a nonnegative integer, k is any integer satisfying $m \geq k$ when m is positive or $m > k$ when $m = 0$. Let $\delta = \min\{|\mathrm{Re}(p_i)|\}_{i=1}^m > 0$ and $\eta = |\mathrm{Re}(q)| > 0$. If s lies on the imaginary axis then $s = j\omega$, $\omega \in \mathbb{R}$. If not, suppose $d(\{p_i\}_{i=1}^m, s) \geq \delta > 0$ and $d(q, s) \geq \eta > 0$. Then there exists $K > 0$ such that

$$\left| \frac{(s-q)^k}{\prod_{i=1}^m (s-p_i)} - (s-q)^{k-m} \right| \leq K\hat{d}(q). \tag{4.53}$$

There is a stronger inequality which will be useful to calculate the $\mathcal{H}_2$ upperbound later,

$$\left\| \frac{|s-q|^k}{\prod_{i=1}^m |s-p_i|} - \frac{1}{|s-q|^{m-k}} \right\|_{\mathcal{H}_2} \leq K_{(m,m-k)}^{(p,q)} \hat{d}(q). \tag{4.54}$$

Proof of Lemma 7: We compute

$$\begin{aligned}
\left| \frac{(s-q)^k}{\prod_{i=1}^m (s-p_i)} - (s-q)^{k-m} \right| &= \frac{|(s-q)^m - \prod_{i=1}^m (s-p_i)|}{|(s-q)^{m-k} \prod_{i=1}^m (s-p_i)|} \\
&\overset{(4.20)}{\leq} \underbrace{\frac{((|q|+2)^m - (|q|+1)^m)\ell(\mathcal{K})^{m-1} \sum_{h=0}^{m-1} |s|^h}{|s-q|^{m-k} \prod_{i=1}^m |s-p_i|}}_{f(s)} \hat{d}(q)
\end{aligned}$$

and (4.52) is proved.

If $s = j\omega$, and m, k follow the assumptions,

$$\begin{aligned}
f(s) &= \frac{((|q|+2)^m - (|q|+1)^m)\ell(\mathcal{K})^{m-1}}{|j\omega - q|^{m-k}} \frac{\sum_{h=0}^{m-1} |\omega|^h}{\prod_{i=1}^m |j\omega - p_i|} \\
&\overset{(4.22)}{\leq} \frac{((|q|+2)^m - (|q|+1)^m)\ell(\mathcal{K})^{m-1}}{(-q_x)^{m-k}} \frac{\sum_{h=0}^{m-1} |\omega|^h}{(a'\omega^2 + b')^{m/2}}.
\end{aligned}$$

Recall the similar analysis for $\mathcal{H}_\infty$ norm in the proof of Corollary 3, here the denominator is an even function, thus we only need to consider the supremum when ω is positive. Then

$$\frac{\sum_{h=0}^{m-1} \omega^h}{(a'\omega^2 + b')^{m/2}} = \frac{\sum_{h=0}^{m-1} \hat{\omega}^h}{a'^{\frac{m}{2}} (\hat{\omega}^2 + b'/a')^{\frac{m}{2}}} \leq \frac{\sum_{h=0}^{m-1} \hat{\omega}^h}{b'^{\frac{m}{2}}}$$

where $\hat{\omega} = 1+\max\{m+1, mb'/a'\}$ from (4.49), by setting $K = \frac{((|q|+2)^m-(|q|+1)^m)\ell(\mathcal{K})^{m-1}\sum_{h=0}^{m-1}\hat{\omega}^h}{(-q_x)^{m-k}b'^{\frac{m}{2}}}$, when $s = j\omega$, otherwise $\frac{((|q|+2)^m-(|q|+1)^m)\ell(\mathcal{K})^{m-1}\sum_{h=0}^{m-1}|s|^h}{\eta^{m-k}\delta^m}$, and (4.53) is proved.

By (4.52), we obtain

$$\left\|\frac{|s-q|^k}{\prod_{i=1}^m|s-p_i|}-\frac{1}{|s-q|^{m-k}}\right\|_{\mathcal{H}_2} \overset{(4.52)}{\leq} \hat{d}(q)((|q|+2)^m-(|q|+1)^m)\ell(\mathcal{K})^{m-1} \left\|\frac{1}{|j\omega-q|^{m-k}}\frac{\sum_{h=0}^{m-1}|\omega|^h}{\prod_{i=1}^m|j\omega-p_i|}\right\|_{\mathcal{H}_2}$$

Therefore, it suffices to analyze the $\mathcal{H}_2$ norm of the last expression and subsequently multiply it by the remaining terms. When $m > k$ and $m \geq 1$

$$\begin{aligned}\left\|\frac{1}{|j\omega-q|^{m-k}}\frac{\sum_{h=0}^{m-1}|\omega|^h}{\prod_{i=1}^m|j\omega-p_i|}\right\|_{\mathcal{H}_2} &\overset{(4.22)}{\leq} \sqrt{\frac{1}{2\pi}\int_{-\infty}^{\infty}\frac{1}{|j\omega-q|^{2m-2k}}\frac{(\sum_{h=0}^{m-1}|\omega|^h)^2}{(a'\omega^2+b')^m}\mathrm{d}\omega} \\ &\overset{\text{c.s.}}{\leq} \frac{1}{\sqrt{2\pi}}\sqrt[4]{\int_{-\infty}^{\infty}\frac{1}{|j\omega-q|^{4m-4k}}\mathrm{d}\omega\int_{-\infty}^{\infty}\frac{(\sum_{h=0}^{m-1}\omega^h)^4}{(a'\omega^2+b')^{2m}}\mathrm{d}\omega} \\ &\overset{(4.25)}{\leq} \frac{1}{\sqrt{2\pi}}\left(2I^{(1,q_x^2)}_{(2m-2k,0)}\right)^{\frac{1}{4}}\left(2\int_0^{\infty}\frac{(\sum_{h=0}^{m-1}\omega^h)^4}{(a'\omega^2+b')^{2m}}\mathrm{d}\omega\right)^{\frac{1}{4}} \\ &\overset{\substack{(4.42)\\(4.27)}}{\leq} \frac{1}{\sqrt{\pi}}\left(I^{(1,q_x^2)}_{(2m-2k,0)}\left(\Gamma_m^{2m-2}I^{(a',b')}_{(2m,2m-2)}\right.\right. \\ &\quad \left.\left.+\sum_{k=0}^{2m-3}\Gamma_m^k\left(I^{(a',b')}_{(2m,k)}+I^{(a',b')}_{(2m,4m-4-k)}\right)\right)\right)^{\frac{1}{4}} = K'^{(p,q)}_{(m,m-k)}\end{aligned}$$

where a' and b' are defined in Lemma 2. When $m = k \geq 1$,

$$\begin{aligned}\left\|\frac{1}{|j\omega-q|^{m-k}}\frac{\sum_{h=0}^{m-1}|\omega|^h}{\prod_{i=1}^m|j\omega-p_i|}\right\|_{\mathcal{H}_2} &\overset{(4.22)}{\leq} \sqrt{\frac{1}{\pi}\int_0^{\infty}\frac{(\sum_{h=0}^{m-1}\omega^h)^2}{(a'\omega^2+b')^m}\mathrm{d}\omega} \\ &\overset{(4.44)}{=} \sqrt{\frac{1}{\pi}\int_0^{\infty}\frac{\sum_{i=0}^{m-2}(i+1)(\omega^i+\omega^{2m-2-i})+m\omega^{m-1}}{(a'\omega^2+b')^m}\mathrm{d}\omega} \\ &\overset{(4.27)}{=} \sqrt{\frac{\sum_{i=0}^{m-2}(i+1)(I^{(a',b')}_{(m,i)}+I^{(a',b')}_{(m,2m-2-i)})+mI^{(a',b')}_{(m,m-1)}}{\pi}}\end{aligned}$$

$$\equiv K'^{(p,q)}_{(m,0)}.$$

When $m = 0 > k$,

$$\left\| \frac{1}{|j\omega - q|^{m-k}} \right\|_{\mathcal{H}_2} \overset{(4.25)}{=} \sqrt{\frac{1}{\pi} I^{(1,q_x^2)}_{(2m-2k,0)}} \equiv K'^{(p,q)}_{(0,-k)}.$$

Define $K^{(p,q)}_{(m,m-k)} = K'^{(p,q)}_{(m,m-k)}((|q|+2)^m - (|q|+1)^m)\ell(\mathcal{K})^{m-1}$, and the upperbound in (4.54) is found. □

Corollary 5 will help bound the error between the optimal and approximating transfer functions in terms of $D(\mathcal{P})$.

Corollary 5 *Let k be a nonnegative integer, m a positive integer. Let s lie on the imaginary axis and $s = j\omega$, $\forall \omega \in \mathbb{R}$ and $q, \lambda, p_1, \ldots, p_m \in \mathcal{K}$ with $d(\lambda, \{p_i\}_{i=1}^m) \geq \delta > 0$ and $d(\lambda, q) \geq \eta > 0$. Denote the diameter of $\mathcal{K}$ as $\ell(\mathcal{K})$. Choose constants c_{p_i} as in (4.16). Then there exists $K > 0$ such that*

$$\left\| \sum_{i=1}^m c_{p_i} (p_i - q)^m J (\lambda - p_i)^{-1} \frac{1}{s - p_i} \right\|_2 \leq K \hat{d}(q)$$
$$\left\| \sum_{i=1}^m c_{p_i} (p_i - q)^m J (\lambda - p_i)^{-1} \frac{1}{s - p_i} \right\|_{\mathcal{H}_2} \leq K \hat{d}(q).$$

Proof of Corollary 5: First we show the upperbound for the spectral norm. By [14, Fact 1], it suffices to show that for each $l \in \{0, \ldots, m_q - 1\}$ there exists $k_l > 0$ such that the lth superdiagonal of the matrix in the desired result satisfies

$$\left| \sum_{i=1}^m c_{p_i} (p_i - q)^m (-1)^l (\lambda - p_i)^{-(l+1)} \frac{1}{s - p_i} \right| \leq k_l \hat{d}(q).$$

First we obtain analogous results by following the proof of [14, Corollary 2(b)], and then replace each following K'_n for $n = \{0, \ldots, k-1\}$ in [14, Lemma 5(b)] with the new bound K by setting $s = \lambda$ in (4.52).

$$\left| \sum_{i=1}^m c_{p_i} (p_i - q)^m (-1)^l (\lambda - p_i)^{-(l+1)} \frac{1}{s - p_i} \right|$$
$$\overset{\text{[14, Corollary 2(b)]}}{\leq} \left| \frac{(s-q)^m}{\prod_{i=1}^m (s - p_i)} - 1 \right| |\lambda - s|^{-l-1} + \frac{|1 - a_0|}{|\lambda - s|^{l+1}} + \sum_{n=1}^l \frac{|a_n|}{|s - \lambda|^{l+1-n}}$$

$$\overset{\substack{s=j\omega\\ \text{Lemma 7}}}{\leq} \left(\frac{((|q|+2)^m - (|q|+1)^m)\ell(\mathcal{K})^{m-1}}{|j\omega-\lambda|^{l+1}} \frac{\sum_{h=1}^{m} |\omega|^{m-h}}{\prod_{i=1}^{m} |j\omega - p_i|} + \frac{K_0'}{|j\omega-\lambda|^{l+1}} + \sum_{n=1}^{l} \frac{K_n'}{|j\omega-\lambda|^{l+1-n}} \right) \hat{d}(q)$$

$$\overset{\substack{\text{merge}\\ \text{terms}}}{=} \left(\frac{((|q|+2)^m - (|q|+1)^m)\ell(\mathcal{K})^{m-1}}{|j\omega-\lambda|^{l+1}} \frac{\sum_{h=1}^{m} |\omega|^{m-h}}{\prod_{i=1}^{m} |j\omega - p_i|} + \sum_{n=0}^{l} \frac{K_n'}{|j\omega-\lambda|^{l+1-n}} \right) \hat{d}(q) \quad (4.55)$$

$$\overset{\text{Lemma 7}}{\leq} \left(\frac{((|q|+2)^m - (|q|+1)^m)\ell(\mathcal{K})^{m-1}}{(-\lambda_x)^{l+1}} \frac{\sum_{h=1}^{m} \hat{\omega}^{m-h}}{{b'}^{\frac{m}{2}}} + \sum_{n=0}^{l} \frac{K_n'}{(-\lambda_x)^{l+1-n}} \right) \hat{d}(q) \equiv k_l \hat{d}(q). \quad (4.56)$$

Here, (4.55) and (4.56) are necessary to compute the $\mathcal{H}_2$ and $\mathcal{H}_\infty$ upperbounds, respectively. The spectral norm is already bounded in (4.56), and then the $\mathcal{H}_\infty$ norm follows directly from its definition.

We now proceed to prove the $\mathcal{H}_2$ bound, enforcing $\mathcal{H}_2$ norm for the lth superdiagonal element of the matrix implies that

$$\left\| \sum_{i=1}^{m} c_{p_i} (p_i - q)^m (-1)^l (\lambda - p_i)^{-(l+1)} \frac{1}{s-p_i} \right\|_{\mathcal{H}_2}$$

$$\overset{\substack{\text{triangle}\\ \text{inequality}\\ (4.55)}}{\leq} \left(\left\| \frac{((|q|+2)^m - (|q|+1)^m)\ell(\mathcal{K})^{m-1}}{|j\omega-\lambda|^{l+1}} \cdot \frac{\sum_{h=1}^{m} |\omega|^{m-h}}{\prod_{i=1}^{m} |j\omega - p_i|} \right\|_{\mathcal{H}_2} + \sum_{n=0}^{l} \left\| \frac{K_n'}{|j\omega-\lambda|^{l+1-n}} \right\|_{\mathcal{H}_2} \right) \hat{d}(q)$$

$$\overset{\text{Lemma 7}}{\leq} \left(K_{(m,l+1)}^{(p,\lambda)} + \sum_{n=0}^{l} K_n' K_{(0,l+1-n)}^{(p,\lambda)} \right) \hat{d}(q) \equiv K_l^* \hat{d}(q). \quad (4.57)$$

Thus

$$\left\| \sum_{i=1}^{m} c_{p_i} (p_i - q)^m J (\lambda - p_i)^{-1} \frac{1}{s-p_i} \right\|_{\mathcal{H}_2}$$

$$= \sqrt{\frac{1}{2\pi} \int_{-\infty}^{\infty} \left\| \sum_{i=1}^{m} c_{p_i} (p_i - q)^m J (\lambda - p_i)^{-1} \frac{1}{s-p_i} \right\|_F^2 \mathrm{d}\omega}$$

$$= \sqrt{\sum_{l=0}^{m_q-1}(m_q-l)\left\|\sum_{i=1}^{m} c_{p_i}\frac{(-1)^l(p_i-q)^m}{(\lambda-p_i)^{(l+1)}(s-p_i)}\right\|_{\mathcal{H}_2}^2}$$

$$\overset{(4.57)}{\leq} \sqrt{\sum_{l=0}^{m_q-1}(m_q-l)K_l^{*2}\hat{d}(q)} \equiv K\hat{d}(q)$$

which completes the proof. □

Now we have prepared everything for proving Lemma 6.

Proof of Lemma 6: The intuition of the proof is to first select an optimal solution (Φ_x^*, Φ_u^*) to (2.3), and then obtain $\|\Phi_u(s) - \Phi_u^*(s)\|_\bullet \leq K_\bullet^u D(\mathcal{P})$ immediately by constructing $\Phi_u(s)$ as Theorem 2. Next $\Phi_x(s)$ is defined as the unique solution to the SLS constraint in (2.4b), then we will show that Φ_x is a feasible solution to (4.10), and that it satisfies the approximation error bounds $\|\Phi_x(s) - \Phi_x^*(s)\|_\bullet \leq K_\bullet^x D(\mathcal{P})$. The main difference in the derivation compared to the discrete-time case in [14] is to show the bound $\|\Phi_x - \Phi_x^*\|_{\mathcal{H}_2} \leq K_2^x D(\mathcal{P})$. According to the proof of [14, Lemma 2], the error bounds are discussed separately for the cases $q \neq \lambda$ and $q = \lambda$.

Case 1: $q \neq \lambda$,

$$\begin{aligned}
&\|\Phi_x(s) - \Phi_x^*(s)\|_{\mathcal{H}_2} \\
&\overset{\substack{[14,\text{ Proof of}\\ \text{Lemma 2}]}}{\leq} \sum_{i=1}^{m}\sum_{l=1}^{i}\left\|G_{(l,i)}^*\right\|_F\left\|\frac{(s-q)^{i-l}}{\prod_{j=1}^{i}(s-p_j^i)} - \frac{1}{(s-q)^l}\right\|_{\mathcal{H}_2} \\
&+ \sum_{i=1}^{m}\left\|G_{(1,i)}^*\right\|_F\left\|\sum_{j=1}^{i} c_j^i\left(p_j^i-q\right)^i J\left(\lambda-p_j^i\right)^{-1}\frac{1}{s-p_j^i}\right\|_{\mathcal{H}_2} \\
&\overset{\substack{s=j\omega\\ \text{Lemma 7}\\ \text{Corollary 5}}}{\leq} \sum_{i=1}^{m}\sum_{l=1}^{i}\left\|G_{(l,i)}^*\right\|_F K_{(i,i-l)}^{(p^i,q)}\hat{d}(q) + \sum_{i=1}^{m}\left\|G_{(1,i)}^*\right\|_F K_i\hat{d}(q) \leq KD(\mathcal{P})
\end{aligned}$$

$$K = \sum_{i=1}^{m}\sum_{l=1}^{i}\left\|G_{(l,i)}^*\right\|_F K_{(i,i-l)}^{(p^i,q)} + \sum_{i=1}^{m}\left\|G_{(1,i)}^*\right\|_F K_i$$

where $K_{(i,i-l)}^{(p^i,q)}$ is from lemma 7 and K_i is from Corollary 5.

Case 2: $q = \lambda$. First we show there exist constants $K_\bullet^i > 0$, $\bullet \in \{2, F\}$, for $i \in$

$\{1,\dots,m\}$ such that

$$\left\|\sum_{j=1}^{i} G_j^i - G_{(1,i)}^*\right\|_\bullet \le K_\bullet^i D(\mathcal{P}). \tag{4.58}$$

To do so, we have the following results as the proof of [14, Lemma 2] analogously

$$\left\|\sum_{j=1}^{i} G_j^i - G_{(1,i)}^*\right\|_\bullet \overset{\substack{[14,\text{ Proof of}\\ \text{Lemma 2}]}}{\le} \left\|J(\lambda-q)^i G_{(1,i)}^*\right\|_\bullet \left\|\sum_{j=1}^{i} c_j^i J\left(\lambda-p_j^i\right)^{-1} - J(\lambda-q)^{-i}\right\|_\bullet.$$

From the proof of [14, (50)], the lth superdiagonal of the difference term between $\sum_{j=1}^{i} c_j^i$ $J\left(\lambda-p_j^i\right)^{-1}$ and $J(\lambda-q)^{-i}$ is shown to be $|\epsilon_{(i,l)}|$ for $l\in\{0,\dots,m_q-1\}$, which is bounded by $k_{(i,l)}D(\mathcal{P})$ in [14, Corollary 2(a)]. This $k_{(i,l)}$ is updated by (4.52). Since $|\epsilon_{(i,l)}|\le K_{(i,l)}D(\mathcal{P})$, where $K_{(i,l)}$ is in (4.52), thus $\|\epsilon_{(i,l)}\|_2 \le K_2' D(\mathcal{P})$ by the [14, Fact 1]. Use the following Fact 4 to yield the Frobenius upperbound for $\|\epsilon_{(i,l)}\|_F$ and we will have $\|\epsilon_i\|_\bullet \le K_\bullet^{i\prime}\hat{d}(q)$, defining $K_\bullet^i = K_\bullet^{i\prime}\left\|J(\lambda-q)^i G_{(1,i)}^*\right\|_\bullet$ finishes the proof of (4.58).

Fact 4. If there exist $k_{i,j}$ and d positive such that $|M_{i,j}|\le k_{i,j}d$ for all i,j then there exists $K>0$ such that $\|M\|_F = \sqrt{\sum_{i,j}|M_{i,j}|^2}\le Kd$.

By (4.58), some results in the proof of [14, Lemma 2] can be extended as follows

$$\left\|\hat{G}_1 - G_1^*\right\|_\bullet \le \sum_{\substack{\hat{q}\in\mathcal{Q}\\ \hat{q}\neq q}}\sum_{i=1}^{m_{\hat{q}}}\left\|G_{(\hat{q},i,1)}^* - \sum_{j=1}^{i} G_{(\hat{q},i,1)}^j\right\|_\bullet \le K_\bullet^1 D(\mathcal{P}), \qquad K_\bullet^1 = \sum_{\substack{\hat{q}\in\mathcal{Q}\\ \hat{q}\neq q}}\sum_{i=1}^{m_{\hat{q}}} K_\bullet^{(\hat{q},i)}.$$

Thus, for $l\in\{1,\dots,m_q\}$ we have

$$\left\|\hat{G}_l - \hat{G}_l^*\right\|_\bullet \le \left\|J(0)^{l-1}\right\|_\bullet \left\|\hat{G}_1 - \hat{G}_1^*\right\|_\bullet \le K_\bullet^l D(\mathcal{P})$$

where $K_\bullet^l = \left\|J(0)^{l-1}\right\|_\bullet K_\bullet^1$. Furthermore, the following inequality will be useful in deriving the error bounds.

$$\begin{aligned}\left\|\sum_{l=1}^{m_q}\left(\hat{G}_l - \hat{G}_l^*\right)\frac{1}{(j\omega-q)^l}\right\|_{\mathcal{H}_2} &\overset{\substack{\text{triangle}\\ \text{inequality}}}{\le} \sum_{l=1}^{m_q}\|\hat{G}_l - \hat{G}_l^*\|_F\sqrt{\frac{1}{2\pi}\int_{-\infty}^{\infty}\frac{1}{|j\omega-q|^{2l}}\mathrm{d}\omega}\\ &\overset{\text{Lemma 3}}{\le} \sum_{l=1}^{m_q} K_F^l\sqrt{\frac{1}{\pi}I_{(l,0)}^{(1,q_x^2)}}D(\mathcal{P})\end{aligned} \tag{4.59}$$

for more details in [14].

$$
\begin{aligned}
&\|\Phi_x(s)-\Phi_x^*(s)\|_{\mathcal{H}_2}\\
&\le \left\|\sum_{i=1}^{m_q+\tilde{m}}\tilde{G}_i\frac{1}{(s-q)^i}+\sum_{i=1+\tilde{m}}^{m}\sum_{j=1+\tilde{m}}^{m}G_j^i\frac{1}{(s-p_j^i)}-\sum_{i=1}^{m_q+m}\tilde{G}_i^*\frac{1}{(s-q)^i}\right\|_{\mathcal{H}_2}\\
&\quad+\left\|\sum_{i=1}^{m_q}\left(\hat{G}_i-\hat{G}_i^*\right)\frac{1}{(s-q)^i}\right\|_{\mathcal{H}_2}\\
&\overset{(4.59)}{\le} \left\|\sum_{i=1}^{m_q+\tilde{m}}\tilde{G}_i\frac{1}{(s-q)^i}+\sum_{i=1+\tilde{m}}^{m}\sum_{j=1+\tilde{m}}^{m}G_j^i\frac{1}{(s-p_j^i)}-\sum_{i=1}^{m_q+m}\tilde{G}_i^*\frac{1}{(s-q)^i}\right\|_{\mathcal{H}_2}\\
&\quad+\sum_{i=1}^{m_q}K_F^i\sqrt{\frac{1}{\pi}I_{(i,0)}^{(1,q_x^2)}}D(\mathcal{P}).
\end{aligned}
$$

For the remainder of the proof let Φ_x and Φ_x^* denote $\sum_{i=1}^{m_q+\tilde{m}}\tilde{G}_i\frac{1}{(s-q)^i}+\sum_{i=1+\tilde{m}}^{m}\sum_{j=1+\tilde{m}}^{m}G_j^i\frac{1}{(s-p_j^i)}$ and $\sum_{i=1}^{m_q+m}\tilde{G}_i^*\frac{1}{(s-q)^i}$, respectively. It suffices to show that there exists $K>0$ such that the first term is bounded in terms of $D(\mathcal{P})$, i.e., the redefined $\|\Phi_x(s)-\Phi_x^*(s)\|_{\mathcal{H}_2}\le KD(\mathcal{P})$. Instead of directly deriving the difference, we consider a similar discussion in the proof of [14, Lemma 2] about each lth superdiagonal element without common BH_i^*.

Recall [14, Lemma 5], for $i\in\{1+\tilde{m},\dots,m\}$ and $l\in\{m_q-i,\dots,m_q-2\}$, the lth superdiagonal of the term multiplying BH_i^* in $\Phi_x(s)-\Phi_x^*(s)$ is

$$
\begin{aligned}
&\left|\frac{(s-q)^{-(l+1+\tilde{m})}}{\prod_{j=1+\tilde{m}}^{i}(s-p_j^i)}-\frac{1}{(s-q)^{i+l+1}}\right|\\
&\qquad\overset{\substack{\text{Lemma 7}\\ s=j\omega}}{\le}\frac{((|q|+2)^{i-\tilde{m}}-(|q|+1)^{i-\tilde{m}})\ell(\mathcal{K})^{i-\tilde{m}}\sum_{h=1}^{i-\tilde{m}}|\omega|^{i-\tilde{m}-h}}{|j\omega-q|^{i+l+1}\prod_{j=1+\tilde{m}}^{i}|j\omega-p_j^i|}\hat{d}(q)
\end{aligned}
\tag{4.60}
$$

for $i\in\{1+\tilde{m},\dots,m\}$, the (m_q-1)th superdiagonal (i.e. $l=m_q-1$) of the term multiplying BH_i^* in $\Phi_x(s)-\Phi_x^*(s)$ is

$$
\begin{aligned}
&\left|\frac{1}{(s-q)^{l+1}}\frac{1}{\prod_{j=1}^{i}(s-p_j^i)}-\frac{1}{(s-q)^{i+l+1}}\right|\\
&\qquad\overset{\substack{\text{Lemma 7}\\ s=j\omega}}{\le}\frac{((|q|+2)^{i}-(|q|+1)^{i})\ell(\mathcal{K})^{i-1}\sum_{h=1}^{i}|\omega|^{i-h}}{|j\omega-q|^{i+l+1}\prod_{j=1}^{i}|j\omega-p_j^i|}\hat{d}(q)
\end{aligned}
$$

for $i \in \{1+\tilde{m}, \ldots, m\}$ and $l \in \{0, \ldots, m_q - i - 1\}$, the lth superdiagonal of the term multiplying BH_i^* in $\Phi_x(s) - \Phi_x^*(s)$ is the same bound in (4.60).

Finally, if $\tilde{m} = 1$, then for $i = 1$ and any $l \in \{0, \ldots, m_q - 1\}$, the lth superdiagonal of the term multiplying BH_1^* in $\Phi_x(s) - \Phi_x^*(s)$ is 0. Thus we have

$$\|(\Phi_x(s) - \Phi_x^*(s))_l^{(i)}\|_{\mathcal{H}_2} \leq K_l^{(i)} D(\mathcal{P})$$

where $K_l^{(i)} = K_{(i-\tilde{m},i+l+1)}^{(p^i,q)}$ for $i \in \{1+\tilde{m}, \ldots, m\}$ and $l \in \{0, \ldots, m_q - i - 1, m_q - i, \ldots, m_q - 2\}$, $K_l^{(i)} = K_{(i,i+l+1)}^{(p^i,q)}$ for $i \in \{1+\tilde{m}, \ldots, m\}$ and $l = m_q - 1$, $K_l^{(1)} = K_{(1,l+2)}^{(p^1,q)}$ for $i = 1$ and $l \in \{0, \ldots, m_q - 1\}$ by Lemma 7. Then

$$\begin{aligned} &\|\Phi_x(s) - \Phi_x^*(s)\|_{\mathcal{H}_2}^2 \\ \leq &\sum_{i=1}^{m} \sum_{l=0}^{m_q-1} (m_q - l) \|(\Phi_x(s) - \Phi_x^*(s))_l^{(i)}\|_{\mathcal{H}_2}^2 \|BH_i^*\|_F^2. \end{aligned}$$

Choosing $K = \sqrt{\sum_{i=1}^{m} \sum_{l=0}^{m_q-1} (m_q - l) K_l^{(i)} \|BH_i^*\|_F^2}$ yields

$$\|\Phi_x(s) - \Phi_x^*(s)\|_{\mathcal{H}_2} \leq K D(\mathcal{P}). \tag{4.61}$$

The statement of $\|\Phi_x(s) - \Phi_x^*(s)\|_{\mathcal{H}_\infty} \leq K D(\mathcal{P})$ is similar with the discrete time in the proof of [14, Lemma 2] except taking the $\mathcal{H}_\infty$ upperbounds which can be easily obtained from Lemma 7. Combine this and (4.61) together, and Lemma 6 is proved. □

Proof of Theorem 6 and Corollary 5: Follow the same argument in the proof of [14, Theorem 1 and Corollary 1]. □

4.5 Conclusion

In this chapter, a new Galerkin-type method for finite-dimensional approximations of discrete-time transfer functions in Hardy space with a selection of simple poles was adapted to the continuous-time setting. For any transfer function in Hardy space, approximation error bounds for SPA were provided which bound the Hardy space norms between the SPA and the target transfer function proportionally to the geometric distance between their poles. These were then used to show that the space of SPAs converges to a compact set of the open left half plane for any space-filling sequence of poles, and to provide a uniform convergence rate that depends purely on the geometry of the SPA pole selection.

Then, SLS with SPA was used to develop the first tractable approach for mixed $\mathcal{H}_2/\mathcal{H}_\infty$ control design with SLS in continuous time. The proposed hybrid domain framework avoids the errors introduced by both discrete time approximations and finite time horizon approximations, enabling accurate evaluation of the $\mathcal{H}_2$ and $\mathcal{H}_\infty$ norms of the closed-loop system. The resulting formulation yields a convex and tractable SDP consisting of LMIs and affine constraints, which can be solved efficiently. A general suboptimality certificate was provided for SLS with SPA, then specialized to the proposed grid pole selection strategy, showing that the control design converges to optimality as the number of poles approaches infinity. A numerical example of frequency and voltage regulation by a power converter interfaced wind turbine showed that SPA showed that the novel method achieved close matching with the optimal solution with only a small number of poles.

Chapter 5

Mixed $\mathcal{H}_2/\mathcal{H}_\infty$ Output Feedback Control in Discrete Time

For many control systems, it is not feasible or cost effective to measure all of the system states. In these situations, it is valuable to perform output feedback control design. Several recent convex reparameterizations have been developed for the output feedback setting in discrete time, including SLS and IOP. However, none of these approaches have been able to establish methods for $\mathcal{H}_2/\mathcal{H}_\infty$ output feedback control design with suboptimality bounds that converge to zero as the number of approximating poles approaches infinity. In this chapter, we develop the first mixed $\mathcal{H}_2/\mathcal{H}_\infty$ output feedback control design methods using four of these recent approaches, including SLS and IOP, for which we can establish suboptimality bounds that converge to zero as the number of poles approaches infinity. Moreover, the suboptimality bounds for these four methods are developed using a single common theoretical framework that applies to all of the methods simultaneously. Section 5.1 introduces the output feedback control synthesis problem, formulates the four convex reparameterizations of the output feedback problem, and applies SPA to the decision variables for each of these approaches. Section 5.2 presents state-space realizations of the closed-loop systems corresponding to each of these four optimization problems. The novel output feedback synthesis methods along with suboptimality guarantees relative to the original infinite dimensional design problem are presented in Section 5.3 and Section 5.4, respectively. Section 5.5 provides detailed derivations of the proposed methods, and Section 5.6 contains the proofs of the theoretical results. Finally, Section 5.7 concludes this chapter.

5.1 Background

We consider the LTI system in discrete time described by the following frequency representation:

$$y(z) = G(z)u(z) + \omega(z) \tag{5.1}$$

where ω is an output disturbance, and plant G is a strictly proper transfer function from u to y, which has the following state space realization

$$\begin{aligned} x(k+1) &= Ax(k) + Bu(k) + \varsigma(k) \\ y(k) &= Cx(k) + \omega(k) \end{aligned} \tag{5.2}$$

where $x(k) \in \mathbb{R}^n$, $u(k) \in \mathbb{R}^p$, $y(k) \in \mathbb{R}^m$ are the state, controller signal, and performance output vectors, $\varsigma(k) \in \mathbb{R}^n$ and $\omega(k) \in \mathbb{R}^m$ are disturbances to states and the output at time step k, respectively. Note that ς is a possible additional disturbance (on states) which is not directly included in the frequency domain representation (i.e., the state space realization does not perfectly match the frequency domain system). The plant G can be obtained as $G = C(zI - A)^{-1}B$.

Consider a linear output feedback control law of the form $u(z) = K(z)y(z) + \upsilon(z)$ where K is a dynamic controller and input disturbance $\upsilon(k) \in \mathbb{R}^p$ in the time domain. Denote the closed-loop transfer functions mapping external disturbances $\begin{bmatrix} \varsigma & \omega & \upsilon \end{bmatrix}^\intercal$ to internal signals $\begin{bmatrix} x & y & u \end{bmatrix}^\intercal$ as

$$\begin{bmatrix} x \\ y \\ u \end{bmatrix} = \underbrace{\begin{bmatrix} T_{\varsigma x} & T_{\omega x} & T_{\upsilon x} \\ T_{\varsigma y} & T_{\omega y} & T_{\upsilon y} \\ T_{\varsigma u} & T_{\omega u} & T_{\upsilon u} \end{bmatrix}}_{=:\, T(z)} \begin{bmatrix} \varsigma \\ \omega \\ \upsilon \end{bmatrix} \tag{5.3}$$

where $T_{ab}(z)$ represents the transfer function mapping from disturbance $a \in \{\varsigma, \omega, \upsilon\}$ to signal $b \in \{x, y, u\}$, and the dimension of each transfer function $T_{ab}(z)$ is $\dim(b) \times \dim(a)$. Let $T_{\omega y}^{\text{des}}(z)$ be a desired closed-loop transfer function for model matching control design, which can also be set to zero if preferred.

The goal of this chapter is to design a controller $K(z)$ that is a solution to the mixed $\mathcal{H}_2/\mathcal{H}_\infty$ control design problem in [1, 20] given by

$$\begin{aligned} \underset{K(z)}{\text{minimize}} \quad & \left\| \begin{bmatrix} T_{\upsilon y}(z) & T_{\omega y}(z) - I - T_{\omega y}^{\text{des}} \\ T_{\upsilon u}(z) - I & T_{\omega u}(z) \end{bmatrix} \right\|_{\mathcal{H}_2/\mathcal{H}_\infty} \\ \text{subject to} \quad & T(z) \in \mathcal{RH}_\infty \end{aligned} \tag{5.4}$$

where the mixed $\mathcal{H}_2/\mathcal{H}_\infty$ norm is given by $\|T\|_{\mathcal{H}_2/\mathcal{H}_\infty} = \|T\|_{\mathcal{H}_2} + \lambda\|T\|_{\mathcal{H}_\infty}$ for some constant $\lambda \in [0, \infty]$. The objective in (5.4) only includes transfer functions from disturbances on input/output to input/output signals (i.e., excluding states) since this is an output feedback formulation, the inclusion of T_{des} for only $T_{\omega y}$ is motivated by applications (it could also be there for the other transfer functions too if desired). Note that T_{vy} is strictly proper whereas $T_{\omega y}$ and T_{vu} are proper with constant term I, which are then subtracted, and the following Assumption A7 ensures a strictly proper $T_{\omega u}$ to make them strictly proper because otherwise their $\mathcal{H}_2$ norms would be infinite. Note that (5.4) is nonconvex in $K(z)$ since all the closed-loop transfer functions of $T(z)$ in (5.3) are, so this problem is challenging to solve in this original form. We make the following feasibility assumptions:

(A6) A solution to (5.4) exists, i.e., (A, B) is stabilizable, (A, C) is detectable, and the optimal closed-loop transfer functions are rational (hence they have finitely many poles).

(A7) $T_{\omega u}(z)$ is strictly proper.

Assumption A6 is a feasibility assumption, similar to A1 for state feedback control design. Assumption A7 ensures a finite $\mathcal{H}_2$ norm in (5.4) and, as we will see, is straightforward to enforce as part of the control design.

Furthermore, [24] showed that the constraint $T(z) \in \mathcal{RH}_\infty$ in (5.4) is redundant and can be equivalently replaced by enforcing any one of the following transfer matrices

$$\begin{bmatrix} T_{\varsigma x} & T_{\omega x} \\ T_{\varsigma u} & T_{\omega u} \end{bmatrix}, \begin{bmatrix} T_{\omega y} & T_{vy} \\ T_{\omega u} & T_{vu} \end{bmatrix}, \begin{bmatrix} T_{\varsigma y} & T_{\omega y} \\ T_{\varsigma u} & T_{\omega u} \end{bmatrix}, \begin{bmatrix} T_{\omega x} & T_{vx} \\ T_{\omega u} & T_{vu} \end{bmatrix} \tag{5.5}$$

to lie in $\mathcal{RH}_\infty$. Replacing the constraint in (5.4) with any choice from (5.5) results in four equivalent optimization problems, which will be explicitly discussed in Section 5.1.1. After representing the closed-loop system in the state space, more precise characteristics of the transfer functions in $T(z)$ can be identified [24]. Specifically, $T_{\omega y}$, T_{vu}, and $T_{\omega u}$ are proper transfer functions. The first two include have constant terms equal to the identity, thus the anti-diagonal entries in (5.4) become strictly proper, while $T_{\omega u}$ contains a constant term corresponding to the direct feedthrough term D in the realization of the dynamic controller K. Since this term would lead to an infinite $\mathcal{H}_2$ norm, the Assumption A7 is made for the remainder of this chapter. All remaining transfer functions in $T(z)$ in (5.3) and $T_{\omega y}^{\text{des}}(z)$ are strictly proper.

5.1.1 Convex Reparameterization Methods

There are four recent convex reparameterization methods that reparameterize each minimal set of closed-loop transfer functions in (5.5) from the original nonconvex optimization problem (5.4) by adding extra affine constraints to render the problem convex. The closed-loop transfer functions from each convex reparameterization method can be found in TABLE 5.1. For the remainder of this chapter, we use "Φ" to denote the reparameterized transfer functions previously denoted by "T" in (5.3).

Table 5.1: Convex Reparameterization Methods for Output Feedback Control Design

Method	Parameterized Transfer Functions (corresponding to matrices in (5.5))
System Level Synthesis [3]	$\begin{bmatrix}\varsigma & \omega\end{bmatrix}^\intercal \mapsto \begin{bmatrix}x & u\end{bmatrix}^\intercal$
Input Output Parameterization [16]	$\begin{bmatrix}\omega & \upsilon\end{bmatrix}^\intercal \mapsto \begin{bmatrix}y & u\end{bmatrix}^\intercal$
Mixed I [24]	$\begin{bmatrix}\varsigma & \omega\end{bmatrix}^\intercal \mapsto \begin{bmatrix}y & u\end{bmatrix}^\intercal$
Mixed II [24]	$\begin{bmatrix}\omega & \upsilon\end{bmatrix}^\intercal \mapsto \begin{bmatrix}x & u\end{bmatrix}^\intercal$

System Level Synthesis

Using SLS, (5.4) can be equivalently reformulated as follows

$$\underset{\substack{\Phi_{\varsigma x}(z),\Phi_{\omega x}(z)\\ \Phi_{\varsigma u}(z),\Phi_{\omega u}(z)}}{\text{minimize}} \quad \left\| \begin{bmatrix} C\Phi_{\varsigma x}B & C\Phi_{\omega x} - T_{\omega y}^{\text{des}} \\ \Phi_{\varsigma u}B & \Phi_{\omega u} \end{bmatrix} \right\|_{\mathcal{H}_2/\mathcal{H}_\infty} \tag{5.6a}$$

$$\text{subject to } \begin{bmatrix} zI - A & -B \end{bmatrix} \begin{bmatrix} \Phi_{\varsigma x} & \Phi_{\omega x} \\ \Phi_{\varsigma u} & \Phi_{\omega u} \end{bmatrix} = \begin{bmatrix} I & 0 \end{bmatrix} \tag{5.6b}$$

$$\begin{bmatrix} \Phi_{\varsigma x} & \Phi_{\omega x} \\ \Phi_{\varsigma u} & \Phi_{\omega u} \end{bmatrix} \begin{bmatrix} zI - A \\ -C \end{bmatrix} = \begin{bmatrix} I \\ 0 \end{bmatrix} \tag{5.6c}$$

$$\Phi_{\omega u}, \Phi_{\varsigma x}, \Phi_{\omega x}, \Phi_{\varsigma u} \in \frac{1}{z}\mathcal{RH}_\infty \tag{5.6d}$$

where $T_{\upsilon y}(z)$, $T_{\omega y}(z)$ and $T_{\upsilon u}(z)$ are calculated as $C\Phi_{\varsigma x}(z)B$, $C\Phi_{\omega x}(z) + I$ and $\Phi_{\varsigma u}(z)B + I$, respectively. Note that (5.6d) ensures stability and well-posedness of the closed-loop system. SLS requires the additional affine constraints (5.6b) and (5.6c). The controller $K = \Phi_{\omega u} - \Phi_{\varsigma u}\Phi_{\varsigma x}^{-1}\Phi_{\omega x}$ can be recovered after solving problem (5.6).

Input Output Parameterization

Using IOP, (5.4) can be equivalently reformulated as follows

$$\underset{\substack{\Phi_{\omega y}(z),\Phi_{\upsilon y}(z)\\ \Phi_{\omega u}(z),\Phi_{\upsilon u}(z)}}{\text{minimize}} \left\| \begin{bmatrix} \Phi_{\upsilon y} & \Phi_{\omega y} - I - T_{\omega y}^{\text{des}} \\ \Phi_{\upsilon u} - I & \Phi_{\omega u} \end{bmatrix} \right\|_{\mathcal{H}_2/\mathcal{H}_\infty} \tag{5.7a}$$

$$\text{subject to} \quad \begin{bmatrix} I & -G \end{bmatrix} \begin{bmatrix} \Phi_{\omega y} & \Phi_{\upsilon y} \\ \Phi_{\omega u} & \Phi_{\upsilon u} \end{bmatrix} = \begin{bmatrix} I & 0 \end{bmatrix} \tag{5.7b}$$

$$\begin{bmatrix} \Phi_{\omega y} & \Phi_{\upsilon y} \\ \Phi_{\omega u} & \Phi_{\upsilon u} \end{bmatrix} \begin{bmatrix} -G \\ I \end{bmatrix} = \begin{bmatrix} 0 \\ I \end{bmatrix} \tag{5.7c}$$

$$\Phi_{\omega y}, \Phi_{\upsilon u} \in \mathcal{RH}_\infty, \ \Phi_{\upsilon y}, \Phi_{\omega u} \in \frac{1}{z}\mathcal{RH}_\infty \tag{5.7d}$$

where (5.7d) ensures stability and well-posedness of the closed-loop system. IOP requires the additional affine constraints (5.7b) and (5.7c). The controller $K = \Phi_{\omega u}\Phi_{\omega y}^{-1}$ can be recovered after solving problem (5.7).

Mixed I

Using MI, (5.4) can be equivalently reformulated as follows

$$\underset{\substack{\Phi_{\varsigma y}(z),\Phi_{\omega y}(z)\\ \Phi_{\varsigma u}(z),\Phi_{\omega u}(z)}}{\text{minimize}} \left\| \begin{bmatrix} \Phi_{\varsigma y}B & \Phi_{\omega y} - I - T_{\omega y}^{\text{des}} \\ \Phi_{\varsigma u}B & \Phi_{\omega u} \end{bmatrix} \right\|_{\mathcal{H}_2/\mathcal{H}_\infty} \tag{5.8a}$$

$$\text{subject to} \quad \begin{bmatrix} I & -G \end{bmatrix} \begin{bmatrix} \Phi_{\varsigma y} & \Phi_{\omega y} \\ \Phi_{\varsigma u} & \Phi_{\omega u} \end{bmatrix} = \begin{bmatrix} G_C & I \end{bmatrix} \tag{5.8b}$$

$$\begin{bmatrix} \Phi_{\varsigma y} & \Phi_{\omega y} \\ \Phi_{\varsigma u} & \Phi_{\omega u} \end{bmatrix} \begin{bmatrix} zI - A \\ -C \end{bmatrix} = 0 \tag{5.8c}$$

$$\Phi_{\omega y} \in \mathcal{RH}_\infty, \ \Phi_{\varsigma y}, \Phi_{\varsigma u}, \Phi_{\omega u} \in \frac{1}{z}\mathcal{RH}_\infty \tag{5.8d}$$

where $T_{\upsilon y}(z)$ and $T_{\upsilon u}(z)$ are calculated as $\Phi_{\varsigma y}(z)B$ and $\Phi_{\varsigma u}(z)B + I$, respectively, and G_C is defined in (2.1). Note that (5.8d) ensures stability and well-posedness of the closed-loop system. MI requires the additional affine constraints (5.8b) and (5.8c). The controller $K = \Phi_{\omega u}\Phi_{\omega y}^{-1}$ can be recovered after solving problem (5.8).

Mixed II

Using MII, (5.4) can be equivalently reformulated as follows

$$\underset{\substack{\Phi_{\omega x}(z),\Phi_{vx}(z)\\ \Phi_{\omega u}(z),\Phi_{vu}(z)}}{\text{minimize}} \quad \left\| \begin{bmatrix} C\Phi_{vx} & C\Phi_{\omega x} - T_{\omega y}^{\text{des}} \\ \Phi_{vu} - I & \Phi_{\omega u} \end{bmatrix} \right\|_{\mathcal{H}_2/\mathcal{H}_\infty} \tag{5.9a}$$

$$\text{subject to } \begin{bmatrix} zI - A & -B \end{bmatrix} \begin{bmatrix} \Phi_{\omega x} & \Phi_{vx} \\ \Phi_{\omega u} & \Phi_{vu} \end{bmatrix} = 0 \tag{5.9b}$$

$$\begin{bmatrix} \Phi_{\omega x} & \Phi_{vx} \\ \Phi_{\omega u} & \Phi_{vu} \end{bmatrix} \begin{bmatrix} -G \\ I \end{bmatrix} = \begin{bmatrix} G_B \\ I \end{bmatrix} \tag{5.9c}$$

$$\Phi_{vu} \in \mathcal{RH}_\infty, \ \Phi_{\omega x}, \Phi_{vx}, \Phi_{\omega u} \in \frac{1}{z}\mathcal{RH}_\infty \tag{5.9d}$$

where $T_{vy}(z)$ and $T_{\omega y}(z)$ are calculated as $C\Phi_{vx}(z)$ and $C\Phi_{\omega x}(z) + I$, respectively, and G_B is defined in (2.1). Note that (5.9d) ensures stability and well-posedness of the closed-loop system. MII requires the additional affine constraints (5.9b) and (5.9c). The controller $K = \Phi_{vu}^{-1}\Phi_{\omega u}$ can be recovered after solving problem (5.9).

Note that the optimizations (5.6)-(5.9) are all now convex, although still infinite dimensional as all design variables in (5.6d)(5.7d)(5.8d)(5.9d) lie in the infinite dimensional function spaces $\frac{1}{z}\mathcal{RH}_\infty$ or $\mathcal{RH}_\infty$.

5.1.2 Simple Pole Approximation

To circumvent this issue, we adapt the approximation method in [14], which approximates the closed-loop transfer functions for state feedback control design using a finite selection of simple stable poles $\mathcal{P}$, closed under complex conjugation, to the output feedback setting using the following approach:

$$\underbrace{\begin{bmatrix} \Phi_{\varsigma x} & \Phi_{\omega x} & \Phi_{vx} \\ \Phi_{\varsigma y} & \Phi_{\omega y} & \Phi_{vy} \\ \Phi_{\varsigma u} & \Phi_{\omega u} & \Phi_{vu} \end{bmatrix}}_{=:\,\Phi(z)} \qquad \begin{array}{l} \blacksquare \ \sum_{p\in\mathcal{P}} H_p^\bullet \frac{1}{z-p} \\ \blacksquare \ \sum_{p\in\mathcal{P}} H_p^\bullet \frac{1}{z-p} + I \end{array} \tag{5.10}$$

for all 9 reparameterized closed-loop transfer functions $\Phi_\bullet$ in $\Phi(z)$, where $H_p^\bullet$ are (complex) coefficient matrices for each $p \in \mathcal{P}$. For notational simplicity, we use the symbol $\bullet \in \{\varsigma x, \varsigma y, \varsigma u, \omega x, \omega y, \omega u, vx, vy, vu\}$ to represent corresponding mappings from disturbances to states, outputs, or control signals. The green shaded entries in (5.10) correspond

to strictly proper transfer functions in $\frac{1}{z}\mathcal{RH}_\infty$, while the blue shaded proper transfer functions $\Phi_{\omega y}$ and Φ_{vu} include identity as constant terms. This SPA renders all four convex optimizations (5.6)-(5.9) finite dimensional, and these problems are referred to as `SLS`, `IOP`, `MI`, and `MII`, respectively.

For SPA, we adopt similar pole selection strategies as recommended in [13] to enhance performance, specifically including stable plant poles and any optimal poles that are known a priori in $\mathcal{P}$, and the remaining poles are chosen from an Archimedes spiral [13, Section III-C]. Since all $\Phi_\bullet(z)$ are real, it is straightforward to show that for any real pole p, $H_p^\bullet$ is real, and for any complex pole p, $H_{\overline{p}}^\bullet = \overline{H_p^\bullet}$. Let $\mathcal{P}_r$ denote the real poles in $\mathcal{P}$, and let $\mathcal{P}_c$ denote its complex poles. Then $\mathcal{P} = \mathcal{P}_r \cup \mathcal{P}_c$.

5.2 Closed-Loop Realization

To derive the proposed hybrid state space and frequency domain control design method for output feedback, we will require state space realizations of the closed-loop transfer functions for four optimizations `SLS`, `IOP`, `MI`, and `MII`. In this section, we propose novel state space realizations of the closed-loop dynamics based on the simple pole approximation.

For any $p \in \mathcal{P}_c$, its conjugate $\overline{p}$ is also in $\mathcal{P}_c$, their corresponding coefficient matrices are:

$$H_p = \mathrm{Re}(H_p) + \mathrm{Im}(H_p)j, \qquad H_{\overline{p}} = \mathrm{Re}(H_p) - \mathrm{Im}(H_p)j. \tag{5.11}$$

We first find real state space realizations for $\Phi_\bullet(z)$. To do so, for each complex conjugate pair $p, \overline{p} \in \mathcal{P}_c$, define the matrix

$$M(p) = \begin{bmatrix} \mathrm{Re}(p) & \mathrm{Im}(p) \\ -\mathrm{Im}(p) & \mathrm{Re}(p) \end{bmatrix},$$

and let $\mathcal{M}_c$ be the collection of $M(p)$ for all such complex conjugate pairs. Let $\mathcal{M}_r$ be the collection of each scalar matrix p for all $p \in \mathcal{P}_r$. Then we can define

$$\overline{A} = \begin{bmatrix} \mathcal{D}(\mathcal{M}_r) & \\ & \mathcal{D}(\mathcal{M}_c) \end{bmatrix} \otimes I,$$
$$\overline{B} = \big[\underbrace{I \quad \cdots \quad I}_{|\mathcal{P}_r|} \quad \underbrace{2I \quad 0 \quad \cdots \quad 2I \quad 0}_{|\mathcal{P}_c|}\big]^\intercal.$$

Next, for each complex conjugate pair $p, \overline{p} \in \mathcal{P}_c$, define the matrices

$$H^\bullet(p) = \begin{bmatrix} \mathrm{Re}(H_p^\bullet) & \mathrm{Im}(H_p^\bullet) \end{bmatrix},$$

and let $\mathcal{H}_c^\bullet$ be the collection of $H^\bullet(p)$ for all such complex conjugate pairs. Let $\mathcal{H}_r^\bullet$ be the collection of $H_p^\bullet$ for each $p \in \mathcal{P}_r$. Then we define

$$\overline{C}_\bullet = \begin{bmatrix} \mathcal{R}(\mathcal{H}_r^\bullet) & \mathcal{R}(\mathcal{H}_c^\bullet) \end{bmatrix}.$$

It is straightforward to verify that $(\overline{A}, \overline{B}, \overline{C}_\bullet, 0)$ is a real state space realization of $\Phi_\bullet(z)$ for each $\bullet \in \{\varsigma x, \varsigma y, \varsigma u, \omega x, \omega y, \omega u, \upsilon x, \upsilon y, \upsilon u\}$. To see this, first note that $\Phi_\bullet(z)$ can be decomposed into the contributions from individual real poles and from complex conjugate pairs of poles since $\overline{A}$ is block diagonal. For any real pole p, it follows

$$H_p^\bullet \left[zI - pI\right]^{-1} = H_p^\bullet \frac{1}{z-p}, \tag{5.12}$$

for any complex conjugate pair of poles p and $\overline{p}$,

$$\begin{aligned} &\begin{bmatrix} \mathrm{Re}(H_p^\bullet) & \mathrm{Im}(H_p^\bullet) \end{bmatrix} \begin{bmatrix} zI - \mathrm{Re}(p)I & -\mathrm{Im}(p)I \\ \mathrm{Im}(p)I & zI - \mathrm{Re}(p)I \end{bmatrix}^{-1} \begin{bmatrix} 2I \\ 0 \end{bmatrix} \\ &= \begin{bmatrix} \mathrm{Re}(H_p^\bullet) & \mathrm{Im}(H_p^\bullet) \end{bmatrix} \frac{1}{(z-p)(z-\overline{p})} \begin{bmatrix} 2zI - 2\mathrm{Re}(p)I \\ -2\mathrm{Im}(p)I \end{bmatrix} \\ &= \frac{2z\mathrm{Re}(H_p^\bullet) - 2\mathrm{Re}(H_p^\bullet)\mathrm{Re}(p) - 2\mathrm{Im}(H_p^\bullet)\mathrm{Im}(p)}{(z-p)(z-\overline{p})} \\ &\overset{(5.11)}{=} H_p^\bullet \frac{1}{z-p} + H_{\overline{p}}^\bullet \frac{1}{z-\overline{p}}, \end{aligned} \tag{5.13}$$

and $\overline{C}(zI - \overline{A})^{-1}\overline{B} = \sum_{\mathcal{P}_r} (5.12) + \sum_{\mathcal{P}_c} (5.13) = \sum_{p \in \mathcal{P}} H_p^\bullet \frac{1}{z-p}$. Therefore, $(\overline{A}, \overline{B}, \overline{C}_\bullet, 0)$ is a real state space realization of $\sum_{p \in \mathcal{P}} H_p^\bullet \frac{1}{z-p}$.

Let $(A_{\mathrm{des}}, B_{\mathrm{des}}, C_{\mathrm{des}}, 0)$ be any real state space realization of T_{des}. Now we can represent the transfer functions in the objectives (5.6a), (5.7a), (5.8a), and (5.9a) using the following

real state space realizations

$$
\begin{aligned}
\tilde{A} &= \begin{bmatrix} \overline{A} & & \\ & \overline{A} & \\ & & A_{\text{des}}^{\omega y} \end{bmatrix}, \quad \underbrace{\begin{bmatrix} \overline{B} & \\ & \overline{B} \\ & B_{\text{des}}^{\omega y} \end{bmatrix}}_{B_1}, \quad \underbrace{\begin{bmatrix} \overline{B}B & \\ & \overline{B} \\ & B_{\text{des}}^{\omega y} \end{bmatrix}}_{B_2} \\
\tilde{C}_{\texttt{SLS}} &= \begin{bmatrix} C\overline{C}_{\varsigma x} & C\overline{C}_{\omega x} & -C_{\text{des}}^{\omega y} \\ \overline{C}_{\varsigma u} & \overline{C}_{\omega u} & \end{bmatrix}, \quad \tilde{B}_{\texttt{SLS}} = B_2 \\
\tilde{C}_{\texttt{IOP}} &= \begin{bmatrix} \overline{C}_{vy} & \overline{C}_{\omega y} & -C_{\text{des}}^{\omega y} \\ \overline{C}_{vu} & \overline{C}_{\omega u} & \end{bmatrix}, \qquad \tilde{B}_{\texttt{IOP}} = B_1 \\
\tilde{C}_{\texttt{MI}} &= \begin{bmatrix} \overline{C}_{\varsigma y} & \overline{C}_{\omega y} & -C_{\text{des}}^{\omega y} \\ \overline{C}_{\varsigma u} & \overline{C}_{\omega u} & \end{bmatrix}, \qquad \tilde{B}_{\texttt{MI}} = B_2 \\
\tilde{C}_{\texttt{MII}} &= \begin{bmatrix} C\overline{C}_{vx} & C\overline{C}_{\omega x} & -C_{\text{des}}^{\omega y} \\ \overline{C}_{vu} & \overline{C}_{\omega u} & \end{bmatrix}, \quad \tilde{B}_{\texttt{MII}} = B_1
\end{aligned}
\tag{5.14}
$$

which satisfies

$$
\tilde{C}_{\circ}(zI - \tilde{A})^{-1}\tilde{B}_{\circ} = \tilde{\Phi}_{\circ}(z). \tag{5.15}
$$

this holds for $\circ \in \{\texttt{SLS}, \texttt{IOP}, \texttt{MI}, \texttt{MII}\}$, where $\tilde{\Phi}_{\circ}(z)$ denotes each transfer function matrix inside the $\mathcal{H}_2/\mathcal{H}_\infty$ norm in each objective (5.6a), (5.7a), (5.8a), (5.9a). Thus, we have obtained an equivalent state space representation of the closed-loop transfer functions $\tilde{\Phi}_{\circ}(z)$ for $\circ \in \{\texttt{SLS}, \texttt{IOP}, \texttt{MI}, \texttt{MII}\}$, which will be used to develop our novel control design methods. Note that for a fixed collection of simple poles $\mathcal{P}$, as used for SPA, $\tilde{A}$ and $\tilde{B}_{\circ}$ are constant matrices, and $\tilde{C}_{\circ}$ are affine functions of all of the variable coefficients $H_p^{\bullet}$.

5.3 Hybrid State Space and Frequency Domain Design

In this section we extend our hybrid state space and frequency domain state feedback control design method in [12] to the output feedback case. This method does not require any finite time horizon approximations for computing the $\mathcal{H}_2$ and $\mathcal{H}_\infty$ norms of the closed-loop transfer functions. As a result, it has reduced suboptimality, better performance, and lower computational cost compared to prior work [14]. The full derivation of the method is presented in Section 5.5, but the key idea is to leave the affine constraints from convex reparameterizations in the frequency domain to maintain their convexity, then combine

them with SPA, and use the state space realizations provided in Section 5.2 together with the KYP lemma to derive an equivalent state space representation of the $\mathcal{H}_2$ and $\mathcal{H}_\infty$ norms of the closed-loop transfer functions as LMIs, that is, the following objective and LMI constraints ($\star$ indicates symmetric blocks)

$$\underset{K_1^\circ, K_2^\circ, Z^\circ, H_p^\bullet, \gamma_1^\circ, \gamma_2^\circ}{\text{minimize}} \quad \gamma_1^\circ + \lambda \gamma_2^\circ \tag{5.16}$$

$$\text{subject to} \quad \begin{bmatrix} K_1^\circ & \star & \star \\ \tilde{A}^\intercal K_1^\circ & K_1^\circ & \star \\ \tilde{B}_\circ^\intercal K_1^\circ & 0 & \gamma_1^\circ I \end{bmatrix} \succ 0 \tag{5.17}$$

$$\begin{bmatrix} K_1^\circ & \star & \star \\ 0 & I & \star \\ \tilde{C}_\circ(H_p^\bullet) & 0 & Z^\circ \end{bmatrix} \succ 0 \tag{5.18}$$

$$\operatorname{Tr}(Z^\circ) < \gamma_1^\circ \tag{5.19}$$

$$\begin{bmatrix} K_2^\circ & \star & \star & \star \\ 0 & \gamma_2^\circ I & \star & \star \\ K_2^\circ \tilde{A} & K_2^\circ \tilde{B}_\circ & K_2^\circ & \star \\ \tilde{C}_\circ(H_p^\bullet) & 0 & 0 & \gamma_2^\circ I \end{bmatrix} \succ 0 \tag{5.20}$$

where $\circ \in \{\texttt{SLS}, \texttt{IOP}, \texttt{MI}, \texttt{MII}\}$ and $\bullet \in \{\varsigma x, \varsigma y, \varsigma u, \omega x, \omega y, \omega u, \upsilon x, \upsilon y, \upsilon u\}$, $K_1^\circ, K_2^\circ \in \mathbb{S}^{2n \times |\mathcal{P}|}$, $Z^\circ \in \mathbb{S}$, and $\gamma_1^\circ, \gamma_2^\circ$ are scalar variables that represent the $\mathcal{H}_2$ and $\mathcal{H}_\infty$ norms of the closed-loop transfer functions, respectively. Recall that $\tilde{A}$, $\tilde{B}_\circ$, and $\tilde{C}_\circ$ were defined in (5.14), but we write $\tilde{C}_\circ = \tilde{C}_\circ(H_p^\bullet)$ to emphasize that $\tilde{C}_\circ$ is an affine function of the coefficients $H_p^\bullet$ for all $p \in \mathcal{P}$. Since, using SPA, we have already selected the closed-loop poles $\mathcal{P}$, $\tilde{A}$ and $\tilde{B}_\circ$ are constant matrices, along with B and C.

While the objectives (5.6a), (5.7a), (5.8a), and (5.9a) have been reformulated as a unified objective (5.16) with state-space LMI constraints (5.17)–(5.20), it is natural to consider expressing the affine constraints in the state space as well. However, the additional affine constraints arising from convex reparameterizations become nonconvex when translated into state space, so we choose to retain their frequency domain representation to preserve their convex (in particular, affine) structure.

To complete the control design formulations, the reformulation of the objective in terms of LMIs using (5.16)-(5.20) should be combined with the affine constraints for each convex reparameterization. Section 5.5 derives in detail the form of these affine constraints after SPA is applied for each of the four approaches (SLS, IOP, MI, MII). It is shown that the constraints which were affine in the closed-loop decision variables remain affine in terms of the new decision variables: the coefficients $H_p^\bullet$ in SPA. Ultimately, the SLS constraints take

the form in (5.27)-(5.31), the `IOP` constraints are given by (5.38)-(5.45), the `MI` constraints are shown as (5.47)-(5.50), and the `MII` constraints are given by (5.52)-(5.55). Thus, combining each set of these constraints with (5.16)-(5.20) results in the four novel control design formulations.

Thus, the objective (5.16) is linear, the constraints (5.17)-(5.20) are LMIs, and the convex reparameterization constraints are linear or affine in the new decision variables of SPA: the coefficients $H_p^\bullet$. Therefore, overall `SLS`, `IOP`, `MI`, `MII` are convex SDPs that can be solved efficiently. Note that the state space realizations of the closed-loop transfer functions from Section 5.2 were deliberately constructed to ensure that the constraints (5.17)-(5.20) become LMIs rather than nonconvex bilinear matrix inequalities by including all the decision variables $H_p^\bullet$ in $\tilde{C}_\circ$ and leaving $\tilde{A}, \tilde{B}_\circ$ as constant matrices.

As we will see in Section 5.5, the objective (5.16) and constraints (5.17)-(5.20) are derived from a state space representation, whereas the constraints (5.27)-(5.31), (5.38)-(5.45), (5.47)-(5.50), (5.52)-(5.55) represent the linear or affine constraints in the frequency domain for each method after convex reparameterization and SPA, which together yield a truly hybrid control design. Notably, the design methods `SLS`, `IOP`, `MI`, `MII` exactly determine the $\mathcal{H}_2$ and $\mathcal{H}_\infty$ norms of the closed-loop transfer function, whereas [14] used Frobenius and spectral norms, respectively, to approximate them over a finite time horizon. The error of this finite time horizon approximation is thus avoided by the proposed design approach.

5.4 Suboptimality Bounds

Recall that $d(z, \mathcal{P})$ is the distance from z to $\mathcal{P}$, that $\max_{z \in Q} d(z, \mathcal{P})$ measures the geometric approximation error between approximating poles $\mathcal{P}$ and optimal poles $\mathcal{Q}$, and $D(\mathcal{P}) = \max_{z \in \mathbb{D}} d(z, \mathcal{P})$ measures the worst case geometric approximation error (for unknown $\mathcal{Q}$). In addition, $r \in (0, 1)$ is such that $\mathcal{P} \subset B_r$, and δ is a measure of the minimum distance between each approximating pole in $\mathcal{P}$ and σ (see [13] for further details). Also, recall Assumptions A1-A5 from [13], and Assumptions A6 and A7 in Section 5.1. Our main theoretical results show that the relative error of the hybrid domain methods decay at least linearly with $D(\mathcal{P})$.

Theorem 7 (SLS General Suboptimality Bound) *Let J^* denote the optimal cost of (5.6), and let $J(\mathcal{P})$ denote the optimal cost of `SLS` (5.16)-(5.20)(5.27)-(5.31) for any choice of $\mathcal{P}$. Suppose Assumptions A6 and A7 are met, and $\mathcal{P}$ satisfies Assumptions A1-A5*

in [13]. Then there exists a constant $\hat{K} = \hat{K}(\mathcal{Q}, H^{\bullet *}_{(q,j)}, r, \delta) > 0$ *such that*

$$\frac{J(\mathcal{P}) - J^*}{J^*} \leq \hat{K} D(\mathcal{P}) \tag{5.21}$$

Theorem 8 (IOP General Suboptimality Bound) *Let* J^* *denote the optimal cost of* (5.7)*, and let* $J(\mathcal{P})$ *denote the optimal cost of* `IOP` (5.16)-(5.20)(5.38)-(5.45) *for any choice of* $\mathcal{P}$*. Suppose Assumptions A6 and A7 are met, and* $\mathcal{P}$ *satisfies Assumptions A1-A5 in [13]. Then there exists a constant* $\hat{K} = \hat{K}(\mathcal{Q}, H^{\bullet *}_{(q,j)}, r, \delta) > 0$ *such that*

$$\frac{J(\mathcal{P}) - J^*}{J^*} \leq \hat{K} D(\mathcal{P}) \tag{5.22}$$

Theorem 9 (MI General Suboptimality Bound) *Let* J^* *denote the optimal cost of* (5.8)*, and let* $J(\mathcal{P})$ *denote the optimal cost of* `MI` (5.16)-(5.20)(5.47)-(5.50) *for any choice of* $\mathcal{P}$*. Suppose Assumptions A6 and A7 are met, and* $\mathcal{P}$ *satisfies Assumptions A1-A5 in [13]. Then there exists a constant* $\hat{K} = \hat{K}(\mathcal{Q}, H^{\bullet *}_{(q,j)}, r, \delta) > 0$ *such that*

$$\frac{J(\mathcal{P}) - J^*}{J^*} \leq \hat{K} D(\mathcal{P}) \tag{5.23}$$

Theorem 10 (MII General Suboptimality Bound) *Let* J^* *denote the optimal cost of* (5.9)*, and let* $J(\mathcal{P})$ *denote the optimal cost of* `MII` (5.16)-(5.20)(5.52)-(5.55) *for any choice of* $\mathcal{P}$*. Suppose Assumptions A6 and A7 are met, and* $\mathcal{P}$ *satisfies Assumptions A1-A5 in [13]. Then there exists a constant* $\hat{K} = \hat{K}(\mathcal{Q}, H^{\bullet *}_{(q,j)}, r, \delta) > 0$ *such that*

$$\frac{J(\mathcal{P}) - J^*}{J^*} \leq \hat{K} D(\mathcal{P}) \tag{5.24}$$

Corollary 6 shows that, for the Archimedes spiral pole selection in [13], the relative error of SPA converges to zero at the rate $(|\mathcal{P}| + 2)^{-1/2}$ since $|\mathcal{P}_n| = 2n - 2$ for each $n > 0$. Corollary 6 applies to all four control design formulations developed above.

Corollary 6 (Spiral Suboptimality Bound) *For each even integer* $n > 0$*, let* $\mathcal{P}_n$ *denote the selection of* $(2n - 2)$ *poles given by* p_k *for* $k \in [-(n-1), n-1]$*, where*

$$\theta_k = 2\sqrt{\pi k}, \qquad r_k = \sqrt{\frac{k}{n}}, \qquad p_k = (r_k, \theta_k), \qquad p_{-k} = (r_k, -\theta_k).$$

Then there exists a constant $\hat{K} = \hat{K}(\mathcal{Q}, H^{\bullet *}_{(q,j)}) > 0$ *and* $N > 0$ *such that* $n \geq N$ *implies*

$$\frac{J(\mathcal{P}_n) - J^*}{J^*} \leq \frac{\hat{K}}{\sqrt{n}} \tag{5.25}$$

Note that N in Corollary 1 only needs to be chosen to ensure that $D(\mathcal{P}_N) < 1$, $|\mathcal{P}_N| \geq m_{\max}$, and that $\delta > 0$ for $\mathcal{P}_N$, and so is typically satisfied in practice with small N (see the remark following [13, Theorem 3]).

5.5 Control Design Derivation

This section presents the derivation of our output feedback control design optimization formulations `SLS`, `IOP`, `MI`, and `MII`, as summarized in Section 5.3. We begin by presenting each problem formulation, namely, (5.6)-(5.9), in conjunction with SPA (5.10).

Our derivation proceeds in two parts. First, we reformulate the SLS constraints (5.6b) (5.6c), IOP constraints (5.7b)(5.7c), MI constraints (5.8b)(5.8c) and MII constraints (5.9b) (5.9c) for SPA. Then, we derive the corresponding state space representations of the objective functions (5.6a), (5.7a), (5.8a), and (5.9a).

The SLS constraints (5.6b) and (5.6c) can be expressed as

$$(zI - A)\Phi_{\varsigma x} - B\Phi_{\varsigma u} = I \tag{5.26a}$$
$$\Phi_{\varsigma x}(zI - A) - \Phi_{\omega x}C = I \tag{5.26b}$$
$$(zI - A)\Phi_{\omega x} - B\Phi_{\omega u} = 0 \tag{5.26c}$$
$$\Phi_{\varsigma u}(zI - A) - \Phi_{\omega u}C = 0. \tag{5.26d}$$

Substituting the SPA reparameterization (5.10) into the constraints (5.26) and matching the coefficients of $\frac{1}{z-p}$ for each $p \in \mathcal{P}$, using the linear independence of these terms, we obtain the following conditions

$$\sum_{p\in\mathcal{P}} H_p^{\varsigma x} = I, \qquad \sum_{p\in\mathcal{P}} H_p^{\omega x} = 0, \qquad \sum_{p\in\mathcal{P}} H_p^{\varsigma u} = 0 \tag{5.27}$$

for the constant terms,

$$(pI - A)H_p^{\varsigma x} - BH_p^{\varsigma u} = 0 \tag{5.28}$$
$$H_p^{\varsigma x}(pI - A) - H_p^{\omega x}C = 0 \tag{5.29}$$
$$(pI - A)H_p^{\omega x} - BH_p^{\omega u} = 0 \tag{5.30}$$
$$H_p^{\varsigma u}(pI - A) - H_p^{\omega u}C = 0 \tag{5.31}$$

for each $p \in \mathcal{P}$. Thus, the SLS constraints (5.6b) and (5.6c) with the SPA (5.10) can be equivalently represented using (5.27)-(5.31).

The IOP constraints (5.7b) and (5.7c) can be equivalently written as

$$\Phi_{\omega y} - G\Phi_{\omega u} = I \tag{5.32a}$$
$$\Phi_{\upsilon y} - G\Phi_{\upsilon u} = 0 \tag{5.32b}$$
$$-\Phi_{\omega y}G + \Phi_{\upsilon y} = 0 \tag{5.32c}$$
$$-\Phi_{\omega u}G + \Phi_{\upsilon u} = I. \tag{5.32d}$$

For the IOP constraints (5.32), substituting SPA (5.10) into (5.32) yields that

$$\sum_{p\in\mathcal{P}} H_p^{\omega y}\frac{1}{z-p} - G\sum_{p\in\mathcal{P}} H_p^{\omega u}\frac{1}{z-p} = 0 \tag{5.33a}$$
$$\sum_{p\in\mathcal{P}} H_p^{\upsilon y}\frac{1}{z-p} - G\left(\sum_{p\in\mathcal{P}} H_p^{\upsilon u}\frac{1}{z-p} + I\right) = 0 \tag{5.33b}$$
$$\sum_{p\in\mathcal{P}} H_p^{\upsilon y}\frac{1}{z-p} - \left(\sum_{p\in\mathcal{P}} H_p^{\omega y}\frac{1}{z-p} + I\right)G = 0 \tag{5.33c}$$
$$\sum_{p\in\mathcal{P}} H_p^{\upsilon u}\frac{1}{z-p} - \sum_{p\in\mathcal{P}} H_p^{\omega u}G\frac{1}{z-p} = 0. \tag{5.33d}$$

The system G can be represented by all plant poles as follows

$$G = \sum_{\lambda\in\sigma}\sum_{k=1}^{m_\lambda} G_\lambda^k \frac{1}{(z-\lambda)^k} \tag{5.34}$$

where σ is the collection of plant poles. Furthermore, the contribution from all simple poles can be split into stable plant poles and others

$$\sum_{p\in\mathcal{P}} H_p^\bullet \frac{1}{z-p} = \sum_{q\in\sigma\cap\mathcal{P}} H_q^\bullet \frac{1}{z-q} + \sum_{p\in\mathcal{P}\setminus\sigma} H_p^\bullet \frac{1}{z-p} \tag{5.35}$$

Then we combine expressions (5.34) and (5.35), the term $G\sum_{p\in\mathcal{P}} H_p^\bullet \frac{1}{z-p}$ expands to

$$\sum_{\lambda\in\sigma}\sum_{k=1}^{m_\lambda}\sum_{p\in\mathcal{P}\setminus\lambda} \frac{G_\lambda^k H_p^\bullet}{(z-\lambda)^k(z-p)} + \sum_{\lambda\in\sigma\cap\mathcal{P}}\sum_{k=1}^{m_\lambda} \frac{G_\lambda^k H_\lambda^\bullet}{(z-\lambda)^{k+1}},$$

applying a partial fraction decomposition (which will be detailed in Lemma 9), we obtain

$$\sum_{\lambda\in\sigma}\sum_{p\in\mathcal{P}\setminus\lambda}\sum_{k=1}^{m_\lambda}\sum_{j=1}^{k} \frac{(-1)^{k-j}1^{(k-j)}}{(k-j)!(\lambda-p)^{1+k-j}} \frac{G_\lambda^k H_p^\bullet}{(z-\lambda)^j}$$

$$+\sum_{\lambda\in\sigma}\sum_{p\in\mathcal{P}\setminus\lambda}\sum_{k=1}^{m_\lambda}\frac{G_\lambda^k H_p^\bullet}{(p-\lambda)^k(z-p)}+\sum_{\lambda\in\sigma\cap\mathcal{P}}\sum_{k=1}^{m_\lambda}\frac{G_\lambda^k H_\lambda^\bullet}{(z-\lambda)^{k+1}}$$

$$=\sum_{\lambda\in\sigma\cap\mathcal{P}}\sum_{\substack{p\in\mathcal{P}\\p\neq\lambda}}\square+\sum_{\lambda\in\sigma\setminus\mathcal{P}}\sum_{p\in\mathcal{P}}\square+\sum_{p\in\sigma\cap\mathcal{P}}\sum_{\substack{\lambda\in\sigma\\\lambda\neq p}}\circ+\sum_{p\in\mathcal{P}\setminus\sigma}\sum_{\lambda\in\sigma}\circ+\sum_{\lambda\in\sigma\cap\mathcal{P}}\sum_{k=2}^{m_\lambda+1}\frac{G_\lambda^{k-1}H_\lambda^\bullet}{(z-\lambda)^k} \tag{5.36}$$

where $\square=\sum_{k=1}^{m_\lambda}\sum_{j=1}^{k}\frac{(-1)^{k-j}1^{(k-j)}}{(k-j)!(\lambda-p)^{1+k-j}}\frac{G_\lambda^k H_p^\bullet}{(z-\lambda)^j}$ and $\circ=\sum_{k=1}^{m_\lambda}\frac{G_\lambda^k H_p^\bullet}{(p-\lambda)^k(z-p)}$. Using the fact that $1^{(k-j)}=(k-j)!$ and cancelling $(-1)^{k-j}$, we have

$$\begin{aligned}\square &\overset{\text{switch sum}}{=}\sum_{j=1}^{m_\lambda}\sum_{k=j}^{m_\lambda}\frac{-1}{(p-\lambda)^{1+k-j}}G_\lambda^k H_p^\bullet\frac{1}{(z-\lambda)^j}\\ &\overset{\substack{\text{define}\\ r=k-j}}{=}\sum_{j=1}^{m_\lambda}\sum_{r=0}^{m_\lambda-j}\frac{-1}{(p-\lambda)^{1+r}}G_\lambda^{j+r}H_p^\bullet\frac{1}{(z-\lambda)^j}\\ &\overset{\substack{\text{change}\\ \text{index}}}{=}\sum_{k=1}^{m_\lambda}\left(\sum_{j=0}^{m_\lambda-k}\frac{-1}{(p-\lambda)^{1+j}}G_\lambda^{k+j}\right)\frac{H_p^\bullet}{(z-\lambda)^k}.\end{aligned} \tag{5.37}$$

Combining (5.34)-(5.37) with the IOP constraints after SPA (5.33), for instance, in (5.33a), and matching the coefficients for $(z-p)^{-1}$ and $(z-\lambda)^{-k}$ implies

$$\sum_{p\in\mathcal{P}}\sum_{j=0}^{m_\lambda-k}\frac{-G_\lambda^{k+j}}{(p-\lambda)^{1+j}}H_p^{\omega u}=0, \qquad \begin{matrix}\forall\lambda\in\sigma\setminus\mathcal{P},\\ \forall k\in I_{m_\lambda}\end{matrix} \tag{5.38}$$

$$H_p^{\omega y}-\sum_{\lambda\in\sigma}\sum_{k=1}^{m_\lambda}\frac{G_\lambda^k}{(p-\lambda)^k}H_p^{\omega u}=0, \qquad \forall p\in\mathcal{P}\setminus\sigma \tag{5.39}$$

and

$$\sum_{\substack{\lambda\in\sigma\\\lambda\neq q}}\sum_{k=1}^{m_\lambda}\frac{G_\lambda^k}{(q-\lambda)^k}H_q^{\omega u}+\sum_{\substack{p\in\mathcal{P}\\p\neq q}}\sum_{j=0}^{m_q-1}\frac{-G_q^{1+j}}{(p-q)^{1+j}}H_p^{\omega u}=H_q^{\omega y} \tag{5.40}$$

$$\sum_{\substack{p\in\mathcal{P}\\p\neq q}}\sum_{j=0}^{m_q-k}\frac{-G_q^{k+j}}{(p-q)^{k+j}}H_p^{\omega u}+G_q^{k-1}H_q^{\omega u}=0, \qquad \forall k\in I_2^{m_q} \tag{5.41}$$

$$G_q^{m_q}H_q^{\omega u}=0, \qquad \forall q\in\sigma\cap\mathcal{P} \tag{5.42}$$

where $I_2^{m_q} = \{2, \ldots, m_q\}$, and the constraints (5.41) would only appear if $m_q \geq 2$ for all $q \in \sigma \cap \mathcal{P}$.

Similarly, the remaining IOP constraints (5.33b)-(5.33d) can be equivalently represented as

$$\begin{aligned}
\sum_{p\in\mathcal{P}} \sum_{j=0}^{m_\lambda - k} \frac{-G_\lambda^{k+j}}{(p-\lambda)^{1+j}} H_p^{\upsilon u} + G_\lambda^k &= 0 \\
\sum_{p\in\mathcal{P}} H_p^{\omega y} \sum_{j=0}^{m_\lambda - k} \frac{-G_\lambda^{k+j}}{(p-\lambda)^{1+j}} + G_\lambda^k &= 0 \\
\sum_{p\in\mathcal{P}} H_p^{\omega u} \sum_{j=0}^{m_\lambda - k} \frac{-G_\lambda^{k+j}}{(p-\lambda)^{1+j}} &= 0
\end{aligned} \tag{5.43}$$

for all $\lambda \in \sigma \setminus \mathcal{P}$ and $k \in I_{m_\lambda}$,

$$\begin{aligned}
H_p^{\upsilon y} - \sum_{\lambda\in\sigma} \sum_{k=1}^{m_\lambda} G_\lambda^k \frac{1}{(p-\lambda)^k} H_p^{\upsilon u} &= 0 \\
H_p^{\upsilon y} - H_p^{\omega y} \sum_{\lambda\in\sigma} \sum_{k=1}^{m_\lambda} G_\lambda^k \frac{1}{(p-\lambda)^k} &= 0 \\
H_p^{\upsilon u} - H_p^{\omega u} \sum_{\lambda\in\sigma} \sum_{k=1}^{m_\lambda} G_\lambda^k \frac{1}{(p-\lambda)^k} &= 0
\end{aligned} \tag{5.44}$$

for all $p \in \mathcal{P} \setminus \sigma$, and

$$
\begin{aligned}
&\sum_{\substack{\lambda\in\sigma\\ \lambda\neq q}}\sum_{k=1}^{m_\lambda}\frac{G_\lambda^k H_q^{\upsilon u}}{(q-\lambda)^k}+\sum_{\substack{p\in\mathcal{P}\\ p\neq q}}\sum_{j=0}^{m_q-1}\frac{-G_q^{1+j}H_p^{\upsilon u}}{(p-q)^{1+j}}+G_q^1=H_q^{\upsilon y}\\
&\sum_{\substack{\lambda\in\sigma\\ \lambda\neq q}}\sum_{k=1}^{m_\lambda}\frac{H_q^{\omega y}G_\lambda^k}{(q-\lambda)^k}+\sum_{\substack{p\in\mathcal{P}\\ p\neq q}}H_p^{\omega y}\sum_{j=0}^{m_q-1}\frac{-G_q^{1+j}}{(p-q)^{1+j}}+G_q^1=H_q^{\upsilon y}\\
&H_q^{\omega u}\sum_{\substack{\lambda\in\sigma\\ \lambda\neq q}}\sum_{k=1}^{m_\lambda}\frac{G_\lambda^k}{(q-\lambda)^k}+\sum_{\substack{p\in\mathcal{P}\\ p\neq q}}H_p^{\omega u}\sum_{j=0}^{m_q-1}\frac{-G_q^{1+j}}{(p-q)^{1+j}}=H_q^{\upsilon u}\\
&\qquad\sum_{\substack{p\in\mathcal{P}\\ p\neq q}}\sum_{j=0}^{m_q-k}\frac{-G_q^{k+j}H_p^{\upsilon u}}{(p-q)^{k+j}}+G_q^{k-1}H_q^{\upsilon u}+G_q^k=0,\qquad \forall k\in I_2^{m_q}\\
&\qquad\sum_{\substack{p\in\mathcal{P}\\ p\neq q}}\sum_{j=0}^{m_q-k}\frac{-H_p^{\omega y}G_q^{k+j}}{(p-q)^{k+j}}+H_q^{\omega y}G_q^{k-1}+G_q^k=0,\qquad \forall k\in I_2^{m_q}\\
&\qquad\sum_{\substack{p\in\mathcal{P}\\ p\neq q}}H_p^{\omega u}\sum_{j=0}^{m_q-k}\frac{-G_q^{k+j}}{(p-q)^{k+j}}+H_q^{\omega u}G_q^{k-1}=0,\qquad \forall k\in I_2^{m_q}\\
&G_q^{m_q}H_q^{\upsilon u}=0,\quad H_q^{\omega y}G_q^{m_q}=0,\quad H_q^{\omega u}G_q^{m_q}=0
\end{aligned}
\tag{5.45}
$$

for all $q \in \sigma \cap \mathcal{P}$.

As in the partial fraction decomposition of G in (5.34), based on the definitions of G_C and G_B in (2.1), their partial fraction decompositions can be obtained as

$$
G_C=\sum_{\lambda\in\sigma}\sum_{k=1}^{m_\lambda}\frac{G_\lambda^k B^\dagger}{(z-\lambda)^k},\qquad\qquad G_B=\sum_{\lambda\in\sigma}\sum_{k=1}^{m_\lambda}\frac{C^\dagger G_\lambda^k}{(z-\lambda)^k}.
$$

The MI constraints (5.8b) and (5.8c) can be equivalently expressed as

$$
\Phi_{\varsigma y}-G\Phi_{\varsigma u}=G_c \tag{5.46a}
$$

$$
\Phi_{\omega y}-G\Phi_{\omega u}=I \tag{5.46b}
$$

$$
\Phi_{\varsigma y}(zI-A)-\Phi_{\omega y}C=0 \tag{5.46c}
$$

$$
\Phi_{\varsigma u}(zI-A)-\Phi_{\omega u}C=0. \tag{5.46d}
$$

For the MI constraints (5.46a) and (5.46b), substituting the SPA (5.10) into them implies that

$$\sum_{p\in\mathcal{P}} H_p^{\varsigma y}\frac{1}{z-p} - G\sum_{p\in\mathcal{P}} H_p^{\varsigma u}\frac{1}{z-p} = G_C$$
$$\sum_{p\in\mathcal{P}} H_p^{\omega y}\frac{1}{z-p} - G\sum_{p\in\mathcal{P}} H_p^{\omega u}\frac{1}{z-p} = 0,$$

applying partial fraction decomposition (as in the derivation of (5.33a)), this yields

$$\begin{aligned}
\sum_{p\in\mathcal{P}}\sum_{j=0}^{m_\lambda-k}\frac{-G_\lambda^{k+j}}{(p-\lambda)^{1+j}}H_p^{\varsigma u} + G_\lambda^k B^\dagger = 0, \quad & \forall \lambda\in\sigma\setminus\mathcal{P}, \\
& \forall k\in I_{m_\lambda} \\
\sum_{p\in\mathcal{P}}\sum_{j=0}^{m_\lambda-k}\frac{-G_\lambda^{k+j}}{(p-\lambda)^{1+j}}H_p^{\omega u} = 0, \quad & \forall \lambda\in\sigma\setminus\mathcal{P}, \\
& \forall k\in I_{m_\lambda} \\
H_p^{\varsigma y} - \sum_{\lambda\in\sigma}\sum_{k=1}^{m_\lambda} G_\lambda^k\frac{1}{(p-\lambda)^k}H_p^{\varsigma u} = 0, \quad & \forall p\in\mathcal{P}\setminus\sigma \\
H_p^{\omega y} - \sum_{\lambda\in\sigma}\sum_{k=1}^{m_\lambda} G_\lambda^k\frac{1}{(p-\lambda)^k}H_p^{\omega u} = 0, \quad & \forall p\in\mathcal{P}\setminus\sigma \\
\sum_{\substack{\lambda\in\sigma\\ \lambda\neq q}}\sum_{k=1}^{m_\lambda}\frac{G_\lambda^k H_q^{\varsigma u}}{(q-\lambda)^k} + \sum_{\substack{p\in\mathcal{P}\\ p\neq q}}\sum_{j=0}^{m_q-1}\frac{-G_q^{1+j}H_p^{\varsigma u}}{(p-q)^{1+j}} + G_q^1 B^\dagger = H_q^{\varsigma y} & \qquad (5.47) \\
\sum_{\substack{\lambda\in\sigma\\ \lambda\neq q}}\sum_{k=1}^{m_\lambda}\frac{G_\lambda^k}{(q-\lambda)^k}H_q^{\omega u} + \sum_{\substack{p\in\mathcal{P}\\ p\neq q}}\sum_{j=0}^{m_q-1}\frac{-G_q^{1+j}}{(p-q)^{1+j}}H_p^{\omega u} = H_q^{\omega y} & \\
\sum_{\substack{p\in\mathcal{P}\\ p\neq q}}\sum_{j=0}^{m_q-k}\frac{-G_q^{k+j}H_p^{\varsigma u}}{(p-q)^{k+j}} + G_q^{k-1}H_q^{\varsigma u} + G_q^k B^\dagger = 0, \quad & \forall k\in I_2^{m_q} \\
\sum_{\substack{p\in\mathcal{P}\\ p\neq q}}\sum_{j=0}^{m_q-k}\frac{-G_q^{k+j}}{(p-q)^{k+j}}H_p^{\omega u} + G_q^{k-1}H_q^{\omega u} = 0, \quad & \forall k\in I_2^{m_q} \\
G_q^{m_q}H_q^{\varsigma u} = 0, \quad G_q^{m_q}H_q^{\omega u} = 0, \quad & \forall q\in\sigma\cap\mathcal{P}
\end{aligned}$$

Then the constraints (5.46c) and (5.46d) can be obtained analogously as the SLS con-

straint (5.26d)

$$\sum_{p\in\mathcal{P}} H_p^{\varsigma y} = C, \qquad \sum_{p\in\mathcal{P}} H_p^{\varsigma u} = 0 \tag{5.48}$$

and

$$H_p^{\varsigma y}(pI - A) - H_p^{\omega y}C = 0 \tag{5.49}$$
$$H_p^{\varsigma u}(pI - A) - H_p^{\omega u}C = 0 \tag{5.50}$$

for each $p \in \mathcal{P}$.

The MII constraints (5.9b) and (5.9c) are equivalently written as

$$(zI - A)\Phi_{\omega x} - B\Phi_{\omega u} = 0 \tag{5.51a}$$
$$(zI - A)\Phi_{\upsilon x} - B\Phi_{\upsilon u} = 0 \tag{5.51b}$$
$$-\Phi_{\omega x}G + \Phi_{\upsilon x} = G_B \tag{5.51c}$$
$$-\Phi_{\omega u}G + \Phi_{\upsilon u} = I. \tag{5.51d}$$

The first two equations (5.51a) and (5.51b) can be handled analogously to the SLS constraint (5.26c), yielding

$$\sum_{p\in\mathcal{P}} H_p^{\omega x} = 0 \qquad \sum_{p\in\mathcal{P}} H_p^{\upsilon x} = B \tag{5.52}$$

and

$$(pI - A)H_p^{\omega x} - BH_p^{\omega u} = 0 \tag{5.53}$$
$$(pI - A)H_p^{\upsilon x} - BH_p^{\upsilon u} = 0 \tag{5.54}$$

for each $p \in \mathcal{P}$.

For the MII constraints (5.51c) and (5.51d), substituting the SPA (5.10) into them implies that

$$-\sum_{p\in\mathcal{P}} H_p^{\omega x}\frac{1}{z-p}G + \sum_{p\in\mathcal{P}} H_p^{\upsilon x}\frac{1}{z-p} = G_B$$
$$-\sum_{p\in\mathcal{P}} H_p^{\omega u}\frac{1}{z-p}G + \sum_{p\in\mathcal{P}} H_p^{\upsilon u}\frac{1}{z-p} = 0,$$

following a procedure analogous to the IOP constraint (5.33d), we obtain

$$
\begin{aligned}
\sum_{p\in\mathcal{P}} H_p^{\omega x} \sum_{j=0}^{m_\lambda-k} \frac{-G_\lambda^{k+j}}{(p-\lambda)^{1+j}} + C^\dagger G_\lambda^k = 0, \qquad & \forall \lambda \in \sigma \setminus \mathcal{P}, \\
& \forall k \in I_{m_\lambda} \\
\sum_{p\in\mathcal{P}} H_p^{\omega u} \sum_{j=0}^{m_\lambda-k} \frac{-G_\lambda^{k+j}}{(p-\lambda)^{1+j}} = 0, \qquad & \forall \lambda \in \sigma \setminus \mathcal{P}, \\
& \forall k \in I_{m_\lambda} \\
H_p^{vx} - H_p^{\omega x} \sum_{\lambda\in\sigma} \sum_{k=1}^{m_\lambda} G_\lambda^k \frac{1}{(p-\lambda)^k} = 0, \qquad & \forall p \in \mathcal{P} \setminus \sigma \\
H_p^{vu} - H_p^{\omega u} \sum_{\lambda\in\sigma} \sum_{k=1}^{m_\lambda} G_\lambda^k \frac{1}{(p-\lambda)^k} = 0, \qquad & \forall p \in \mathcal{P} \setminus \sigma \\
\sum_{\substack{\lambda\in\sigma \\ \lambda\neq q}} \sum_{k=1}^{m_\lambda} \frac{H_q^{\omega x} G_\lambda^k}{(q-\lambda)^k} + \sum_{\substack{p\in\mathcal{P} \\ p\neq q}} \sum_{j=0}^{m_q-1} \frac{-H_p^{\omega x} G_q^{1+j}}{(p-q)^{1+j}} + C^\dagger G_q^1 = H_q^{vx} \qquad & \\
H_q^{\omega u} \sum_{\substack{\lambda\in\sigma \\ \lambda\neq q}} \sum_{k=1}^{m_\lambda} \frac{G_\lambda^k}{(q-\lambda)^k} + \sum_{\substack{p\in\mathcal{P} \\ p\neq q}} H_p^{\omega u} \sum_{j=0}^{m_q-1} \frac{-G_q^{1+j}}{(p-q)^{1+j}} = H_q^{vu} \qquad & \\
\sum_{\substack{p\in\mathcal{P} \\ p\neq q}} \sum_{j=0}^{m_q-k} \frac{-H_p^{\omega x} G_q^{k+j}}{(p-q)^{k+j}} + H_q^{\omega x} G_q^{k-1} + C^\dagger G_q^k = 0, \qquad & \forall k \in I_2^{m_q} \\
\sum_{\substack{p\in\mathcal{P} \\ p\neq q}} H_p^{\omega u} \sum_{j=0}^{m_q-k} \frac{-G_q^{k+j}}{(p-q)^{k+j}} + H_q^{\omega u} G_q^{k-1} = 0, \qquad & \forall k \in I_2^{m_q} \\
H_q^{\omega x} G_q^{m_q} = 0, \quad H_q^{\omega u} G_q^{m_q} = 0, \qquad & \forall q \in \sigma \cap \mathcal{P}
\end{aligned}
\tag{5.55}
$$

Next, we will express the $\mathcal{H}_2$ and $\mathcal{H}_\infty$ norms of the closed-loop transfer functions from the objective functions (5.6a), (5.7a), (5.8a), and (5.9a) using state space representations. To do so, analogously like [12], we begin with the real state space realization $(\tilde{A}, \tilde{B}_\circ, \tilde{C}_\circ, 0)$ from (5.14), which is a realization of each closed-loop transfer function $\tilde{\Phi}_\circ(z)$ by (5.15). In order to calculate the objectives (5.6a), (5.7a), (5.8a), and (5.9a), we replace $\|\tilde{\Phi}_\circ(z)\|_{\mathcal{H}_2} + \lambda\|\tilde{\Phi}_\circ(z)\|_{\mathcal{H}_\infty}$ in these objectives by the minimization of $\gamma_1+\lambda\gamma_2$ subject to the two inequality constraints $\|\tilde{\Phi}_\circ(z)\|_{\mathcal{H}_2} < \gamma_1$ and $\|\tilde{\Phi}_\circ(z)\|_{\mathcal{H}_\infty} < \gamma_2$, which will become tight at optimality. Note that $\tilde{A}$ is Schur by construction because its eigenvalues consist of the poles $\mathcal{P}$ from SPA, which all lie inside the unit disk, so the assumptions of KYP lemma are automatically

satisfied and those two inequality constraints that bound the $\mathcal{H}_2$ and $\mathcal{H}_\infty$ norms can then be transformed into LMIs using state space representations $(\tilde{A}, \tilde{B}_\circ, \tilde{C}_\circ, 0)$ by the KYP lemma.

Thus, combining these LMIs and previous linear or affine constraints (5.27)-(5.31), (5.38)-(5.45), (5.47)-(5.50), (5.52)-(5.55), we arrive at the final control design optimization problems `SLS`, `IOP`, `MI`, `MII`, which are equivalent to (5.6)-(5.9) with the SPA (5.10), resepectively.

5.6 Proofs

The next two lemmas provide useful identities for developing the Corollary 7, which implies the suboptimality bounds for all four reparameterization methods.

Lemma 8 *For any positive integer m, i $(m \geq i)$, let $p_1, \ldots, p_m \in B_r$, $q \in \mathbb{D}$, $z, \lambda \in \partial\mathbb{D}$, $\mathcal{P} = \{p_l\}_{l=1}^{i} \cup \{p_k\}_{k=i+1}^{m}$ and $I_m = \{1, 2, \ldots, m\}$. Let $\hat{d}(q) = \max_{p\in\mathcal{P}} |p-q|$ and assume that $\hat{d}(q) < 1$. We allow the potential existence of the repeated poles in $\{p_l\}_{l=1}^{i}$ and $\{p_k\}_{k=i+1}^{m}$, (e.g., $p_{i+1} = p_i$). Then*

$$\left| \frac{1}{(\lambda - q)^{m-i}(z-q)^i} - \frac{1}{\prod_{k=i+1}^{m}(\lambda - p_k)\prod_{l=1}^{i}(z-p_l)} \right| \leq \frac{(|q|+2)^m - (|q|+1)^m}{d(q, \partial\mathbb{D})^m (1-r)^m} \hat{d}(q).$$

Proof of Lemma 8: Note that this Lemma will degenerate to the [13, Corollary 2] when $m = i$, thus it suffices to show the case when $m > i$. We compute

$$\begin{aligned}
&\prod_{k=i+1}^{m}(\lambda - p_k)\prod_{l=1}^{i}(z-p_l) - (\lambda-q)^{m-i+1}(z-q)^i \\
&\overset{\text{binomial theorem}}{=} \left(\sum_{k=0}^{m-i} \sum_{\substack{S\subset I_{m-i} \\ |S|=k}} \lambda^{m-i-k} \prod_{j\in S}(-p_{j+i}) \right) \left(\sum_{l=0}^{i} \sum_{\substack{T\subset I_i \\ |T|=l}} z^{i-l} \prod_{j\in T}(-p_j) \right) \\
&\quad - \left(\sum_{k=0}^{m-i} \binom{m-i}{k} \lambda^{m-i-k}(-q)^k \right) \left(\sum_{l=0}^{i} \binom{i}{l} z^{i-l}(-q)^l \right) \\
&\overset{\text{cancelling } \lambda^{m-i}z^i}{=} \sum_{k=0}^{m-i} \sum_{\substack{S\subset I_{m-i} \\ |S|=k}} \sum_{\substack{l=0 \\ l+k\neq 0}}^{i} \sum_{\substack{T\subset I_i \\ |T|=l}} \lambda^{m-i-k} z^{i-l} \left(\prod_{j\in\tilde{S}}(-p_j) \prod_{j\in T}(-p_j) - (-q)^{k+l} \right)
\end{aligned}$$

where $\tilde{S} = S + i$ represents the set after adding i to each elements in S and the last equality follows since the number of terms in $\sum_{\substack{S\subset I_{m-i}\\|S|=k}}$ is the number of ways to select k poles out of $m-i$ poles, which is $\binom{m-i}{k}$, similarly for $\binom{i}{l}$. Then, recalling that $z, \lambda \in \partial\mathbb{D}$ so $|z| = |\lambda| = 1$, and applying [13, Lemma 2] to poles $-q$ and new constructed $\{-p_j\}_{j\in\tilde{S}\cup T}$ for each set S and T in the sum yields

$$
\begin{aligned}
&\left|\prod_{k=i+1}^{m}(\lambda-p_k)\prod_{l=1}^{i}(z-p_l)-(\lambda-q)^{m-i}(z-q)^i\right| \\
&\overset{\substack{\text{triangle}\\\text{inequality}}}{\leq} \sum_{k=0}^{m-i}\sum_{\substack{S\subset I_{m-i}\\|S|=k}}\sum_{\substack{l=0\\l+k\neq 0}}^{i}\sum_{\substack{T\subset I_i\\|T|=l}}\left|\lambda^{m-i-k}z^{i-l}\right|\left|\prod_{j\in\tilde{S}}(-p_j)\prod_{j\in T}(-p_j)-(-q)^{k+l}\right| \\
&\overset{\substack{|z|\leq 1\\|\lambda|\leq 1}}{\leq} \sum_{k=0}^{m-i}\sum_{\substack{S\subset I_{m-i}\\|S|=k}}\sum_{\substack{l=0\\l+k\neq 0}}^{i}\sum_{\substack{T\subset I_i\\|T|=l}}\left|\prod_{j\in\tilde{S}\cup T}(-p_j)-(-q)^{k+l}\right| \\
&\overset{[13,\text{ Lemma 2}]}{\leq} \sum_{k=0}^{m-i}\sum_{\substack{S\subset I_{m-i}\\|S|=k}}\sum_{\substack{l=0\\l+k\neq 0}}^{i}\sum_{\substack{T\subset I_i\\|T|=l}}\sum_{n=1}^{k+l}\sum_{\substack{R\subset\tilde{S}\cup T\\|R|=n}}|q|^{k+l-n}\prod_{j\in R}|p_j-q| \\
&\overset{[13,\ (10)]}{\leq} \sum_{k=0}^{m-i}\sum_{\substack{S\subset I_{m-i}\\|S|=k}}\sum_{\substack{l=0\\l+k\neq 0}}^{i}\sum_{\substack{T\subset I_i\\|T|=l}}((|q|+\hat{d}(q))^{k+l}-|q|^{k+l}) \\
&= \sum_{k=0}^{m-i}\sum_{\substack{S\subset I_{m-i}\\|S|=k}}(|q|+\hat{d}(q))^k\sum_{\substack{l=0\\l+k\neq 0}}^{i}\sum_{\substack{T\subset I_i\\|T|=l}}(|q|+\hat{d}(q))^l-\sum_{k=0}^{m-i}\sum_{\substack{S\subset I_{m-i}\\|S|=k}}|q|^k\sum_{\substack{l=0\\l+k\neq 0}}^{i}\sum_{\substack{T\subset I_i\\|T|=l}}|q|^l \\
&= \left(\sum_{k=0}^{m-i}\binom{m-i}{k}(|q|+\hat{d}(q))^k\right)\left(\sum_{l=0}^{i}\binom{i}{l}(|q|+\hat{d}(q))^l\right)-1 \\
&\quad -\left(\left(\sum_{k=0}^{m-i}\binom{m-i}{k}|q|^k\right)\left(\sum_{l=0}^{i}\binom{i}{l}|q|^l\right)-1\right) \\
&\overset{\substack{\text{binomial}\\\text{theorem}}}{=} (1+|q|+\hat{d}(q))^m-(1+|q|)^m.
\end{aligned}
$$

By [13, Corollary 2],

$$\begin{aligned}
&\left|\frac{1}{(\lambda-q)^{m-i}(z-q)^i}-\frac{1}{\prod_{k=i+1}^{m}(\lambda-p_k)\prod_{l=1}^{i}(z-p_l)}\right| \\
&\leq \frac{\left|\prod_{k=i+1}^{m}(\lambda-p_k)\prod_{l=1}^{i}(z-p_l)-(\lambda-q)^{m-i}(z-q)^i\right|}{d(q,\partial\mathbb{D})^m\prod_{i=1}^{m}d(p_i,\partial\mathbb{D})} \\
&\leq \frac{(|q|+2)^m-(|q|+1)^m}{d(q,\partial\mathbb{D})^m(1-r)^m}\hat{d}(q).
\end{aligned}$$

□

Lemma 9 *Let k,i,m be positive integers, $z\in\partial\mathbb{D}$, $\lambda\in\overline{\mathbb{D}}$, and $q,p_1,\ldots,p_m\in\mathbb{D}$ with $d(\lambda,\{p_l\}_{l=1}^m)\geq\delta>0$ and $d(\lambda,q)\geq\eta>0$. Choose constants c_{p_l} as in [14, Lemma 4], then*

a.

$$\frac{1}{(z-\lambda)^k(z-q)^i}=\sum_{j=1}^{k}\frac{\varphi_j}{(z-\lambda)^j}+\sum_{l=1}^{i}\frac{\psi_l}{(z-q)^l} \tag{5.56}$$

where

$$\varphi_{k-n}=\frac{(-1)^n i^{(n)}}{n!(\lambda-q)^{i+n}}, \qquad n=\{0,\ldots,k-1\} \tag{5.57}$$

$$\psi_{i-n}=\frac{(-1)^n k^{(n)}}{n!(q-\lambda)^{k+n}}, \qquad n=\{0,\ldots,i-1\}. \tag{5.58}$$

b. There exist $k_0,\ldots,k_{k-1}>0$ such that

$$\frac{1}{(z-\lambda)^k\prod_{l=1}^{m}(z-p_l)}=\sum_{j=1}^{k}\frac{\iota_j}{(z-\lambda)^j}+\sum_{l=1}^{m}\frac{\kappa_l}{(z-p_l)} \tag{5.59}$$

where

$$\iota_{k-n}=\frac{(-1)^n m^{(n)}}{n!(\lambda-q)^{m+n}}+\epsilon_n, \qquad n=\{0,\ldots,k-1\} \tag{5.60}$$

$$|\epsilon_n|\leq k_n\hat{d}(q),$$

$$\kappa_l=\frac{c_{p_l}}{(p_l-\lambda)^k}, \qquad l=\{1,\ldots,m\}. \tag{5.61}$$

c. The difference between case (a) and (b) is

$$\begin{aligned}\frac{1}{(z-\lambda)^k(z-q)^i} - \frac{1}{(z-\lambda)^k\prod_{l=1}^{i}(z-p_l)} \\ = \sum_{j=1}^{k}\frac{-\epsilon_{k-j}}{(z-\lambda)^j} + \sum_{l=1}^{i}\left(\frac{\psi_l}{(z-q)^l} - \frac{\kappa_l}{(z-p_l)}\right)\end{aligned} \tag{5.62}$$

where

$$\sum_{l=1}^{i}\frac{\kappa_l}{z-p_l} = \sum_{l=1}^{i}\frac{c_{p_l}}{(\lambda-p_l)^k}\frac{1}{z-p_l} = \sum_{l=1}^{i}\frac{1}{\prod_{j=1}^{l}(z-p_j)}\sum_{\substack{v\in\mathbb{Z}_+^{i-l+1}\\ \|v\|_1=k+i-l}}\prod_{j=l}^{i}\frac{1}{(\lambda-p_j)^{v_{j-l+1}}} \tag{5.63}$$

and there exist $K>0$ such that

$$\left|\sum_{l=1}^{i}\left(\frac{\psi_l}{(z-q)^l} - \frac{\kappa_l}{z-p_l}\right)\right| \le K\hat{d}(q). \tag{5.64}$$

Building some intuition will aid the derivation of the proof. Given the expression

$$\sum_{\substack{v\in\mathbb{Z}_+^{i-l+1}\\ \|v\|_1=k+i-l}}\prod_{j=l}^{i}\frac{1}{(\lambda-p_j)^{v_{j-l+1}}} \tag{5.65}$$

which can be expanded as

$$\sum_{\substack{\sum_{n=1}^{i-l+1}v_n=k+i-l\\ 1\le v_n\le k+i-l-1,\forall n}}\frac{1}{(\lambda-p_l)^{v_1}(\lambda-p_{l+1})^{v_2}\cdots(\lambda-p_i)^{v_{i-l+1}}}.$$

This expression sums over all possible compositions of $k+i-l$ into $i-l+1$ positive integers, weighted by the product of reciprocal powers of $(\lambda-p_j)$ from $j=l$ to $j=i$. (e.g., if $i=4,l=3,k=2$ then (5.65) is $(\lambda-p_3)^{-2}(\lambda-p_4)^{-1}$ and $(\lambda-p_3)^{-1}(\lambda-p_4)^{-2}$.)

Proof of Lemma 9: First consider case (a). For any nonnegative n, define

$$b_n^a = \left(\frac{\mathrm{d}}{\mathrm{d}z^n}\sum_{l=1}^{k}a_l(z-\lambda)^{k-l}\right)(\lambda)$$

$$= \sum_{l=1}^{k-n} a_l (k-l)_n (z-\lambda)^{k-l-n}|_{z=\lambda} = n! a_{k-n}$$

$$d_n = \left(\frac{\mathrm{d}}{\mathrm{d}z^n} \prod_{l=1}^{m} (z - p_l) \right)(\lambda) = \sum_{\substack{v \in \mathbb{R}^n \\ v_i \in I_m \forall i \\ v_i \neq v_j \text{ for } i \neq j}} \prod_{\substack{k \in I_m \\ k \notin v}} (\lambda - p_k)$$

$$e_n = \left(\frac{\mathrm{d}}{\mathrm{d}z^n} (z-q)^i \right)(\lambda) = i_n (\lambda - q)^{i-n}$$

where a_l is any constant coefficient.

Multiplying both sides of (5.56) by $(z-\lambda)^k (z-q)^i$ yields

$$1 = (z-q)^i \sum_{l=1}^{k} \varphi_l (z-\lambda)^{k-l} + (z-\lambda)^k \sum_{l=1}^{i} \psi_l (z-q)^{i-l}.$$

Differentiating it $n = \{0, \ldots, k-1\}$ times with respect to z and evaluating at $z = \lambda$ implies that

$$\varphi_k = \frac{1}{(\lambda - q)^i} \tag{5.66}$$

for $n = 0$,

$$0 = \sum_{s=0}^{n} \binom{n}{s} b^{\varphi}_{n-s} e_s$$

$$0 = n! \varphi_{k-n} (\lambda - q)^i + \sum_{s=1}^{n} \frac{n!}{s!} \varphi_{k-(n-s)} i_s (\lambda - q)^{i-s}$$

$$\varphi_{k-n} = -\sum_{s=1}^{n} \frac{i_s \varphi_{k-(n-s)}}{s! (\lambda - q)^s} \tag{5.67}$$

for $n = \{1, \ldots, k-1\}$. We claim that

$$\varphi_{k-n} = \frac{(-1)^n i^{(n)}}{n! (\lambda - q)^{i+n}} \tag{5.68}$$

for $n = \{0, \ldots, k-1\}$. We prove (5.68) by strong induction. By (5.66) the base case is verified.

For the induction step, assume that (5.68) holds for all $n-s \in \{0,\dots,n-1\}$, together with (5.67)

$$\begin{aligned}
\varphi_{k-n} &\overset{(5.67)}{=} -\sum_{s=1}^{n} \frac{i_s \varphi_{k-(n-s)}}{s!(\lambda-q)^s} \overset{(5.68)}{=} -\sum_{s=1}^{n} \frac{i_s(-1)^{n-s} i^{(n-s)}}{s!(n-s)!(\lambda-q)^{i+n}} \\
&\overset{[14,\text{ Fact 3}]}{=} -\frac{1}{n!(\lambda-q)^{i+n}} \sum_{s=1}^{n} \binom{n}{s} i_s (-i)_{n-s} \\
&= -\frac{1}{n!(\lambda-q)^{i+n}} \left(\sum_{s=0}^{n} \binom{n}{s} i_s (-i)_{n-s} - i_0 \cdot (-i)_n \right) \\
&\overset{[14,\text{ Fact 4}]}{=} -\frac{1}{n!(\lambda-q)^{i+n}} (0_n - (-i)_n) \\
&\overset{[14,\text{ Fact 3}]}{=} -\frac{(-1)^n i^{(n)}}{n!(\lambda-q)^{i+n}}.
\end{aligned}$$

Thus, (5.68) holds.

The proof of (5.58) follows exactly the same derivation but differentiating $n = \{0,\dots,i-1\}$ times and evaluating at $z = q$.

Next consider Case (b): To find partial fraction decomposition in (5.59), we multiply both sides of (5.59) by $(z-\lambda)^k \prod_{l=1}^{m}(z-p_l)$ yields

$$(z-\lambda)^k \sum_{l=1}^{m} \kappa_l \prod_{\substack{j=1 \\ j\neq l}}^{m} (z-p_j) + \sum_{j=1}^{k} \iota_j (z-\lambda)^{k-j} \prod_{l=1}^{m} (z-p_l) = 1.$$

Evaluating at $z = p_l$ implies that

$$\kappa_l = \frac{c_{p_l}}{(p_l-\lambda)^k}$$

where c_{p_l} is referred in (5.69). Evaluating at $z = \lambda$ implies that

$$\iota_k = \frac{1}{\prod_{l=1}^{m}(\lambda-p_l)}.$$

After differentiating $n = \{1,\dots,k-1\}$ times with respect to z and evaluating at $z = \lambda$, similar results from above

$$0 = \left(\frac{\mathrm{d}}{\mathrm{d}z^n} \sum_{j=1}^{k} \iota_j (z-\lambda)^{k-j} \prod_{l=1}^{m} (z-p_l) \right)(\lambda)$$

$$= \sum_{s=0}^{n} \binom{n}{s} b_{n-s}(\lambda) d_s = \sum_{s=0}^{n} \binom{n}{s} \iota_{k-(n-s)} (n-s)! d_s$$
$$= \iota_{k-n} n! d_0 + \sum_{s=1}^{n} \frac{n!}{s!} \iota_{k-(n-s)} d_s.$$

Thus

$$\iota_{k-n} = -\sum_{s=1}^{n} \frac{1}{s!} \iota_{k-(n-s)} \frac{d_s}{d_0}$$

where

$$\frac{d_n}{d_0} = \sum_{\substack{v \in \mathbb{R}^n \\ v_i \in I_m \forall i \\ v_i \neq v_j \text{ for } i \neq j}} \prod_{k \in v} \frac{1}{\lambda - p_k}$$

is defined similarly in [14, Lemma 5]. We claim that

$$\iota_{k-j} = \frac{(-1)^j m^{(j)}}{j!(\lambda - q)^{m+j}} + \epsilon_j, \qquad |\epsilon_j| \leq k_j \hat{d}(q)$$

for $j = \{0, \ldots, k-1\}$. The proof shares a similar flow in [14, Proof of Lemma 5(a)] by using strong induction.

For case (c), it's straightforward to show (5.62) by taking the difference of (5.59) and (5.56). The following two properties (5.70) and (5.71) will help to derive (5.63).

Recall the partial fraction decomposition in [13, eq. (5)(6)]

$$\sum_{l=1}^{i} c_{p_l} \frac{1}{z - p_l} = \frac{1}{\prod_{l=1}^{i} (z - p_l)} \qquad c_{p_l} = \frac{1}{\prod_{\substack{j=1 \\ j \neq l}}^{i} (p_l - p_j)}. \tag{5.69}$$

It's straightforward to verify that

$$\sum_{l=1}^{m} c_{p_l} \frac{\prod_{j=m+1}^{i} (p_l - p_j)}{z - p_l} = \frac{1}{\prod_{l=1}^{m} (z - p_l)} \tag{5.70}$$

for all $m = \{1, \ldots, i-1\}$. The following property is also useful to factor out $p_i - p_j$ from the difference of $(\lambda - p_i)^{-n}$ and $(\lambda - p_j)^{-n}$ by the difference of powers formula

$$\begin{aligned}
&\frac{1}{(\lambda - p_i)^n} - \frac{1}{(\lambda - p_j)^n} = \frac{(\lambda - p_j)^n - (\lambda - p_i)^n}{(\lambda - p_i)^n (\lambda - p_j)^n} \\
&= \frac{(p_i - p_j) \sum_{k=0}^{n-1} (\lambda - p_j)^{n-1-k} (\lambda - p_i)^k}{(\lambda - p_i)^n (\lambda - p_j)^n} \\
&= (p_i - p_j) \sum_{k=1}^{n} \frac{1}{(\lambda - p_j)^k (\lambda - p_i)^{n-k+1}}.
\end{aligned} \tag{5.71}$$

To show (5.63), the argument proceeds by iteratively decomposing the partial fraction sum through a telescoping construction. The high-level proof strategy is to isolate the highest-subscript-pole piece in sum by adding and subtracting compensatory terms sharing a common λ-dependence factor, combine the piece and the adding terms and use the first property (5.70) after extracting the λ-dependence factor. Then apply the second property (5.71) for the remaining terms in the sum and the subtracting terms, which are iterated down to $l = 1$. More details are showed explicitly in the following first two iterations

$$\begin{aligned}
&\sum_{l=1}^{i} \frac{c_{p_l}}{(\lambda - p_l)^k} \frac{1}{z - p_l} \\
&= \sum_{l=1}^{i} \frac{c_{p_l}}{(\lambda - p_l)^k} \frac{1}{z - p_l} + \frac{1}{(\lambda - p_i)^k} \sum_{l=1}^{i-1} \frac{c_{p_l}}{z - p_l} - \frac{1}{(\lambda - p_i)^k} \sum_{l=1}^{i-1} \frac{c_{p_l}}{z - p_l} \\
&= \sum_{l=1}^{i-1} \frac{c_{p_l}}{z - p_l} \left(\frac{1}{(\lambda - p_l)^k} - \frac{1}{(\lambda - p_i)^k} \right) + \frac{1}{(\lambda - p_i)^k} \sum_{l=1}^{i} \frac{c_{p_l}}{z - p_l} \\
&\overset{(5.69)}{=} \sum_{l=1}^{i-1} \frac{c_{p_l}}{z - p_l} \left(\frac{1}{(\lambda - p_l)^k} - \frac{1}{(\lambda - p_i)^k} \right) + \frac{1}{(\lambda - p_i)^k \prod_{l=1}^{i} (z - p_l)} \\
&\overset{(5.71)}{=} \frac{1}{(\lambda - p_i)^k \prod_{l=1}^{i} (z - p_l)} + \sum_{l=1}^{i-1} \frac{c_{p_l} (p_l - p_i)}{z - p_l} \sum_{i_1=1}^{k} \frac{1}{(\lambda - p_i)^{i_1} (\lambda - p_l)^{k-i_1+1}}.
\end{aligned}$$

It can be seen that the original sum is split into one accumulated denominator products and one residual correction terms, and we keep peeling off the latter

$$\sum_{l=1}^{i-1} \frac{c_{p_l} (p_l - p_i)}{z - p_l} \sum_{i_1=1}^{k} \frac{1}{(\lambda - p_i)^{i_1} (\lambda - p_l)^{k-i_1+1}}$$

$$
\begin{aligned}
&= \sum_{l=1}^{i-1} \frac{c_{p_l}(p_l - p_i)}{z - p_l} \sum_{i_1=1}^{k} \frac{1}{(\lambda - p_i)^{i_1}(\lambda - p_l)^{k-i_1+1}} \\
&\quad + \sum_{l=1}^{i-2} \frac{c_{p_l}(p_l - p_i)}{z - p_l} \sum_{i_1=1}^{k} \frac{1}{(\lambda - p_i)^{i_1}(\lambda - p_{i-1})^{k-i_1+1}} \\
&\quad - \sum_{l=1}^{i-2} \frac{c_{p_l}(p_l - p_i)}{z - p_l} \sum_{i_1=1}^{k} \frac{1}{(\lambda - p_i)^{i_1}(\lambda - p_{i-1})^{k-i_1+1}} \\
&\overset{(5.70)}{=} \frac{1}{\prod_{l=1}^{i-1}(z - p_l)} \sum_{i_1=1}^{k} \frac{1}{(\lambda - p_i)^{i_1}(\lambda - p_{i-1})^{k-i_1+1}} \\
&\quad + \sum_{l=1}^{i-2} \frac{c_{p_l}(p_l - p_i)}{z - p_l} \sum_{i_1=1}^{k} \frac{1}{(\lambda - p_i)^{i_1}} \left(\frac{1}{(\lambda - p_l)^{k-i_1+1}} - \frac{1}{(\lambda - p_{i-1})^{k-i_1+1}} \right) \\
&\overset{(5.71)}{=} \frac{1}{\prod_{l=1}^{i-1}(z - p_l)} \sum_{i_1=1}^{k} \frac{1}{(\lambda - p_i)^{i_1}(\lambda - p_{i-1})^{k-i_1+1}} \\
&\quad + \sum_{l=1}^{i-2} \frac{c_{p_l}(p_l - p_i)(p_l - p_{i-1})}{z - p_l} \sum_{i_1=1}^{k} \frac{1}{(\lambda - p_i)^{i_1}} \sum_{i_2=1}^{k-i_1+1} \frac{1}{(\lambda - p_{i-1})^{i_2}(\lambda - p_l)^{k-i_1-i_2+2}}.
\end{aligned}
$$

Following this recipe and iterating for the residual terms after $i-3$ times yields

$$
\begin{aligned}
&\sum_{l=1}^{i-2} \frac{c_{p_l}(p_l - p_i)(p_l - p_{i-1})}{z - p_l} \sum_{i_1=1}^{k} \frac{1}{(\lambda - p_i)^{i_1}} \sum_{i_2=1}^{k-i_1+1} \frac{1}{(\lambda - p_{i-1})^{i_2}(\lambda - p_l)^{k-i_1-i_2+2}} \\
&= \sum_{l=2}^{i-2} \frac{1}{\prod_{j=1}^{l}(z - p_j)} \sum_{\substack{v \in \mathbb{Z}_+^{i-l+1} \\ \|v\|_1 = k+i-l}} \prod_{j=l}^{i} \frac{1}{(\lambda - p_j)^{v_{j-l+1}}} \\
&\quad + \frac{c_{p_1} \prod_{j=2}^{i}(p_1 - p_j)}{z - p_1} \sum_{i_1=1}^{k} \frac{1}{(\lambda - p_i)^{i_1}} \sum_{i_2=1}^{k-i_1+1} \frac{1}{(\lambda - p_{i-1})^{i_2}} \\
&\quad \cdot \ldots \cdot \sum_{i_{i-1}=1}^{k-\sum_{j=1}^{i-2}(i_j-1)} \frac{1}{(\lambda - p_2)^{i_{i-1}}(\lambda - p_1)^{k-\sum_{j=1}^{i-1}(i_j-1)}}
\end{aligned}
$$

note that $c_{p_1} \prod_{j=2}^{i}(p_1 - p_j) = 1$, and the nested summations is exactly the expression of (5.65) when $l = 1$. Tracking back the recursive iteration finishes the proof of (5.63).

Observe the combinatorial structure of (5.65): The sum enumerates all possible ways to write $k+i-l$ as a sum of $i-l+1$ positive integers (i.e., integer compositions). Thus there are $\binom{k+i-l-1}{i-l}$ elements in (5.65) and all with the same exponents $k+i-l$ after adding up v_{j-l+1} by the constraint $\|v\|_1 = k+i-l$.

Evaluating the absolute value of $\sum_{l=1}^{i}\left(\frac{\psi_l}{(z-q)^l}-\frac{\kappa_l}{z-p_l}\right)$ after substituting coefficients ψ_l in (5.58) and κ_l in (5.61) implies that

$$
\begin{aligned}
&\left|\sum_{l=1}^{i}\left(\frac{(-1)^{i-l}k^{(i-l)}}{(i-l)!(q-\lambda)^{k+i-l}}\frac{1}{(z-q)^l}-\frac{c_{p_l}}{(p_l-\lambda)^k}\frac{1}{z-p_l}\right)\right| \\
&=\left|(-1)^k\left(\sum_{l=1}^{i}\frac{k^{(i-l)}}{(i-l)!(\lambda-q)^{k+i-l}}\frac{1}{(z-q)^l}-\sum_{l=1}^{i}\frac{c_{p_l}}{(\lambda-p_l)^k}\frac{1}{z-p_l}\right)\right| \\
&=\left|\sum_{l=1}^{i}\frac{k^{(i-l)}}{(i-l)!(\lambda-q)^{k+i-l}}\frac{1}{(z-q)^l}-\sum_{l=1}^{i}\frac{c_{p_l}}{(\lambda-p_l)^k}\frac{1}{z-p_l}\right| \\
&\overset{(5.63)}{=}\left|\sum_{l=1}^{i}\binom{k+i-l-1}{i-l}\frac{1}{(\lambda-q)^{k+i-l}}\frac{1}{(z-q)^l}\right. \\
&\qquad\left.-\sum_{l=1}^{i}\frac{1}{\prod_{j=1}^{l}(z-p_j)}\sum_{\substack{v\in\mathbb{Z}_+^{i-l+1}\\ \|v\|_1=k+i-l}}\prod_{j=l}^{i}\frac{1}{(\lambda-p_j)^{v_{j-l+1}}}\right| \\
&\overset{\substack{\text{triangle}\\ \text{inequality}}}{\leq}\sum_{l=1}^{i}\left|\binom{k+i-l-1}{i-l}\frac{1}{(\lambda-q)^{k+i-l}}\frac{1}{(z-q)^l}\right. \\
&\qquad\left.-\frac{1}{\prod_{j=1}^{l}(z-p_j)}\sum_{\substack{v\in\mathbb{Z}_+^{i-l+1}\\ \|v\|_1=k+i-l}}\prod_{j=l}^{i}\frac{1}{(\lambda-p_j)^{v_{j-l+1}}}\right| \\
&\overset{\text{Lemma 8}}{\leq}\sum_{l=1}^{i}\binom{k+i-l-1}{i-l}\frac{(|q|+2)^{k+i}-(|q|+1)^{k+i}}{d(q,\partial\mathbb{D})^{k+i}(1-r)^{k+i}}\hat{d}(q) \\
&=\binom{k+i-1}{k}\frac{(|q|+2)^{k+i}-(|q|+1)^{k+i}}{d(q,\partial\mathbb{D})^{k+i}(1-r)^{k+i}}\hat{d}(q)=K\hat{d}(q)
\end{aligned}
$$

this completes the proof of (5.64). □

The key technical result required to establish suboptimality bounds for all four methods is stated in Corollary 7, which provides an upper bound on the discrepancy between a feasible solution satisfying the generalized affine constraints and SPA, and any real, rational, stable, and (strictly) proper transfer functions satisfying the constraints.

Corollary 7 *For any strictly proper plant G and transfer functions U, V (0 is included). Let $(\hat{X}, \hat{Y})$ and $(\hat{Z}, \hat{W})$ denote any pair of real, rational, stable, and (strictly) proper transfer functions which satisfy*

$$X = GY + U, \tag{5.72}$$
$$Z = WG + V \tag{5.73}$$

respectively. Then there exist SPA $(X, Y) \in \mathcal{RH}_\infty$ and $(Z, W) \in \mathcal{RH}_\infty$ which are feasible solutions to relationships (5.72) and (5.73), respectively, and constants $\hat{K}^x_\bullet, \hat{K}^y_\bullet, \hat{K}^w_\bullet, \hat{K}^z_\bullet > 0$, $\bullet \in \{2, \infty\}$, such that

$$\|X - \hat{X}\|_{\mathcal{H}_\bullet} \leq \hat{K}^x_\bullet D(\mathcal{P}), \ \|Y - \hat{Y}\|_{\mathcal{H}_\bullet} \leq \hat{K}^y_\bullet D(\mathcal{P}), \tag{5.74}$$
$$\|Z - \hat{Z}\|_{\mathcal{H}_\bullet} \leq \hat{K}^z_\bullet D(\mathcal{P}), \ \|W - \hat{W}\|_{\mathcal{H}_\bullet} \leq \hat{K}^w_\bullet D(\mathcal{P}) \tag{5.75}$$

respecively.

Proof of Corollary 7: First we consider (5.72), for any fixed $(\hat{X}, \hat{Y})$ satisfying (5.72), since $\hat{Y}$ is real rational stable and (strictly) proper, $\hat{Y}$ has a partial fraction decomposition which does not include polynomial terms or unstable poles, and in which all poles have finite multiplicity. Denote

$$\hat{Y} = \sum_{q \in \mathcal{Q}} \sum_{i=1}^{m_q} \hat{H}_{(q,i)} \frac{1}{(z-q)^i} + \hat{Y}_0$$

where $\hat{H}_{(q,i)}$ is the constant coefficient matrix in terms of pole q and corresponding power i ranging from 1 to its multiplicity m_q, $\hat{Y}_0$ is the potential constant matrix and will be 0 if $\hat{Y}$ is strictly proper, and then construct

$$Y = \sum_{q \in \mathcal{Q}} \sum_{i=1}^{m_q} \sum_{j=1}^{i} H_j^{(q,i)} \frac{1}{z - p_j^i} + Y_0, \qquad \begin{aligned} H_j^{(q,i)} &= c_j^{(q,i)} \hat{H}_{(q,i)}, \\ Y_0 &= \hat{Y}_0 \end{aligned}$$

by [13, Theorem 1], which implies the approximating error bounds for Y of (5.74) are satisfied. Then, $\hat{X}$ and X are defined as the unique solution of (5.72) by $\hat{X} = G\hat{Y} + U$

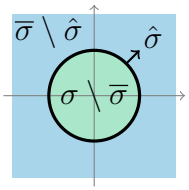

Symbol	Meaning
σ	plant poles
$\overline{\sigma}$	unstable plant poles
$\hat{\sigma}$	plant poles on the unit circle

Figure 5.1: Notation of plant poles

and $X = GY + U$ respectively. The partial fraction decomposition of the system G can be found in (5.34). For clarity, we distinguish all plant poles using the notation introduced in Fig. 5.1, which will be used throughout the remainder of the proof.

To prove the approximating error bounds of X in (5.74), our goal is to show there exists a constant K such that

$$\|G\hat{Y} - GY\|_2 \leq KD(\mathcal{P}). \tag{5.76}$$

To do so, $G\hat{Y} - GY = G(\hat{Y} - Y)$ is

$$\sum_{\lambda\in\sigma}\sum_{q\in\mathcal{Q}}\sum_{k=1}^{m_\lambda} G_\lambda^k \frac{1}{(z-\lambda)^k}\sum_{i=1}^{m_q}\hat{H}_{(q,i)}\left(\frac{1}{(z-q)^i} - \frac{1}{\prod_{j=1}^{i}(z-p_j^i)}\right) = \sum_{\lambda\in\overline{\sigma}}\bullet + \sum_{\lambda\in\sigma\setminus\overline{\sigma}}\bullet$$

where $\overline{\sigma}$ is the collection of unstable plant poles, and the remaining stable plant poles are represented as $\sigma \setminus \overline{\sigma}$. We have

$$\begin{aligned}
&\left\|\sum_{\lambda\in\sigma\setminus\overline{\sigma}}\sum_{q\in\mathcal{Q}}\sum_{k=1}^{m_\lambda} G_\lambda^k \frac{1}{(z-\lambda)^k}\sum_{i=1}^{m_q}\hat{H}_{(q,i)}\left(\frac{1}{(z-q)^i} - \frac{1}{\prod_{j=1}^{i}(z-p_j^i)}\right)\right\|_2 \\
&\overset{\text{triangle inequality}}{\leq} \sum_{\lambda\in\sigma\setminus\overline{\sigma}}\sum_{q\in\mathcal{Q}}\left\|\sum_{k=1}^{m_\lambda} G_\lambda^k \frac{1}{(z-\lambda)^k}\sum_{i=1}^{m_q}\hat{H}_{(q,i)}\left(\frac{1}{(z-q)^i} - \frac{1}{\prod_{j=1}^{i}(z-p_j^i)}\right)\right\|_2 \\
&\overset{\text{triangle inequality}}{\leq} \sum_{\lambda\in\sigma\setminus\overline{\sigma}}\sum_{q\in\mathcal{Q}}\sum_{k=1}^{m_\lambda}\frac{\|G_\lambda^k\|_2}{|z-\lambda|^k}\sum_{i=1}^{m_q}\|\hat{H}_{(q,i)}\|_2\left|\frac{1}{(z-q)^i} - \frac{1}{\prod_{j=1}^{i}(z-p_j^i)}\right| \\
&\overset{\text{[14, Lem 3]}}{\leq} KD(\mathcal{P})
\end{aligned}$$

where

$$K = \sum_{\lambda\in\sigma\setminus\overline{\sigma}}\sum_{q\in\mathcal{Q}}\sum_{k=1}^{m_\lambda}\frac{\|G_\lambda^k\|_2}{(1-|\lambda|)^k}\sum_{i=1}^{m_q}\|\hat{H}_{(q,i)}\|_2 k_{(q,i)}$$

for all $\lambda \in \sigma \setminus \overline{\sigma}$. Similar uppberbound can be immediately obtained for all unstable poles outside unit disk by setting $K = \sum_{\lambda\in\overline{\sigma}\setminus\hat{\sigma}} \sum_{q\in\mathcal{Q}} \sum_{k=1}^{m_\lambda} \frac{\|G_\lambda^k\|_2}{(|\lambda|-1)^k} \sum_{i=1}^{m_q} \|\hat{H}_{(q,i)}\|_2 k_{(q,i)}$. Thus, it suffices to show there exists a constant K such that

$$\left\| \sum_{q\in\mathcal{Q}} \sum_{k=1}^{m_\lambda} G_\lambda^k \frac{1}{(z-\lambda)^k} \sum_{i=1}^{m_q} \hat{H}_{(q,i)} \left(\frac{1}{(z-q)^i} - \frac{1}{\prod_{j=1}^{i}(z-p_j^i)} \right) \right\|_2 \leq K\hat{d}(q) \tag{5.77}$$

for all $\lambda \in \hat{\sigma}$. However, it is not valid to apply the triangle inequality directly to upper bound (5.77) as other two cases, because when z spans the entire unit circle, the term $1/(z-\lambda)$ may become arbitrarily large, and thus there doesn't exist distance between z and λ to provide a uniform bound.

In order to deal with these unstable plant poles $\lambda \in \hat{\sigma}$, we first tease out the partial fraction decomposition for $G\hat{Y}$ and GY with respect to all unstable plant pole $\overline{\sigma}$ and characteristics of potential poles of U. Although U is cancelled after taking the difference between X and $\hat{X}$ in (5.76), here the argument goes to X and $\hat{X}$ are stable independently, thus all coefficient matrices of their unstable poles should be zero as they are both stable. The contribution of all unstable plant poles of $G\hat{Y}$ that can be written as

$$\begin{aligned} G\hat{Y}|_{\overline{\sigma}} &= \sum_{\lambda\in\overline{\sigma}} \sum_{q\in\mathcal{Q}} \sum_{k=1}^{m_\lambda} G_\lambda^k \frac{1}{(z-\lambda)^k} \left(\sum_{i=1}^{m_q} \hat{H}_{(q,i)} \frac{1}{(z-q)^i} + \hat{Y}_0 \right) \\ &\overset{(5.56)}{=} \sum_{\lambda\in\overline{\sigma}} \sum_{q\in\mathcal{Q}} \sum_{k=1}^{m_\lambda} \sum_{i=1}^{m_q} G_\lambda^k \hat{H}_{(q,i)} \left(\sum_{j=1}^{k} \frac{\varphi_j}{(z-\lambda)^j} + \sum_{l=1}^{i} \frac{\psi_l}{(z-q)^l} \right) + \sum_{\lambda\in\overline{\sigma}} \sum_{k=1}^{m_\lambda} G_\lambda^k \hat{Y}_0 \frac{1}{(z-\lambda)^k} \end{aligned}$$

and the partial fraction decomposition of U is $\sum_{u\in\mathcal{U}} \sum_{l=1}^{m_u} U_u^l \frac{1}{(z-u)^l}$. It is important to emphasize that the poles of U are either stable or unstable; however, all unstable poles of U must lie within the collection of unstable plant poles $\overline{\sigma}$ and the multiplicity should be less than or equal to the multiplicity of corresponding unstable plant poles (or all coefficient matrices of other unstable poles have to be zero) in order to ensure the stability of $\hat{X}$. Consequently, U can be decomposed as follows

$$U = \sum_{\lambda\in\overline{\sigma}} \sum_{k=1}^{m_\lambda} U_\lambda^k \frac{1}{(z-\lambda)^k} + \sum_{u\in\mathcal{U}\setminus\overline{\sigma}} \sum_{l=1}^{m_u} U_u^l \frac{1}{(z-u)^l}$$

where $\mathcal{U} \setminus \overline{\sigma}$ represents all the other stable poles of U.

The coefficient matrices of each unstable pole of $G\hat{Y}+U$ should be zero since $\hat{X} \in \mathcal{RH}_\infty$, similarly like the derivation in (5.37), that is,

$$\sum_{q\in\mathcal{Q}} \sum_{i=1}^{m_q} \sum_{j=0}^{m_\lambda-k} \varphi_{k-j}^{(\lambda,q,i)} G_\lambda^{k+j} \hat{H}_{(q,i)} + G_\lambda^k \hat{Y}_0 + U_\lambda^k = 0$$

for all $\lambda \in \overline{\sigma}$ and $k = \{1, \ldots, m_\lambda\}$, where $\varphi_{k-j}^{(\lambda,q,i)}$ is defined in (5.57). Applying similar arguments, we arrive at the analogous results for X, i.e.,

$$\sum_{q\in\mathcal{Q}} \sum_{i=1}^{m_q} \sum_{j=0}^{m_\lambda - k} \iota_{k-j}^{(\lambda,q,i)} G_\lambda^{k+j} \hat{H}_{(q,i)} + G_\lambda^k Y_0 + U_\lambda^k = 0$$

for all $\lambda \in \overline{\sigma}$ and $k = \{1, \ldots, m_\lambda\}$, where $\iota_{k-j}^{(\lambda,q,i)}$ is defined in (5.60).

From now we restrict our attention to the unstable poles in the unit circle $\hat{\sigma} \subset \overline{\sigma}$, since all coefficient matrices of unstable poles $\hat{\sigma}$ are zero, then $(G\hat{Y} - GY)|_{\hat{\sigma}}$ is

$$\sum_{\lambda\in\hat{\sigma}} \sum_{q\in\mathcal{Q}} \sum_{k=1}^{m_\lambda} \sum_{i=1}^{m_q} G_\lambda^k \hat{H}_{(q,i)} \sum_{l=1}^{i} \left(\frac{\psi_l}{(z-q)^l} - \frac{\kappa_l}{z-p_l} \right)$$

where ψ_l and κ_l are from Lemma 9.

$$\begin{aligned}
&\left\| \sum_{\lambda\in\hat{\sigma}} \sum_{q\in\mathcal{Q}} \sum_{k=1}^{m_\lambda} \sum_{i=1}^{m_q} G_\lambda^k \hat{H}_{(q,i)} \sum_{l=1}^{i} \left(\frac{\psi_l}{(z-q)^l} - \frac{\kappa_l}{z-p_l} \right) \right\|_2 \\
&\overset{\text{triangle inequality}}{\leq} \sum_{\lambda\in\hat{\sigma}} \sum_{q\in\mathcal{Q}} \sum_{k=1}^{m_\lambda} \sum_{i=1}^{m_q} \left\| G_\lambda^k \hat{H}_{(q,i)} \right\|_2 \left| \sum_{l=1}^{i} \left(\frac{\psi_l}{(z-q)^l} - \frac{\kappa_l}{z-p_l} \right) \right| \\
&\overset{(5.64)}{\leq} \sum_{\lambda\in\hat{\sigma}} \sum_{q\in\mathcal{Q}} \sum_{k=1}^{m_\lambda} \sum_{i=1}^{m_q} \left\| G_\lambda^k \hat{H}_{(q,i)} \right\|_2 \binom{k+i-1}{k} \frac{(|q|+2)^{k+i} - (|q|+1)^{k+i}}{d(q,\partial\mathbb{D})^{k+i}(1-r)^{k+i}} \hat{d}(q) \\
&= KD(\mathcal{P}).
\end{aligned}$$

Thus, (5.77) is proved. Combining (5.76) and (5.77) completes the proof of (5.74).

The proof of (5.75) proceeds analogously. It begins by constructing a transfer function W with simple poles to approximate $\hat{W}$, and then follows the same reasoning as in the proof of (5.74), except that G now post-multiplies the corresponding terms. □

Lemma 10 *Let $(\Phi_{\varsigma x}^*, \Phi_{\omega x}^*, \Phi_{\varsigma u}^*, \Phi_{\omega u}^*)$ denote the optimal solution in (5.6). Then there exist $\Phi_{\omega u} \in \mathcal{RH}_\infty$, $\Phi_{\varsigma x}, \Phi_{\omega x}, \Phi_{\varsigma u} \in \frac{1}{z}\mathcal{RH}_\infty$ which are a feasible solution to relationships (5.6b) and (5.6c) after SPA, and constants $K_{\varsigma x}^\bullet, K_{\omega x}^\bullet, K_{\varsigma u}^\bullet, K_{\omega u}^\bullet > 0$, $\bullet \in \{2, \infty\}$, such that*

$$\|\Phi_{\omega x} - \Phi_{\omega x}^*\|_{\mathcal{H}_\bullet} \leq K_{\omega x}^\bullet D(\mathcal{P}), \|\Phi_{\omega u} - \Phi_{\omega u}^*\|_{\mathcal{H}_\bullet} \leq K_{\omega u}^\bullet D(\mathcal{P}) \tag{5.78}$$

$$\|\Phi_{\varsigma u} - \Phi_{\varsigma u}^*\|_{\mathcal{H}_\bullet} \leq K_{\varsigma u}^\bullet D(\mathcal{P}), \|\Phi_{\varsigma x} - \Phi_{\varsigma x}^*\|_{\mathcal{H}_\bullet} \leq K_{\varsigma x}^\bullet D(\mathcal{P}) \tag{5.79}$$

Proof of Lemma 10: For arbitrary fixed optimal solution $(\Phi^*_{\varsigma x}, \Phi^*_{\omega x}, \Phi^*_{\varsigma u}, \Phi^*_{\omega u})$, it satisfies these relationships in (5.26a)-(5.26d) shown as the equivalent expression of SLS constraints (5.6b) and (5.6c). For $\Phi^*_{\omega x} = (zI - A)^{-1}B\Phi^*_{\omega u}$ in (5.26c), by setting $G = (zI - A)^{-1}B$ and $U = 0$ in case (5.72) of Corollary 7, there exist $\Phi_{\omega u}$ and $\Phi_{\omega x}$ in $\mathcal{RH}_\infty$ which also satisfy (5.26c) and the approximating error bounds in (5.78) are guaranteed.

We also have $\Phi^*_{\varsigma u} = \Phi^*_{\omega u}C(zI-A)^{-1}$ by (5.26d), by setting $G = C(zI-A)^{-1}$ and $V = 0$ in case (5.73) of Corollary 7, there exists $\Phi_{\varsigma u} \in \mathcal{RH}_\infty$ approximating $\Phi^*_{\varsigma u}$ with respect to error bounds in (5.79).

The optimal solution $(\Phi^*_{\varsigma x}, \Phi^*_{\varsigma u})$ satisfies (5.26a), which is the same constraint in SLS state feedback policy, by [14, Lemma 2], the approximation error bounds for $\Phi_{\varsigma x}$ are assured. □

Lemma 11 *Let $(\Phi^*_{\omega y}, \Phi^*_{\upsilon y}, \Phi^*_{\omega u}, \Phi^*_{\upsilon u})$ denote the optimal solution in (5.7). Then there exist $\Phi_{\omega y}, \Phi_{\omega u}, \Phi_{\upsilon u} \in \mathcal{RH}_\infty$, $\Phi_{\upsilon y} \in \frac{1}{z}\mathcal{RH}_\infty$ which are a feasible solution to relationships (5.7b) and (5.7c) after SPA, and constants $K^\bullet_{\omega y}, K^\bullet_{\omega u}, K^\bullet_{\upsilon u}, K^\bullet_{\upsilon y}$, $\bullet \in \{2, \infty\}$, such that*

$$\|\Phi_{\omega y} - \Phi^*_{\omega y}\|_{\mathcal{H}_\bullet} \le K^\bullet_{\omega y} D(\mathcal{P}), \|\Phi_{\omega u} - \Phi^*_{\omega u}\|_{\mathcal{H}_\bullet} \le K^\bullet_{\omega u} D(\mathcal{P}) \tag{5.80}$$

$$\|\Phi_{\upsilon u} - \Phi^*_{\upsilon u}\|_{\mathcal{H}_\bullet} \le K^\bullet_{\upsilon u} D(\mathcal{P}), \|\Phi_{\upsilon y} - \Phi^*_{\upsilon y}\|_{\mathcal{H}_\bullet} \le K^\bullet_{\upsilon y} D(\mathcal{P}) \tag{5.81}$$

Proof of Lemma 11: For any fixed optimal solution $(\Phi^*_{\omega y}, \Phi^*_{\upsilon y}, \Phi^*_{\omega u}, \Phi^*_{\upsilon u})$, it satisfies these relationships in (5.32a)-(5.32d). For $\Phi^*_{\omega y} = G\Phi^*_{\omega u} + I$ in (5.32a), by setting $U = I$ in case (5.72) of Corollary 7, there exist $\Phi_{\omega y}$ and $\Phi_{\omega u}$ in $\mathcal{RH}_\infty$ which also satisfy (5.32a) and the approximating error bounds in (5.80) are guaranteed.

Analogously for $\Phi^*_{\upsilon y} = \Phi^*_{\omega y}G$ from (5.32c) and $\Phi^*_{\upsilon u} = \Phi^*_{\omega u}G + I$ from (5.32d), apply Corollary 7 case (5.73) with $V = 0$ and $V = I$ respectively to obtain error bounds in (5.81). □

Lemma 12 *Let $(\Phi^*_{\varsigma y}, \Phi^*_{\omega y}, \Phi^*_{\varsigma u}, \Phi^*_{\omega u})$ denote the optimal solution in (5.8). Then there exist $\Phi_{\omega y}, \Phi_{\omega u} \in \mathcal{RH}_\infty$, $\Phi_{\varsigma y}, \Phi_{\varsigma u} \in \frac{1}{z}\mathcal{RH}_\infty$ which are a feasible solution to relationships (5.8b) and (5.8c) after SPA, and constants $K^\bullet_{\varsigma y}, K^\bullet_{\omega y}, K^\bullet_{\varsigma u}, K^\bullet_{\omega u}$, $\bullet \in \{2, \infty\}$, such that*

$$\|\Phi_{\omega y} - \Phi^*_{\omega y}\|_{\mathcal{H}_\bullet} \le K^\bullet_{\omega y} D(\mathcal{P}), \|\Phi_{\omega u} - \Phi^*_{\omega u}\|_{\mathcal{H}_\bullet} \le K^\bullet_{\omega u} D(\mathcal{P}) \tag{5.82}$$

$$\|\Phi_{\varsigma u} - \Phi^*_{\varsigma u}\|_{\mathcal{H}_\bullet} \le K^\bullet_{\varsigma u} D(\mathcal{P}), \|\Phi_{\varsigma y} - \Phi^*_{\varsigma y}\|_{\mathcal{H}_\bullet} \le K^\bullet_{\varsigma y} D(\mathcal{P}) \tag{5.83}$$

Proof of Lemma 12: For any fixed optimal solution $(\Phi^*_{\varsigma y}, \Phi^*_{\omega y}, \Phi^*_{\varsigma u}, \Phi^*_{\omega u})$, it satisfies constraints (5.46). For $\Phi^*_{\omega y} = G\Phi^*_{\omega u} + I$ from (5.46b), by setting $U = I$ in case (5.72) of

Corollary 7, there exist transfer functions $\Phi_{\omega y}$ and $\Phi_{\omega u}$ in $\mathcal{RH}_\infty$ which also satisfy (5.46b), and the corresponding approximation error bounds stated in (5.82) are guaranteed.

By taking a right inverse of $zI - A$ in (5.46c) and (5.46d), and observing that $\Phi^*_{\varsigma y} = \Phi^*_{\omega y} G_c$ from (5.46c) and $\Phi^*_{\varsigma u} = \Phi^*_{\omega u} G_c$ from (5.46d), we can apply Corollary 7, case (5.73) with $V = 0$, to similarly obtain the approximation error bounds in (5.83). □

Lemma 13 *Let* $(\Phi^*_{\omega x}, \Phi^*_{\upsilon x}, \Phi^*_{\omega u}, \Phi^*_{\upsilon u})$ *denote the optimal solution in* (5.9). *Then there exist* $\Phi_{\omega u}, \Phi_{\upsilon u} \in \mathcal{RH}_\infty$, $\Phi_{\omega x}, \Phi_{\upsilon x} \in \frac{1}{z}\mathcal{RH}_\infty$ *which are a feasible solution to relationships* (5.9b) *and* (5.9c) *after SPA, and constants* $K^\bullet_{\omega x}, K^\bullet_{\upsilon x}, K^\bullet_{\omega u}, K^\bullet_{\upsilon u}$, $\bullet \in \{2, \infty\}$, *such that*

$$\|\Phi_{\upsilon u} - \Phi^*_{\upsilon u}\|_{\mathcal{H}_\bullet} \le K^\bullet_{\upsilon u} D(\mathcal{P}), \|\Phi_{\omega u} - \Phi^*_{\omega u}\|_{\mathcal{H}_\bullet} \le K^\bullet_{\omega u} D(\mathcal{P}) \tag{5.84}$$

$$\|\Phi_{\upsilon x} - \Phi^*_{\upsilon x}\|_{\mathcal{H}_\bullet} \le K^\bullet_{\upsilon x} D(\mathcal{P}), \|\Phi_{\omega x} - \Phi^*_{\omega x}\|_{\mathcal{H}_\bullet} \le K^\bullet_{\omega x} D(\mathcal{P}) \tag{5.85}$$

Proof of Lemma 13: For any fixed optimal solution $(\Phi^*_{\omega x}, \Phi^*_{\upsilon x}, \Phi^*_{\omega u}, \Phi^*_{\upsilon u})$, it satisfies constraints (5.51). To show (5.84) and (5.85), one possible approach is to follow a derivation similar to the proof of Lemma 12. Here we provide a more straightforward method as well.

Observe that $\Phi^*_{\upsilon x} = \Phi^*_{\omega x} G + G_B$ from (5.51c) and $\Phi^*_{\upsilon u} = \Phi^*_{\omega u} G + I$ from (5.51d). By setting $V = G_B$ and $V = I$, respectively, in case (5.73) of Corollary 7, we obtain transfer functions $\Phi_{\upsilon x}$, $\Phi_{\omega x}$ and $\Phi_{\upsilon u}$, $\Phi_{\omega u}$ in $\mathcal{RH}_\infty$ which also satisfy (5.51c) and (5.51d), respectively. Moreover, the corresponding approximation error bounds stated in (5.85) and (5.84) are guaranteed. □

Proof of Theorem 7: The proof follows similarly to the [14, Proof of Theorem 1] by applying the approximation error bounds of Lemma 10 to the optimal solution of (5.4) to obtain the desired suboptimality bounds. □

Proof of Theorem 8: The proof follows similarly to the [14, Proof of Theorem 1] by applying the approximation error bounds of Lemma 11 to the optimal solution of (5.4) to obtain the desired suboptimality bounds. □

Proof of Theorem 9: The proof follows similarly to the [14, Proof of Theorem 1] by applying the approximation error bounds of Lemma 12 to the optimal solution of (5.4) to obtain the desired suboptimality bounds. □

Proof of Theorem 10: The proof follows similarly to the [14, Proof of Theorem 1] by applying the approximation error bounds of Lemma 13 to the optimal solution of (5.4) to obtain the desired suboptimality bounds. □

5.7 Conclusion

This chapter presented a unified framework for $\mathcal{H}_2/\mathcal{H}_\infty$ output feedback control synthesis by combining four recently developed convex reparameterization methods with the SPA. By adapting the hybrid state space and frequency domain approach from state feedback to output feedback, we formulated convex and tractable SDPs consisting of LMIs and affine constraints, which avoid the approximation errors inherent in finite-horizon norm evaluations and can be solved efficiently. We provided, for the first time, suboptimality certificates for output feedback control design methods under each convex reparameterization. These results characterize how the suboptimality tends to zero as the number of poles approaches infinity and were further specialized to include a convergence rate for a particular pole selection along an Archimedes spiral.

Chapter 6

Constrained $\mathcal{H}_2/\mathcal{H}_\infty$ Control Design of Dynamic Virtual Power Plants

In this chapter, the hybrid state space control design framework is extended to aggregative synthesis. The proposed hybrid domain method offers bounded suboptimality [12], handles state, input, output, and coupling constraints without conservatism, and avoids manual controller tuning. Its effectiveness is demonstrated in Section 6.4, where coordinated DER control enables grid-level voltage and frequency regulation. Some DVPP background is introduced in Section 6.1. A valuable state space realization of the aggregate closed-loop system and the derivation of the control design methods are presented in Section 6.2. A novel multicontrol design method is shown in Section 6.3. A case study is provided in Section 6.4. Finally, Section 6.5 offers concluding remarks.

6.1 DVPP Control Setup

Consider a DVPP control framework comprising a collection of heterogeneous DERs [17]. All units within the DVPP are assumed to be connected to the same bus of the transmission grid, where they receive common input signals, the measured bus frequency deviation Δf and voltage magnitude deviation Δv. The active and reactive power deviation output of each device i, namely Δp_i and Δq_i, respectively (deviating from the respective power set point), sum up to the aggregate active and reactive power deviation output of the DVPP, namely Δp_{agg} and Δq_{agg} , respectively, i.e.,

$$\begin{bmatrix} \Delta p_{\text{agg}} \\ \Delta q_{\text{agg}} \end{bmatrix} = \sum_{i \in \mathcal{N}} \begin{bmatrix} \Delta p_i \\ \Delta q_i \end{bmatrix}. \tag{6.1}$$

Table 6.1: List of Notation for the DVPP Control Setup

Description	Symbol
Set of DVPP devices	$\mathcal{N}$
DVPP devices index	i
Measured bus frequency deviation	Δf
Measured bus voltage magnitude deviation	Δv
Active power deviation output of device i	Δp_i
Reactive power deviation output of device i	Δq_i
Aggregate active power deviation output of the DVPP	Δp_{agg}
Aggregate reactive power deviation output of the DVPP	Δq_{agg}
Desired active power deviation output of the DVPP	Δp_{des}
Desired reactive power deviation output of the DVPP	Δq_{des}
Local closed-loop transfer matrix of device i	$T_i(z)$
Desired MIMO transfer matrix of the DVPP	$T_{\text{des}}(z)$
Desired DVPP transfer function for the f-p channel	$T_{\text{des}}^{\text{fp}}(z)$
Desired DVPP transfer function for the v-q channel	$T_{\text{des}}^{\text{vq}}(z)$

The local closed-loop transfer matrices $T_i(z) \in \mathbb{R}^{2\times 2}$ associated with the devices $i \in \mathcal{N}$ can be systematically shaped through the design of suitable feedback controllers. More details can be found in Section 6.1.1.

The aggregate behavior of the DVPP is characterized by

$$\begin{bmatrix} \Delta p_{\text{agg}}(z) \\ \Delta q_{\text{agg}}(z) \end{bmatrix} = \sum_{i\in\mathcal{N}} T_i(z) \begin{bmatrix} \Delta f(z) \\ \Delta v(z) \end{bmatrix}. \tag{6.2}$$

To replicate the ancillary services traditionally provided by synchronous generators in transmission systems, a decoupled active power frequency (f-p) and reactive power voltage (v-q) dynamic response is prescribed for the aggregate DVPP as a desired diagonal MIMO transfer matrix as

$$\begin{bmatrix} \Delta p_{\text{des}}(z) \\ \Delta q_{\text{des}}(z) \end{bmatrix} = \underbrace{\begin{bmatrix} T_{\text{des}}^{\text{fp}}(z) & 0 \\ 0 & T_{\text{des}}^{\text{vq}}(z) \end{bmatrix}}_{=: T_{\text{des}}(z)} \begin{bmatrix} \Delta f(z) \\ \Delta v(z) \end{bmatrix}. \tag{6.3}$$

The DVPP control design problem is to find local controllers for the controllable devices

$\mathcal{C}$, such that the following aggregation condition holds:

$$\sum_{i \in \mathcal{N}} T_i(z) \stackrel{!}{=} T_{\text{des}}(z) \tag{6.4}$$

where "$\stackrel{!}{=}$" indicates that the terms on the left hand side of the equality achieve the right side as closely as possible.

During control design, it is essential to respect each device's physical limits, such as bandwidth, power availability, and current capacity, under normal operation. Moreover, the DVPP must be sufficiently diverse to span all relevant time scales and power levels. We assume the desired reference T_{des} is specified by the system operator so that it is achievable by the ensemble, guarantees closed-loop stability, and remains robust to grid uncertainties and parameter variations.

6.1.1 $\mathcal{H}_2/\mathcal{H}_\infty$ Control Design

To find local feedback controls for the devices $\mathcal{N}$ to ensure their closed-loop transfer matrices T_i satisfy the aggregation condition (6.4), we consider LTI systems in discrete time described by the following state space representation:

$$\begin{aligned} x_i^{k+1} &= A_i x_i^k + B_i u_i^k + \hat{B}_i w^k \\ y_i^k &= C_i x_i^k \end{aligned} \tag{6.5}$$

where $x_i^k \in \mathbb{R}^n$, $u_i^k \in \mathbb{R}^p$, $y_i^k \in \mathbb{R}^m$ are the states, controller signal, and performance output vectors at time step k for each device $i \in \mathcal{N}$, respectively, note that all devices are subject to a common disturbance input $w^k \in \mathbb{R}^q$ as they are connected in parallel. It will be useful to define the signal $v_i^k = \hat{B}_i w^k$.

In this chapter, the mixed $\mathcal{H}_2/\mathcal{H}_\infty$ state feedback control design framework of Section 2.2 is extended to accommodate multicontroller scenarios. We consider linear state feedback control laws of the form $u_i(z) = K_i(z)x_i(z)$ for each device $i \in \mathcal{N}$, where $K_i(z)$ is a dynamic controller. The closed-loop transfer function mapping disturbance w to each output y_i is $T_{w \to y_i}(z)$, and $T_{w \to u_i}(z)$, $T_{v_i \to x_i}(z)$, and $T_{v_i \to u_i}(z)$ are defined analogously. And $T_{\text{des}}(z)$ in (6.3) is the desired closed-loop transfer function for model matching control design.

The goal of this chapter is to design local controllers $K_i(z)$ such that their collection is

a solution to the following mixed $\mathcal{H}_2/\mathcal{H}_\infty$ model matching problem

$$\begin{aligned} \underset{\{K_i(z)\}_{i\in\mathcal{N}}}{\text{minimize}} \quad & \left\| \begin{bmatrix} Q & 0 \\ 0 & R \end{bmatrix} \begin{bmatrix} \sum_{i\in\mathcal{N}} T_{w\to y_i}(z) - T_{\text{des}}(z) \\ \sum_{i\in\mathcal{N}} T_{w\to u_i}(z) \end{bmatrix} \right\|_{\mathcal{H}_2/\mathcal{H}_\infty} \\ \text{subject to} \quad & T_{v_i\to x_i}(z), T_{v_i\to u_i}(z) \in \mathcal{R}_i, \ \forall i \in \mathcal{N} \end{aligned} \tag{6.6}$$

where the mixed $\mathcal{H}_2/\mathcal{H}_\infty$ norm is given by $\|T\|_{\mathcal{H}_2/\mathcal{H}_\infty} = \|T\|_{\mathcal{H}_2} + \lambda\|T\|_{\mathcal{H}_\infty}$ for some constant $\lambda \in [0,\infty]$. The constant matrices Q and R represent the weights on output and input, respectively. $\mathcal{R}_i$ is the Hardy space of real, rational, strictly proper, and stable transfer functions for device i, that additionally satisfy time-dependent constraints:

i) The trajectories of the *states, inputs, and outputs* induced by known disturbance signals $w^{0:T}$ over a finite horizon T are given by

$$x_i^{0:T} = \mathcal{C}^{0:T}[T_{v_i\to x_i}(z)]v_i^{0:T}, \tag{6.7}$$
$$u_i^{0:T} = \mathcal{C}^{0:T}[T_{v_i\to u_i}(z)]v_i^{0:T}, \tag{6.8}$$
$$y_i^{0:T} = \mathcal{C}^{0:T}[T_{v_i\to y_i}(z)]v_i^{0:T}, \tag{6.9}$$

and are required to satisfy the prescribed bounds $m_{x,i}$, $m_{u,i}$, and $m_{y,i}$, respectively.

ii) *Steady state gain* in response to a unit step input exists and can be computed using the final value theorem as

$$y_i^\infty = \lim_{z\to 1} T_{w\to y_i}(z) \tag{6.10}$$

for all devices $i \in \mathcal{N}$. Note that (6.6) is nonconvex in $\{K_i(z)\}_{i\in\mathcal{N}}$ since $T_{w\to y_i}(z)$ and $T_{w\to u_i}(z)$ are, so this problem is challenging to solve in this form.

Similar to the approach in Section 2.2 using SLS, equations (6.6)-(6.10) can be equivalently reformulated as follows:

$$\underset{\{\Phi_{x,i},\Phi_{u,i}\}_{i\in\mathcal{N}}}{\text{minimize}} \quad \left\| \begin{bmatrix} Q & 0 \\ 0 & R \end{bmatrix} \begin{bmatrix} \sum_{i\in\mathcal{N}} \tilde{\Phi}_{x,i} - T_{\text{des}} \\ \sum_{i\in\mathcal{N}} \tilde{\Phi}_{u,i} \end{bmatrix} \right\|_{\mathcal{H}_2/\mathcal{H}_\infty} \tag{6.11a}$$

$$\text{subject to} \quad (zI - A_i)\Phi_{x,i}(z) - B_i\Phi_{u,i}(z) = I, \tag{6.11b}$$

$$\Phi_{x,i}(z), \Phi_{u,i}(z) \in \frac{1}{z}\mathcal{R}\mathcal{H}_\infty \tag{6.11c}$$

$$x_i^k = \sum_{l=0}^{k} \mathcal{J}^{k-l}\left[\Phi_{x,i}\right]\hat{B}_i w^l \le m_{x,i}, \ \forall i \in \mathcal{N}, \ \forall k \in [0,T] \tag{6.11d}$$

$$u_i^k = \sum_{l=0}^{k} \mathcal{J}^{k-l} \left[\Phi_{u,i}\right] \hat{B}_i w^l \leq m_{u,i},\ \forall i \in \mathcal{N},\ \forall k \in [0,T] \tag{6.11e}$$

$$y_i^k = \sum_{l=0}^{k} C_i \mathcal{J}^{k-l} \left[\Phi_{x,i}\right] \hat{B}_i w^l \leq m_{y,i},\ \forall i \in \mathcal{N},\ \forall k \in [0,T] \tag{6.11f}$$

$$y_i^T = C_i \Phi_{x,i}(1) \hat{B}_i,\ \forall i \in \mathcal{N} \tag{6.11g}$$

where $\Phi_{x,i}(z)$ and $\Phi_{u,i}(z)$ are the design variables, corresponding to the closed-loop transfer functions $T_{v_i \to x_i}(z)$ and $T_{v_i \to u_i}(z)$, respectively. We define $\tilde{\Phi}_{x,i}(z) = T_{w \to y_i}(z) = C_i \Phi_{x,i}(z) \hat{B}_i$ and $\tilde{\Phi}_{u,i}(z) = T_{w \to u_i}(z) = \Phi_{u,i}(z) \hat{B}_i$. The constraint (6.11c) guarantees the stability and well-posedness of the closed-loop system, while (6.11b) imposes an additional affine constraint required by SLS. By expressing the relevant transfer functions using the SLS variables and representing convolution operators through impulse responses, state, input and output constraints (6.7)–(6.9) naturally lead to (6.11d)–(6.11f) at time k. Furthermore, the steady-state gain constraint in (6.10) is captured by (6.11g) over the steady state gain is accurate over an infinite time horizon by the final value theorem. The controller for each device can be recovered locally as $K_i(z) = \Phi_{u,i}(z) \Phi_{x,i}^{-1}(z)$ based only on local information, i.e., $\Phi_{x,i}(z)$ and $\Phi_{u,i}(z)$. Note that (6.11) becomes convex under this reparameterization, although still infinite-dimensional since $\Phi_{x,i}(z)$ and $\Phi_{u,i}(z)$ lie in the infinite dimensional function space $\frac{1}{z}\mathcal{RH}_\infty$.

To circumvent this issue, as single control design in Section 4.2 approximates the closed-loop transfer functions using a finite selection of simple stable poles $\{\mathcal{P}_i\}_{i \in \mathcal{N}}$, closed under complex conjugation, as

$$\Phi_{x,i}(z) = \sum_{p \in \mathcal{P}_i} G_{p,i} \frac{1}{z-p},\ \Phi_{u,i}(z) = \sum_{p \in \mathcal{P}_i} H_{p,i} \frac{1}{z-p} \tag{6.12}$$

where $G_{p,i}$ and $H_{p,i}$ are (complex) coefficient matrices for each $p \in \mathcal{P}_i$ and $i \in \mathcal{N}$. This simple pole approximation (SPA) renders (6.11) finite dimensional. In [12], a hybrid state space and frequency domain control design framework is proposed to address the optimization after (6.11) and (6.12) as a semidefinite program, and the suboptimality of the solution of SLS with SPA will tend to zero as the number of poles approaches infinity. In the following part of the chapter, we extend this framework to the multi-controller design problem for DVPP control.

For SPA, since $\Phi_{x,i}(z)$ and $\Phi_{u,i}(z)$ are real, it is straightforward to show that for any real pole p, $G_{p,i}$ and $H_{p,i}$ are real, and for any complex pole p, $G_{\overline{p},i} = \overline{G_{p,i}}$ and $H_{\overline{p},i} = \overline{H_{p,i}}$. Let $\mathcal{P}_{r,i}$ denote the real poles in $\mathcal{P}_i$, and let $\mathcal{P}_{c,i}$ denote its complex poles in device $i \in \mathcal{N}$. Then $\mathcal{P}_i = \mathcal{P}_{r,i} \cup \mathcal{P}_{c,i}$.

6.2 Control Design Derivation

To derive the proposed hybrid state space and frequency domain control design method, we will require a state space realization of the closed-loop transfer functions. In this section, we propose novel state space realizations of the entire closed-loop dynamics in DVPP based on the simple pole approximation, and then the control design will be derived.

For any $p \in \mathcal{P}_{c,i}$, its conjugate $\overline{p}$ is also in $\mathcal{P}_{c,i}$, their corresponding coefficient matrices are:

$$\begin{aligned} G_{p,i} &= \mathrm{Re}(G_{p,i}) + \mathrm{Im}(G_{p,i})j \quad G_{\overline{p},i} = \mathrm{Re}(G_{p,i}) - \mathrm{Im}(G_{p,i})j, \\ H_{p,i} &= \mathrm{Re}(H_{p,i}) + \mathrm{Im}(H_{p,i})j \quad H_{\overline{p},i} = \mathrm{Re}(H_{p,i}) - \mathrm{Im}(H_{p,i})j. \end{aligned} \tag{6.13}$$

For simplicity, the subscript i in $G_{p,i}$ and $H_{p,i}$ is omitted whenever it does not cause ambiguity.

We first find the realization of the individual closed-loop transfer functions $\tilde{\Phi}_{x,i}(z)$ and $\tilde{\Phi}_{u,i}(z)$ for each device $i \in \mathcal{N}$. To do so, for each complex conjugate pair $p, \overline{p} \in \mathcal{P}_{c,i}$, define the matrix

$$M(p) = \begin{bmatrix} \mathrm{Re}(p) & \mathrm{Im}(p) \\ -\mathrm{Im}(p) & \mathrm{Re}(p) \end{bmatrix},$$

and let $\mathcal{M}_{c,i}$ be the collection of $M(p)$ for all such complex conjugate pairs. Let $\mathcal{M}_{r,i}$ be the collection of each scalar matrix p for all $p \in \mathcal{P}_{r,i}$. Then we can define

$$\begin{aligned} \overline{A}_i &= \begin{bmatrix} \mathcal{D}(\mathcal{M}_{r,i}) & \\ & \mathcal{D}(\mathcal{M}_{c,i}) \end{bmatrix} \otimes I, \\ \overline{B}_i &= \big[\underbrace{I \quad \cdots \quad I}_{|\mathcal{P}_{r,i}|} \quad \underbrace{2I \quad 0 \quad \cdots \quad 2I \quad 0}_{|\mathcal{P}_{c,i}|} \big]^{\mathsf{T}} \hat{B}_i. \end{aligned}$$

Next, for each complex conjugate pair $p, \overline{p} \in \mathcal{P}_{c,i}$, define the matrices

$$G(p) = \begin{bmatrix} \mathrm{Re}(G_{p,i}) & \mathrm{Im}(G_{p,i}) \end{bmatrix}, H(p) = \begin{bmatrix} \mathrm{Re}(H_{p,i}) & \mathrm{Im}(H_{p,i}) \end{bmatrix},$$

and let $\mathcal{G}_{c,i}$ and $\mathcal{H}_{c,i}$ be the collection of $G(p)$ and $H(p)$, respectively, for all such complex conjugate pairs. Let $\mathcal{G}_{r,i}$ and $\mathcal{H}_{r,i}$ be the collection of G_p and H_p, respectively, for each $p \in \mathcal{P}_{r,i}$. Then we define

$$\begin{aligned} \overline{C}_{x,i} &= C \begin{bmatrix} \mathcal{R}(\mathcal{G}_{r,i}) & \mathcal{R}(\mathcal{G}_{c,i}) \end{bmatrix}, \\ \overline{C}_{u,i} &= \begin{bmatrix} \mathcal{R}(\mathcal{H}_{r,i}) & \mathcal{R}(\mathcal{H}_{c,i}) \end{bmatrix}. \end{aligned}$$

It is straightforward to verify that $(\overline{A}_i, \overline{B}_i, \overline{C}_{x,i}, 0)$ is a real state space realization of $\tilde{\Phi}_{x,i}(z)$, and that $(\overline{A}_i, \overline{B}_i, \overline{C}_{u,i}, 0)$ is a real state space realization of $\tilde{\Phi}_{u,i}(z)$ from Section 3.3.

Let $(A_{\text{des}}, B_{\text{des}}, C_{\text{des}}, 0)$ be any real state space realization of T_{des}. Now we can represent the transfer function in the objective (6.11a) using the following real state space realization

$$\begin{aligned}\tilde{A} &= \begin{bmatrix} \overline{A}_1 & 0 & \cdots & 0 & 0 \\ 0 & \overline{A}_2 & \cdots & 0 & 0 \\ \vdots & \vdots & \ddots & \vdots & \vdots \\ 0 & 0 & \cdots & \overline{A}_{|\mathcal{N}|} & 0 \\ 0 & 0 & \cdots & 0 & A_{\text{des}} \end{bmatrix}, \quad \tilde{B} = \begin{bmatrix} \overline{B}_1 \\ \overline{B}_2 \\ \vdots \\ \overline{B}_{|\mathcal{N}|} \\ B_{\text{des}} \end{bmatrix}, \\ \tilde{C} &= \begin{bmatrix} Q\overline{C}_{x,1} & Q\overline{C}_{x,2} & \cdots & Q\overline{C}_{x,|\mathcal{N}|} & -QC_{\text{des}} \\ R\overline{C}_{u,1} & R\overline{C}_{u,2} & \cdots & R\overline{C}_{u,|\mathcal{N}|} & 0 \end{bmatrix}. \end{aligned} \tag{6.14}$$

which satisfies

$$\tilde{C}(zI - \tilde{A})^{-1}\tilde{B} = \begin{bmatrix} Q & 0 \\ 0 & R \end{bmatrix} \begin{bmatrix} \sum_{i\in\mathcal{N}} \tilde{\Phi}_{x,i} - T_{\text{des}} \\ \sum_{i\in\mathcal{N}} \tilde{\Phi}_{u,i} \end{bmatrix} =: \Phi(z). \tag{6.15}$$

Thus, we have obtained an equivalent state space representation of the closed-loop transfer function $\Phi(z)$, which will be used to develop our novel control design method. Note that for a fixed collection of simple poles $\cup_{i\in\mathcal{N}}\mathcal{P}_i$, as used for SPA, $\tilde{A}$ and $\tilde{B}$ are constant matrices, and $\tilde{C}$ is an affine function of all of the variable coefficients $G_{p,i}$ and $H_{p,i}$.

The control design optimization problem is derived analogously to the single controller case in Section 3.3, with the notable exceptions that time-dependent constraints are incorporated and the state-space representation characterizes the aggregate closed-loop system. We begin with the SLS problem formulation (6.11) combined with SPA (6.12). The SLS constraints (6.11b) are represented for each device as in (3.6)-(3.8). The remaining constraints are formulated after applying SPA. Following similar arguments as in Section 3.3, we then express the objective function (6.11a) in terms of LMIs using the KYP lemma with the state-space representation of the objective.

For the SLS constraint (6.11b), substituting in the SPA (6.12) and matching coefficients of $\frac{1}{z-p}$ for each pole $p \in \mathcal{P}_i$ since these functions are linearly independent, we obtain

$$I = \sum_{p\in\mathcal{P}_{r,i}} G_{p,i} + 2\sum_{p\in\mathcal{P}_{c,i}} \text{Re}(G_{p,i}) = \sum_{p\in\mathcal{P}_i} G_{p,i} \tag{6.16}$$

for each $i \in \mathcal{N}$,

$$0 = (pI - A_i)\, G_{p,i} - B_i H_{p,i} \tag{6.17}$$

for each $i \in \mathcal{N}$ and $p \in \mathcal{P}_i$. Thus, the SLS constraint (6.11b) with the SPA (6.12) can be equivalently represented using (6.16)-(6.17).

Then, we address the design constraints on the state, input, output, and steady-state behavior using SPA. By [14], We denote the impulse response of $\Phi_{x,i}$ and $\Phi_{u,i}$ at time step k as $\mathcal{J}^k[\Phi_{x,i}] \coloneqq \sum_{p\in\mathcal{P}_i} G_{p,i}p^{k-1}$ and $\mathcal{J}^k[\Phi_{u,i}] \coloneqq \sum_{p\in\mathcal{P}_i} H_{p,i}p^{k-1}$, respectively. Thus we have

$$\sum_{l=0}^{k}\sum_{p\in\mathcal{P}_i} G_{p,i}p^{k-l-1}\hat{B}_i w^l \leq m_{x,i} \tag{6.18}$$

$$\sum_{l=0}^{k}\sum_{p\in\mathcal{P}_i} H_{p,i}p^{k-l-1}\hat{B}_i w^l \leq m_{u,i} \tag{6.19}$$

$$\sum_{l=0}^{k}\sum_{p\in\mathcal{P}_i} p^{k-l-1}C_i G_{p,i}\hat{B}_i w^l \leq m_{y,i} \tag{6.20}$$

$$C_i \sum_{p\in\mathcal{P}_i} G_{p,i}\frac{1}{1-p}\hat{B}_i = y_i^T. \tag{6.21}$$

Next, the $\mathcal{H}_2$ and $\mathcal{H}_\infty$ norms of the closed-loop transfer functions from the objective function (6.11a) are transferred as LMIs by using KYP lemma with the real state space realization $(\tilde{A}, \tilde{B}, \tilde{C}, 0)$ from (6.14) (more details can be found in Section 3.3).

6.3 DVPP Control Synthesis

In this section we present our hybrid state space and frequency domain DVPP control design method which does not require any finite time horizon approximations for computing the $\mathcal{H}_2$ and $\mathcal{H}_\infty$ norms of the closed-loop transfer functions. As a result, it has reduced suboptimality, better performance, and lower computational cost compared to prior work [14]. Combining constraints and LMIs derivation stated in Section 3.1, we obtain the following multicontrol design formulation for the solution to (6.11) with the SPA (6.12)

$$\underset{K_1,K_2,Z,\{G_{p,i},H_{p,i}\}_{i\in\mathcal{N}},\gamma_1,\gamma_2}{\text{minimize}} \quad \gamma_1 + \lambda\gamma_2 \tag{6.22a}$$

$$\text{subject to} \quad \begin{bmatrix} K_1 & K_1\tilde{A} & K_1\tilde{B} \\ \tilde{A}^\intercal K_1 & K_1 & 0 \\ \tilde{B}^\intercal K_1 & 0 & \gamma_1 I \end{bmatrix} \succ 0 \tag{6.22b}$$

$$\begin{bmatrix} K_1 & 0 & \tilde{C}(G_{p,i}, H_{p,i})^\intercal \\ 0 & I & 0 \\ \tilde{C}(G_{p,i}, H_{p,i}) & 0 & Z \end{bmatrix} \succ 0 \tag{6.22c}$$

$$\mathrm{Tr}(Z) < \gamma_1 \tag{6.22d}$$

$$\begin{bmatrix} K_2 & 0 & \tilde{A}^\intercal K_2 & \tilde{C}(G_{p,i}, H_{p,i})^\intercal \\ 0 & \gamma_2 I & \tilde{B}^\intercal K_2 & 0 \\ K_2\tilde{A} & K_2\tilde{B} & K_2 & 0 \\ \tilde{C}(G_{p,i}, H_{p,i}) & 0 & 0 & \gamma_2 I \end{bmatrix} \succ 0 \tag{6.22e}$$

$$\sum_{p \in \mathcal{P}_i} G_{p,i} = I, \qquad \forall i \in \mathcal{N} \tag{6.22f}$$

$$(pI - A_i)\, G_{p,i} - B_i H_{p,i} = 0, \qquad \forall p \in \mathcal{P}_i, \quad \forall i \in \mathcal{N} \tag{6.22g}$$

$$(6.18), (6.19), (6.20), (6.21), \qquad \forall k \in [0, T], \quad \forall i \in \mathcal{N} \tag{6.22h}$$

where $K_1, K_2 \in \mathbb{S}^{n \times (|\mathcal{P}||\mathcal{N}|)}$, $Z \in \mathbb{S}^m$, and γ_1, γ_2 are scalar variables that represent the $\mathcal{H}_2$ and $\mathcal{H}_\infty$ norms of the closed-loop transfer functions, respectively. Recall that $\tilde{A}$, $\tilde{B}$, and $\tilde{C}$ were defined in (6.14), but we write $\tilde{C} = \tilde{C}(G_{p,i}, H_{p,i})$ to emphasize that $\tilde{C}$ is an affine function of the coefficients $G_{p,i}$ and $H_{p,i}$ for all $p \in \mathcal{P}_i$.

Since, using SPA, we have already selected the closed-loop poles $\cup_{i \in \mathcal{N}} \mathcal{P}_i$, $\tilde{A}$ and $\tilde{B}$ are constant matrices, along with A, B, and C. Thus, the objective (6.22a) and the constraint (6.22g) are linear, the constraints (6.22f) and (6.21) are affine, the constraints (6.18)-(6.20) are affine inequalities since the disturbance w is known and the poles are fixed, so these are affine in the decision variables $G_{p,i}$ and $H_{p,i}$, and the constraints (6.22b)-(6.22e) are LMIs in the decision variables. Therefore, overall (6.22) is a convex SDP that can be solved efficiently. Note that the state space realizations of the closed-loop transfer functions from Section 6.2 were deliberately constructed to ensure that the constraints (6.22b)-(6.22e) become LMIs rather than nonconvex bilinear matrix inequalities by including all the decision variables $G_{p,i}, H_{p,i}$ in $\tilde{C}$ and leaving $\tilde{A}, \tilde{B}$ as constant matrices.

The hybrid state space and frequency domain control design method has been extended to multi controller systems. The suboptimality bound from [14, Corollary 1] applies immediately to this new design method, thus the suboptimality will tend to zero as the number of poles approaches infinity. As we will see in the test case in Section 6.4, only a small number of poles can often result in low suboptimality and good performance.

6.4 Test Case

To demonstrate the effectiveness of the proposed control design, we investigate a multi-variable DVPP setup that replaces the fast frequency and voltage control traditionally provided by a thermal-based generator. The DVPP consists of an aggregation of DERs, including wind turbines (WTs), photovoltaics (PVs), and energy storage systems (ESs), which collectively provide fast frequency and voltage regulation services to the power grid. Specifically, we consider the IEEE 9-bus power system [4], a benchmark network comprising nine nodes, three synchronous generators, three loads, six transmission lines, and three transformers. In our setup, the thermal-based power plant at bus 3 is replaced by a DVPP, which includes a wind power plant, a PV system, and a battery energy storage system (BESS). The DVPP is designed to replicate f-p and v-q control characteristics of the original thermal unit. To assess system performance, we consider a disturbance from a step change in the load.

For individual DER, the continuous-time model in [17] shown here

$$\begin{aligned} \dot{x}_{pll} &= v^q \\ \dot{\theta}_{pll} &= k_{p,pll} v^q + k_{i,pll} x_{pll} \\ C\dot{v} &= -C\omega^* J_2 v + i_s - i \\ L\dot{i}_s &= -\left(L\omega^* J_2 + RI_2\right) i_s + v_s - v \end{aligned} \tag{6.23}$$

is normalized to define c_d and c_q. The outputs are the active and reactive power injections. Key model parameters include the phase locked loop gains $k_{p,\text{pll}}$ and $k_{i,\text{pll}}$, the sampling time h, and the time constants τ_d and τ_q associated with the d- and q-axis current control loops, where we set $k_{i,\text{pll}} = 1700, k_{p,\text{pll}} = 150$ and $h = 0.0167$ in the simulation process. The parameter τ_i is the time constant of each DER and is equal to 1.5, 0.6 and 0.2 seconds for WT, PV and ES, respectively.

In addition, we want to substitute the services of the thermal-based power plant, and specify a f-p and v-q control as

$$\begin{bmatrix} \Delta p \\ \Delta q \end{bmatrix} = \begin{bmatrix} \frac{-1.1052}{z-0.944} & \\ & \frac{-1.1389}{z-0.944} \end{bmatrix} \begin{bmatrix} \Delta f \\ \Delta v \end{bmatrix}, \tag{6.24}$$

then we employ the $\mathcal{H}_2/\mathcal{H}_\infty$ matching control method in the outer control loop of each grid-side converter to match the desired accumulated by closed-loop dynamics of the DVPP 3 devices. We now aim to regulate the entire reference current to participate in the desired f-p and v-q control of DVPP 3 in (6.24). In this regard, we consider the previous converter

model in (6.23), as well as the active and reactive power outputs as our plant model for control design.

For the control design, we choose $Q = I_2$, $R = 0.01I_2$, and $\lambda = 0.5$. For the SPA pole selection $\mathcal{P}$, we set the maximum number of closed-loop poles at $l = 15$. To form $\mathcal{P}$ we first incorporate the plant poles and the poles of the desired transfer function. The remaining poles are chosen along an Archimedes spiral as in [13]. We solve the SDP for the control design using MOSEK [2] in conjunction with YALMIP [19] in MATLAB.

The step responses for the desired transfer function in (6.24) and the aggregate response of all DVPP devices are shown in Fig. 6.1, where the DVPP output almost perfectly matches the desired response, demonstrating the extraordinary performance of the DVPP control design. Fig. 6.2 depicts the individual step responses of WT, PV, and ES to a unit disturbance. In the active-power plots (left), storage delivers a fast, brief pulse, PV provides a moderate sustained adjustment, and wind ramps slowly to the largest offset. In the reactive-power plots (right), storage is again fastest, PV is intermediate, and wind is slowest with the highest magnitude. Together, these complementary dynamics ensure that the aggregate DVPP can provide fast initial support via storage, sustained correction via PV, and long-term compensation via wind, which demonstrates the overall system's benefits arising from DER heterogeneity.

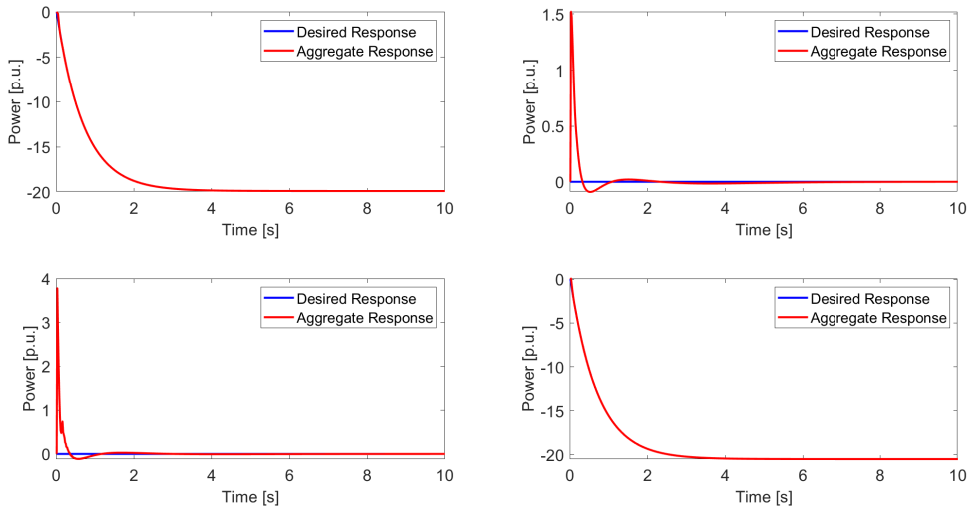

Figure 6.1: Aggregate DVPP step response

Fig. 6.3 plots each device's apparent power output (solid) alongside its limit (dashed). Following a small disturbance, all devices exhibit only minor transients and remain strictly within their apparent-power bounds, confirming that the imposed constraints are satisfied.

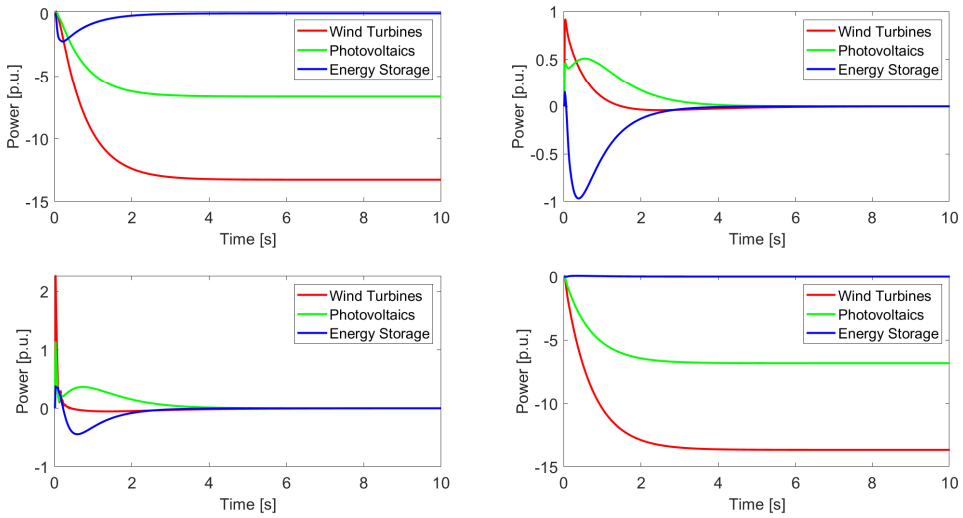

Figure 6.2: Individual step response of each device

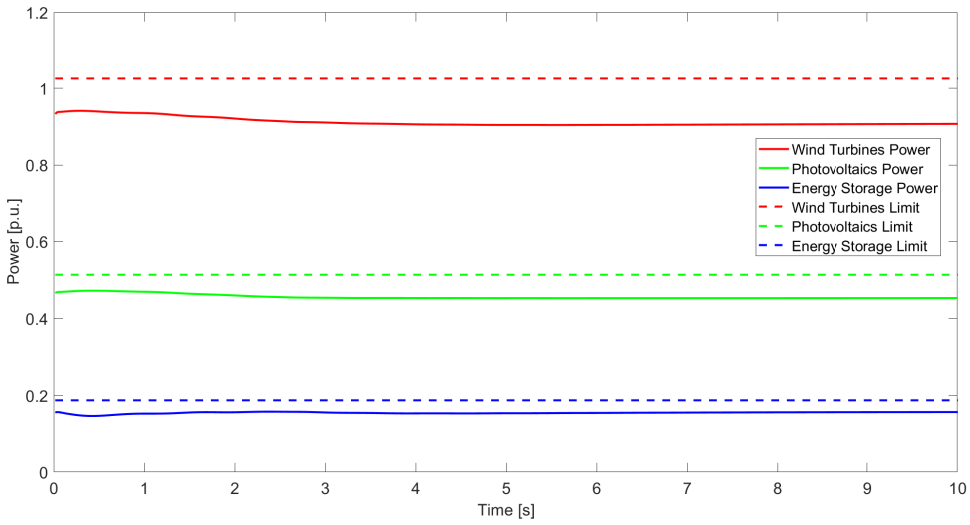

Figure 6.3: Individual device apparent power disturbance responses

6.5 Conclusion

We have presented a tractable control framework for DVPPs that rigorously addresses the joint challenges of renewable variability and device-level constraints. By extending SLS with SPA to a multi-controller setting, our method yields a convex semidefinite program whose solutions come with guaranteed suboptimality bounds. Local linear state feedback $\mathcal{H}_2/\mathcal{H}_\infty$ controllers synthesized in this way ensure that the aggregate DVPP response closely matches a desired reference model while enforcing state, input, and output limits on each DER. A comprehensive case study on the IEEE nine-bus system demonstrates the efficacy of our approach. The results confirm that heterogeneous converter-interfaced DERs can be coordinated to deliver reliable frequency and voltage regulation in aggregate to the power grid while respecting individual device limitations.

Chapter 7

Conclusion and Outlook

A novel hybrid state space and frequency domain method for mixed $\mathcal{H}_2/\mathcal{H}_\infty$ state feedback control design was developed in discrete time. The method uses SLS with SPA, but unlike prior work it does not require any finite time horizon approximations to evaluate the $\mathcal{H}_2$ and $\mathcal{H}_\infty$ norms of the closed-loop transfer functions. This proposed method represents the $\mathcal{H}_2$ and $\mathcal{H}_\infty$ norms of the closed-loop transfer functions in the state space as LMIs by using KYP applied to a deliberately constructed state space realization of the closed-loop transfer functions, and then leaves the additional SLS affine constraints in the frequency domain to maintain their convexity. The formulation obtained eliminates the need for a finite time horizon approximation, and results in a convex and tractable SDP for the control design. Suboptimality bounds are provided for the method which guarantee convergence to the global optimum of the infinite dimensional problem as the number of poles approaches infinity with a convergence rate that depends on the geometry of the pole selection.

We adapted SPA approximation error bounds to the more challenging setting of continuous time due to the noncompactness of the domain of integration for $\mathcal{H}_2$ and $\mathcal{H}_\infty$ norms, and recovered similar results to the discrete time. The first ever tractable control design method for $\mathcal{H}_2/\mathcal{H}_\infty$ control with SLS in continuous time is developed, which avoids the errors introduced by both discrete time approximations and finite time horizon approximations, enabling accurate evaluation of the $\mathcal{H}_2$ and $\mathcal{H}_\infty$ norms of the closed-loop system. Suboptimality bounds are provided for the more challenging continuous-time setting, with results similar to those obtained in discrete time, showing that the control design converges to optimality as the number of poles approaches infinity.

The hybrid framework for only four known output feedback convex reparameterizations without relying on coprime decomposition in discrete time (SLS, IOP, MI, MII) is developed after SPA, avoiding the error of finite time horizon approximation, which are all convex

and tractable SDPs and can be solved efficiently. We developed a unified proof framework for providing suboptimality bounds, and applied it to simultaneously establish the first suboptimality bounds for output feedback design using all four convex reparameterization methods that yield results analogous to the state feedback setting.

Applications to power converter control and dynamic virtual power plants demonstrate the framework's practical effectiveness, with case studies showing superior performance in frequency regulation, voltage control, and aggregative control scenarios.

Future work will focus on the suboptimality bounds of the hybrid framework after incorporating state and input constraints in both discrete time and continuous time. This framework can also be adapted in multi agent systems for distributed control synthesis, revealing many new areas for future research.

References

[1] Alborz Alavian and Michael C. Rotkowitz. Q-parametrization and an sdp for $\mathcal{H}_\infty$-optimal decentralized control. *IFAC Proceedings Volumes*, 46(27):301–308, 2013. 4th IFAC Workshop on Distributed Estimation and Control in Networked Systems (2013).

[2] Erling D Andersen and Knud D Andersen. The mosek interior point optimizer for linear programming: an implementation of the homogeneous algorithm. In *High performance optimization*, pages 197–232. Springer, 2000.

[3] James Anderson, John C Doyle, Steven H Low, and Nikolai Matni. System level synthesis. *Annual Reviews in Control*, 47:364–393, 2019.

[4] P.M. Anderson, A.A. Fouad, Institute of Electrical, and Electronics Engineers. *Power System Control and Stability*. IEEE Press power engineering series Power system control and stability. Wiley, 2003.

[5] Athanasios C. Antoulas. *Approximation of Large-Scale Dynamical Systems*. SIAM, 2005.

[6] Shimon Awerbuch and Alistair Preston. *The virtual utility: Accounting, technology & competitive aspects of the emerging industry*, volume 26. Springer Science & Business Media, 2012.

[7] Denis S Bernstein and Wassim M Haddad. Lqg control with an $\mathcal{H}_\infty$ performance bound: A riccati equation approach. In *1988 American Control Conference*, pages 796–802. IEEE, 1988.

[8] D.S. Bernstein and W.M. Haddad. Lqg control with an h/sup infinity / performance bound: a riccati equation approach. *IEEE Transactions on Automatic Control*, 34(3):293–305, 1989.

[9] Yuxiao Chen and James Anderson. System level synthesis with state and input constraints. In *2019 IEEE 58th Conference on Decision and Control (CDC)*, pages 5258–5263. IEEE, 2019.

[10] Emiliano Dall'Anese, Swaroop S. Guggilam, Andrea Simonetto, Yu Christine Chen, and Sairaj V. Dhople. Optimal regulation of virtual power plants. *IEEE Transactions on Power Systems*, 33(2):1868–1881, 2018.

[11] John Doyle. Robust and optimal control. In *Proceedings of 35th IEEE Conference on Decision and Control*, volume 2, pages 1595–1598. IEEE, 1996.

[12] Zhong Fang and Michael W. Fisher. Hybrid state space and frequency domain system level synthesis for sparsity-promoting $\mathcal{H}_2/\mathcal{H}_\infty$ control design. In *2024 IEEE 63rd Conference on Decision and Control (CDC)*, pages 8473–8478, 2024.

[13] Michael W. Fisher, Gabriela Hug, and Florian Dörfler. Approximation by simple poles—part i: Density and geometric convergence rate in hardy space. *IEEE Transactions on Automatic Control*, 69(8):4894–4909, 2024.

[14] Michael W. Fisher, Gabriela Hug, and Florian Dörfler. Approximation by simple poles—part ii: System level synthesis beyond finite impulse response. *IEEE Transactions on Automatic Control*, 70(3):1411–1426, 2025.

[15] Pascal Frey and Paul George. Mesh generation: Application to finite elements: Second edition. *Mesh Generation: Application to Finite Elements: Second Edition*, 01 2008.

[16] Luca Furieri, Yang Zheng, Antonis Papachristodoulou, and Maryam Kamgarpour. An input–output parametrization of stabilizing controllers: Amidst youla and system level synthesis. *IEEE Control Systems Letters*, 3(4):1014–1019, 2019.

[17] Verena Häberle, Michael W Fisher, Eduardo Prieto-Araujo, and Florian Dörfler. Control design of dynamic virtual power plants: An adaptive divide-and-conquer approach. *IEEE Transactions on Power Systems*, 37(5):4040–4053, 2021.

[18] Rick Wallace Kenyon, Anderson Hoke, Jin Tan, and Bri-Mathias Hodge. Grid-following inverters and synchronous condensers: a grid-forming pair? In *2020 Clemson University Power Systems Conference (PSC)*, pages 1–7. IEEE, 2020.

[19] Johan Lofberg. Yalmip: A toolbox for modeling and optimization in matlab. In *2004 IEEE international conference on robotics and automation (IEEE Cat. No. 04CH37508)*, pages 284–289. IEEE, 2004.

[20] M. Rotkowitz and S. Lall. A characterization of convex problems in decentralized control$^a st$. *IEEE Transactions on Automatic Control*, 51(2):274–286, 2006.

[21] H. Saboori, M. Mohammadi, and R. Taghe. Virtual power plant (vpp), definition, concept, components and types. In *2011 Asia-Pacific Power and Energy Engineering Conference*, pages 1–4, 2011.

[22] Carsten Scherer and Siep Weiland. Linear matrix inequalities in control. *Lecture Notes, Dutch Institute for Systems and Control, Delft, The Netherlands*, 3(2), 2000.

[23] Dante Youla, Hamid Jabr, and Jr Bongiorno. Modern wiener-hopf design of optimal controllers–part ii: The multivariable case. *IEEE Transactions on Automatic Control*, 21(3):319–338, 1976.

[24] Yang Zheng, Luca Furieri, Maryam Kamgarpour, and Na Li. System-level, input–output and new parameterizations of stabilizing controllers, and their numerical computation. *Automatica*, 140:110211, 2022.

[25] Yang Zheng, Luca Furieri, Antonis Papachristodoulou, Na Li, and Maryam Kamgarpour. On the equivalence of youla, system-level, and input–output parameterizations. *IEEE Transactions on Automatic Control*, 66(1):413–420, 2020.